Modelling Sub-Reef Thermodynamics to Predict Coral Bleaching: A Case Study at Scott Reef, WA

by

James C. Bird
Sc.B. with Honours from Brown University, USA

Advisors: T. Hardy and L. Bode

MASTERS THESIS
March 2005

Submitted in partial fulfilment of the requirement for the degree of Masters of Engineering Science by Research at James Cook University.

Appendix 2

STATEMENT OF ACCESS

I, the undersigned, author of this work, understand that James Cook University will make this thesis available for use within the University Library and, via the Australian Digital Theses network, for use elsewhere.

I understand that, as an unpublished work, a thesis has significant protection under the Copyright Act and;

I do not wish to place any further restriction on access to this work.

~~Or~~

~~I wish this work to be embargoed until :~~

~~Or~~

~~I wish the following restrictions to be placed on this work :~~

Signature

25/3/05
Date

Appendix 3

STATEMENT OF SOURCES

DECLARATION

I declare that this thesis is my own work and has not been submitted in any form for another degree or diploma at any university or other institution of tertiary education. Information derived from the published or unpublished work of others has been acknowledged in the text and a list of references is given.

25/3/05

Signature

Date

Appendix 3

ELECTRONIC COPY

I, the undersigned, the author of this work, declare that the electronic copy of this thesis provided to the James Cook University Library is an accurate copy of the print thesis submitted, within the limits of the technology available.

Signature

25/3/05
Date

Statement of Contribution

Fees: Waived by James Cook University

Stipend support: Australian–American Fulbright Commission

Supporting institutions external to JCU: Australian Institute of Marine Science (AIMS)

Supervision: Thomas Hardy, Craig Steinberg (AIMS), and Lance Bode

Other collaborations: Woodside Energy Ltd. and NOAA / NESDIS (National Oceanic and Atmospheric Administration /National Environmental Satellite, Data, and Information Service)

Statistical support: Steve Delean (AIMS) [suggested statistical models and reviewed statistical analysis]

Editorial assistance: Craig Steinberg (AIMS), Thomas Hardy, Lance Bode, Richard Brinkman (AIMS), Kathleen Corriveau [all edited thesis manuscript]

Research assistance: Luciano Mason [2D modelling], Craig Steinberg (AIMS), Richard Brinkman (AIMS) [oceanography], Luke Smith (AIMS) [coral ecology].

Project costs: $600,000 in field data, $4,000 in AIMS bench fees, and $3,000 in transport to AIMS all paid for by the joint project between AIMS and Woodside Energy Ltd. Additional project costs, such as JCU supervision and computer resources were provided by JCU.

Use of infrastructure internal to JCU: *Hydra* supercomputer used for numerical simulations.

This thesis research forms part of a three-year project between AIMS and Woodside Energy Ltd. The overall design and goals of the project were developed by my advisors at AIMS prior to my involvement. Additionally, all field measurements were collected by AIMS before I began the project. My contributions were to develop the methodology to achieve the overall design and goals, process and analyse the field data, develop appropriate forcings for the numerical models, and analyse the results.

Acknowledgements

This project and thesis would not have been possible without the help and commitment of several people. I would like to thank my supervisors Tom Hardy, Craig Steinberg, and Lance Bode, as well as my unofficial advisors Lou Mason and Richard Brinkman, for the invaluable support and guidance with which they all provided me over the course of this project. I would also like to thank Janice Lough, Terry Done, Steve Delean, and Severine Choukroun for their advice and support.

Additionally, this thesis would not have been written without the emotional support of my family and friends. I thank my flatmates for helping me to keep my work in perspective, and my girlfriend, Kathleen Corriveau. Although she was physically living halfway around the world, she was always by my side and in my heart.

Abstract

Coral bleaching occurs when corals become stressed, which typically occurs during periods of elevated water temperatures. If water temperatures remain elevated for a sufficient length of time, the corals often die. Coral bleaching affects reefs around the world and the recent increase in the frequency and severity of bleaching episodes has raised considerable concern.

A clear understanding of the physics that elevate water temperatures may improve coral bleaching predictions and lead to more effective reef management. Currently, the best method to detect bleaching-like conditions is through a time integration of sea surface temperatures observed by satellite. Unfortunately, these observations only reveal the thermal structure for the top millimetre of water averaged over large areas (presently 2500 km^2). The aim of this study is to use environmental physics to predict water temperatures at the reef and sub-reef scales. The study then goes a step further and translates these thermodynamic models into bleaching predictions.

Simulations are run using atmospheric and oceanographic data from Scott Reef, a 40 km-wide atoll 300 km off the northwest coast of Australia. Scott Reef presents an ideal test site as it experienced a severe bleaching event in 1998 that was well documented. Averaged coral cover in exposed sites dropped from 54% to less than 10% over the top 30 metres. Additionally, the bathymetry around Scott Reef has been thoroughly surveyed and in 2003 an extensive array of oceanographic instruments was deployed for three months at strategic locations.

A one-dimensional turbulence model is used to determine the vertical temperature structure of the water column around Scott Reef. Scott Reef is in a data-sparse region so that all of the heat fluxes have to be estimated from atmospheric conditions recorded at distant weather stations. The model results are verified with the 2003 field data. By driving the model with the appropriate atmospheric conditions, the simulated temperature profiles match the field observations. The model is next used to hindcast the temperature profiles during the 1998 bleaching event. Simulations indicate that anomalously-warm water most likely reached depths of 30 metres, a result that supports the claim that the deep bleaching was due to thermal stress.

Field observations confirm that water currents around Scott Reef are predominantly tidal. Additionally, the observations demonstrate that the upper layers of certain regions within Scott Reef cool during strong tides. This finding is characteristic of tidal cooling, a common phenomenon where tides mix cooler, deeper water with warmer surface water.

A map of sub-reef regions at Scott Reef that might experience tidal cooling is revealed by the numerical modelling. In a novel approach, stratified waters from the vertical model can be well-mixed in zones identified by a two-dimensional hydrodynamic model. There is a strong correlation between areas where bleached corals survived and locations that are predicted to have access to cooler well-mixed deep waters.

The techniques used in this work are applicable to other reef systems. Therefore the results in this thesis are significant as they improve two aspects of coral bleaching prediction. First, the methods can determine if coral at different depths are at risk of bleaching. Second, the methods can distinguish regions within individual reefs that are more susceptible to coral bleaching.

Table of Contents

List of Tables

List of Figures

Preface

This thesis describes how a combination of thermodynamic and hydrodynamic models can be used to improve coral bleaching prediction. The model results have been compared to extensive field observations at Scott Reef, an isolated reef off the coast of northwest Australia. That said, the techniques presented within this thesis are not restricted to a particular geographic location and it is the author's hope that they might one day improve coral bleaching predictions worldwide.

In the introduction I discuss coral bleaching and why it is becoming an increasingly important issue. The spatial patterns that have been observed during bleaching events are mentioned with particular emphasis on how they may be caused. I describe two methods that are used to predict where coral bleaching is most likely to occur. I then identify the limitations of these techniques and outline how the work carried out in this project addresses these issues.

The second chapter focuses on the local oceanography around the test site, Scott Reef. I review what is currently known about the oceanography in the area and describe the 2003 field campaign, which was completed prior to my involvement in the project. Almost half of the work in the thesis involved compiling and analysing the field data; therefore considerable attention is given in explaining all the required steps. Finally, the noteworthy oceanographic characteristics are discussed; the results form a foundation that is referred to often in later chapters.

The third chapter describes the techniques used to estimate the heat transfer across the air-sea interface. The heat transfer depends on atmospheric conditions and the methods used to approximate these conditions are described. Finally, I discuss how the atmospheric conditions are applied to approximate the heat fluxes.

The fourth chapter explains how a numerical model was used to calculate the water temperature at various depths around Scott Reef. Simulations are first performed to calibrate and validate the model with the field data collected in 2003. The model is then run to calculate the temperature profiles which may have been present during the 1998 bleaching episode at Scott Reef. The impact of these temperature profiles on coral bleaching is discussed.

The fifth chapter investigates whether certain regions around Scott Reef are persistently cooler than other regions. Coral records at Scott Reef demonstrate that the coral mortality in 1998 differed among the sites sampled. Under the assumption that the spatial variability may be due to tidal mixing, a hydrodynamic model is used to calculate the tidal currents around the reef. Tidal currents and local bathymetry are combined to estimate mixing and potential cooling around the reef. Finally, the results are related to coral records as well as to temperature data.

The sixth and final chapter summarizes the techniques and results precented in this thesis. The two key objectives of the thesis are reiterated: first the investigation of water temperature at various depths, and second the examination of whether certain spatial locations are more susceptible to coral bleaching. I summarize the results of the numerical simulations and describe how these simulations are helpful in predicting coral bleaching. Finally, future research initiatives are identified and briefly discussed.

Chapter 1 – Introduction

Coral Bleaching

Coral are comprised of communities of individual coral polyps. The polyps support themselves by feeding on surrounding plankton; however, they receive most of their energy from algae called zooxanthellae. Zooxanthellae live in a symbiotic relationship within the polyps and give corals their colour. The zooxanthellae benefit from ammonia and phosphate given off as waste products from the coral and in return supply corals with surplus photosynthetic products. Coral bleaching occurs when corals purge the inhabiting zooxanthellae and as result become white, or bleached.

Abnormal levels of UV radiation, salinity, or concentrations of chemicals can all contribute to coral bleaching; however the dominant cause for large-scale bleaching is increased water temperature (Hoegh-Guldberg, 1999). Corals live at the upper-limits of their thermal environment such that water temperature elevated by only one degree Celsius above the maximum monthly average in summer is considered to have reached a bleaching threshold (Goreau and Hayes, 1994). Prolonged exposure to "bleaching temperatures" will eventually kill the coral; however, if temperatures quickly return to normal levels, the corals have a chance to reabsorb the zooxanthellae and recover. Many studies have also emphasized the effect of solar radiation on coral bleaching (e.g. Coles and Brown, 2003; Lesser, 1996; Mumby et al., 2001), although it is unclear whether high irradiance acts independently of water temperature (Fitt et al., 2001) or merely "aggravates the effect of temperature" (Hoegh-Guldberg, 1999).

In recent years, laboratory data have provided evidence for a third type of coral stress, stagnant water. Experiments have demonstrated that corals in moving water (50–70 cm s^{-1}) are less likely to bleach (and are more likely to recover from bleaching) than corals in slowly moving water (2–3 cm s^{-1}) (Nakamura and van Woesik, 2001; Nakamura et al., 2003). Nakamura et al. attribute their results to the slow mass transfer of necessary gases and molecules to the coral. It is important to note that corals can thrive in slow-moving water; the corals in Nakamura et al.'s studies only bleached when surrounded by elevated temperatures.

Prior to 1998, coral bleaching was generally considered a minor threat to coral communities. This attitude drastically changed following the 1997-1998 mass-bleaching episode, the most severe bleaching event ever recorded (Wilkinson, 2000). Coral bleaching and mortality was observed around the world. Reefs in Sri Lanka, Maldives, India, Kenya, Tanzania, and Seychelles experienced mortalities of up to 90% (Wilkinson et al., 1999). The Great Barrier Reef experienced the worst bleaching event on record for the region; bleaching was observed on 42% of the reefs (Berkelmans and Oliver, 1999). Not surprisingly, the global bleaching event coincided with record-breaking water temperatures (Karl et al., 2000) that have been attributed to one of the strongest El Nino events ever recorded (McPhaden, 1999).

While the thermal stress on corals may have been unprecedented during 1997-1998, the event was not as improbable as it first may have seemed. Sea-surface temperatures (SSTs) have significantly warmed over the last hundred years, and spikes of extreme SSTs have increased in frequency during the last thirty years (Lough, 2000). In fact on the Great Barrier Reef, the 1998 event held the record of worst-bleaching for only four years. In 2002, the coral bleaching on the Great Barrier Reef was even more severe than in 1998 with 54% of reefs bleached to some extent (Berkelmans et al., 2004). The link between global warming and mass-coral bleaching is now considered "incontrovertible" (Hughes et al., 2003), and results from global warming models have suggested that over half of the coral reefs in the world may be gone by 2030 (Wilkinson, 2002).

Coral communities form the foundation of a diverse ecosystem in otherwise nutrient-poor regions. Therefore a significant decrease in coral cover can have a devastating impact on the rest of the ecosystem. Economically, reef preservation is crucial as the reef ecosystem supports multi-billion-dollar tourism and fishing industries, and the corals themselves provide coastal protection and biochemicals that have the potential for new drug discoveries (Hoegh-Guldberg, 1999). There is therefore a pressing need for coral reef habitats to be protected.

While ocean heating is a global issue and is difficult for individual countries to combat, predicting where and when bleaching events are likely to occur is a first step in mitigating the problem. Effective prediction would allow scientists to better research and document the phenomenon. Due to the size of reef systems, the extent and severity of bleaching can evade scientists as they may not know where to conduct surveys.

Additionally, better coral bleaching prediction can help managers design more effective Marine Protected Areas. These areas protect the enclosed reefs by restricting various levels of human interaction: restrictions range from no-fishing to no-trespassing. Unfortunately, the 1998 bleaching event demonstrated that corals in the marine-protected areas were as likely to bleach and die as corals in non-protected sites (Wilkinson, 2000). This observation highlights the need for managers to take coral bleaching into consideration when designating conservation sites. Since the only way to improve site design would be to include reefs that have been identified as less prone to bleaching-induced mortality, reef-wide prediction capabilities are required.

Spatial Variability in Bleaching

The idea that some patches of corals may be less susceptible to bleaching than other nearby patches is based on the considerable spatial variability observed in bleaching and bleaching-induced mortality. Spatial variability in coral bleaching is well documented (e.g. Berkelmans et al., 2004) and is observed between reefs, within reefs, and even within single coral colonies (see Figure 1.1). The processes that cause this variability can be broken into two groups, biology and physics.

Figure 1.1 Healthy (pink) and bleached (white) corals lying side by side. *Photograph courtesy of Ray Berkelmans.*

Reaction to Stress

Biological explanations of bleaching variability focus on the coral's reaction to the stress causing the bleaching. Different types of coral have varying reactions to thermal stress; branching corals such as *Acropora* are more prone to bleaching and temperature-induced mortality than the massive corals, such as *Porites* (e.g. Marshall and Baird, 2000). In addition, the relationship between bleaching and mortality varies between taxa. Some types of corals tend to bleach and subsequently survive, whereas other types will die without ever losing

their colour. That said, the most typical reaction to warm water across taxa is a combination of bleaching and mortality (McClanahan, 2004).

Corals can adapt to their environment such that a coral in warmer, tropical water is apt to have a greater tolerance to high temperatures than the same species living in cooler, subtropical regions (Berkelmans, 2002). Furthermore, reefs that have survived a bleaching episode tend to be more resilient when faced with a subsequent thermal stress (Coles and Brown, 2003). Therefore, an accurate prediction of whether a particular reef will bleach requires information regarding its location, species composition, and bleaching history. There is of course one other crucial component to include in any bleaching prediction, and that is the location and intensity of the stress itself.

Location of Stress

Physical oceanography can also explain the spatial variability of coral bleaching. Unlike the biological approach which focuses on the coral's reaction to stress, the physical approach investigates where the stress is located. If the water in certain areas of a reef becomes hotter than other areas during a bleaching period, spatial variability in bleaching would be expected. The main stressors associated with mass coral bleaching are elevated temperature, increased irradiance and slow water movement. Spatial patterns of coral bleaching may be attributed to the spatial variability that naturally occurs in each of these stressors.

The amount of irradiance entering the atmosphere depends on latitude and time-of-year. For example in February the Great Barrier Reef is exposed to greater levels of irradiance than the Caribbean. At smaller scales, spatial patterns of cloud cover (Mumby et al., 2001) and water clarity (Phongsuwan, 1998) will lead to varying levels of irradiance on corals and may factor into bleaching patterns.

Water flow rates in nearby locations (<100 metres apart) can vary significantly. The flow rate depends on local features, such as bathymetry, and also requires a forcing mechanism. Ocean currents, tides, and wind can all influence the flow rate across coral reefs (e.g. Brinkman et al., 2001; Coutis and Middleton, 1999).

Temperatures can also vary significantly over small distances. Solar radiation increases water temperatures; therefore, any spatial patterns of irradiance may also lead to similar

spatial patterns of elevated temperatures. In addition, spatial variations in atmospheric conditions such as humidity and wind speed can lead to horizontal temperature gradients. Finally spatial patterns in temperatures can occur from the advection of warm or cool water. The spatial variability observed on reefs in Okinawa in 1998 has been attributed to the horizontal advection of warmer water (Nadaoka et al., 2001). At the same time, it is believed that some reefs in the Bahamas and South Africa avoided bleaching because of the upwelling of nearby cool, deep water (Riegl and Piller, 2003). Related to the cooling potential of upwelling is the idea of tidal mixing around reefs (Skirving and Steinberg, 2003). Skirving and Steinberg have noted that tidal flows can initiate local mixing (Simpson and Hunter, 1974) and subsequently cool down surface waters (Pingree and Griffiths, 1978). Because the tidal flow rates vary along reefs, tidal cooling is expected to vary along reefs as well and may be partly responsible for the spatial variability observed in coral bleaching.

Predicting Coral Bleaching and Mortality

Any coral bleaching prediction requires locating potential stressors, such as warm water, as well as approximating the coral's reaction to that stressor. Present prediction models are based, at least in part, on SST which can be obtained remotely by satellite.

The most widely-available bleaching predictions rely solely on remotely sensed SSTs. The technique, which I will call the 'Remote Sensing Approach', presumes that the stress caused by high temperatures dominates any stress from irradiation and water speed. At the same time, the coral's reaction to the water temperature is assumed to be related to the upper range of water temperature observed in the area. These predictions have been highly successful at large-scales (Liu et al., 2003), yet have been sharply criticized for their simplicity (e.g. Fitt et al., 2001).

A new, more complex prediction method consists of a Bayesian belief network (Wooldridge and Done, 2004). The network uses information from past events to "learn" what combinations of events are likely to lead to future bleaching. Wooldridge and Done's model relies on satellite-derived SST data as well as information regarding the ecology of the modelled reef sites.

Remote Sensing Approach

Since the late 1990s, large-scale coral bleaching predictions have been possible through remote sensing. Areas of elevated temperatures identified from satellite images are used as a proxy for thermal stress on coral reefs. These patches of hot water can be tracked in near real-time, and are generally referred to as "hot spots" (Goreau and Hayes, 1994). NOAA has been tracking hot spots since the late 1990s and provides twice-weekly charts of hot spots around the world. It is important to differentiate a hot spot from a temperature anomaly. Hot spots are defined with coral stress in mind. Since it is believed that corals have generally acclimated to their particular environment, warm water is only considered a "spot" when it has surpassed the upper limits of typical water in the region (more specifically, when the maximum mean-monthly summer temperature has been surpassed). For example, suppose a temperature of 31 degrees is detected in April when temperatures are typically 29 degrees. Additionally suppose that at this particular location, February was climatologically the warmest month with an average of 30 degrees. In this case, there is a two degree temperature anomaly; however, the hot spot value is only one degree.

Hot spots are limited to identifying the possible location and degree of thermal stress; however, they do not give an indication of the coral's reaction to the stress. The length of time that the coral is exposed to the water anomaly is crucial in determining the likely outcome. Corals can survive a brief period of hot temperatures, but will bleach after a longer period of moderately elevated water temperatures. For this reason, NOAA also integrates exposure time with above-average heating to create a Degree-Heating-Week (DHW) map. The DHW value represents the time-integrated effect of thermal stress on coral, and is calculated as the product of the exposure-time and degrees of thermal stress over a rolling 12-week time period. For example, a two-week period of a four-degree increase in temperatures is given the same index as a four-week period of a two-degree temperature increase; both are given a value of 8 provided that there was no other thermal stress observed over the 12-week period. Field observations indicate that a DHW value of approximately 4 coincides with the onset of bleaching. By the time the DHW value reaches 8 degree-weeks there is a high probability of widespread bleaching with some mortality (Liu et al., 2003).

The hot spot and DHW predictions are presently too coarse to discern reef-wide bleaching. At the moment, the satellite images have a resolution of 50 km by 50 km which means that any cooling features smaller than 2500 square kilometres would be obscured by the temperature of the surrounding water. There are plans to improve the resolution to 4 km by 4 km (Liu et al., 2003) and eventually to resolutions as fine as 1 km by 1 km (W. Skirving, personal communication). These refinements will improve SST predictions; however, the amount that they might improve bleaching predictions is unclear as coral bleaching and bleaching-induced mortality depend on additional factors.

Bayesian Belief Network Approach

Bayesian Belief Networks (BBNs) offer a holistic approach to coral bleaching predictions. The network is comprised of several "evidence" nodes that describe a certain aspect of the system. For example, one node might reflect the water temperature while another denotes the coral habitat. Still other nodes describe the outcome, such as coral bleaching or mortality. The nodes are connected with directional links indicating a directed influence from one node to another. For example, the water temperature node would point toward the bleaching node because water temperature can lead to coral bleaching. Note that the arrow would not point from the bleaching node to water temperature node as bleached coral does not affect the water temperature. Once the links between the nodes have been established, an algorithm strengthens or weakens the links based on field observations. The result is a probabilistic model which indicates the likelihood of bleaching or mortality from various conditions.

Bayesian Belief Networks offer promising solution to many of the simplifications used in the hot spot and DHW predictions. For example, a concern regarding the Degree-Heat-Weeks index is its over-simplified method to calculate the accumulated heat stress. The accumulated heat stress is estimated as the product of the degree of heating and exposure time, which tacitly assumes bleaching/mortality curves follow the hyperbola, $y = c/x$. Highly non-linear bleaching curves were determined experimentally for several sites in the Great Barrier Reef (Berkelmans, 2002). However, the bleaching curves demonstrated that there was no clear relation between temperatures and exposure time that leads to bleaching. BBNs could determine appropriate relationships between

temperature, exposure time, and bleaching and include any number of additional considerations, such as habitat or taxa.

The difficulty in setting up a BBN is that it requires a large amount of input data. In addition, the accuracy of the models will depend on what the nodes measure. For example, Wooldridge and Done (2004) decided not to include irradiance or water velocity as nodes in their network. If these potential stressors are important in coral bleaching predictions, then a model that does not include them will be less accurate and less reliable than a model that does. In spite of all this, there appears to be potential for Bayesian networks to improve coral bleaching prediction as well as to discover the relative strength of interactions and relationships between the physics and ecology leading to a bleaching event.

Limitations of Prediction Approaches

The Hot Spot and Degree-Heating-Weeks products proved quite successful in monitoring the 2002 mass bleaching event (Liu et al., 2003), and there are indications that the Bayesian approach of Wooldridge and Done will yield excellent results in the Great Barrier Reef (Wooldridge and Done, 2004). Yet there are two limitations which should be addressed. First, the thermal stress used in both techniques is restricted to the surface skin layer. The second limitation is that neither of these products gives any insight to the physical mechanisms that are the root cause of anomalous temperatures. These limitations will be discussed in detail below.

Bleaching at Depth

'Hot Spots' and DHW prediction techniques do not give any indication of the thermal stress and coral response at varying depths. The DHW product may indicate that bleaching is likely at a particular location, but the observations are restricted to the skin-surface. The same is true for the Bayesian network setup (Wooldridge and Done, 2004) since the model used SST rather than the temperature surrounding the coral.

Satellite imagery detects water temperature of only the top 10 microns of water, often referred to as the skin layer. Because this layer is in contact with air, the difference in temperature between this layer and water a centimetre below can be as much as one

degree Celsius (Maurer, 2002). This slight temperature difference can have a significant effect on coral health. Also, due to thermal stratification, temperature differences throughout the water column may be even more pronounced. Water temperature for corals near the surface will correlate reasonably well with skin layer temperatures; however, corals can live up to 50 m below the surface and a wide variety of temperatures environments, different from that at the surface, can exist. Coral bleaching predictions would greatly benefit from knowing the water temperature surrounding the coral rather than just the water temperature at the surface.

In fact, coral bleaching research in general would profit by taking account of these temperature differences. While some studies have pointed to radiation as the source of the coral bleaching, this does not rule out the possibility that these results were caused instead by thermal stratification (e.g. Mumby et al., 2001; Phongsuwan, 1998). For example, it has been noted that corals in turbid water are less likely to bleach than those in clearer water; this observation has been used as evidence of the effects of UV stress on corals (Phongsuwan, 1998). There is no doubt that particles in turbid water attenuate the amount of solar radiation that can penetrate to the depths of the coral; however, a decrease in solar radiation leads to a decrease in solar heating in the deeper water. Therefore in relatively still water, greater turbidity increases the thermal stratification of the water column and can have the effect of insulating deeper corals from warm surface waters.

Another example is a recent study by Mumby et al. (2001) which hypothesized that cloud cover reduced radiative stress and thus prevented corals from bleaching at a particular site. The study noted that SSTs in 1998 surpassed a "bleaching threshold" for the study site, but that bleaching was not observed. The investigators used quadratic discriminate analysis to predict coral bleaching at the site using SST, wind, and cloud cover records. Their results showed that when cloud cover was removed from the analysis, the model predicted bleaching for 1998; however when cloud cover was included in the analysis, no bleaching was predicted.

These results may also be more a result of thermal stratification than cloud cover. The corals that were investigated were located 14 metres below the surface, yet their analysis assumes that the temperatures at this depth were the same as at the surface.

A close analysis of the SST data of Mumby et al. (Figure 1 in their paper), reveals that surface temperatures a month prior to the expected (but not observed) 1998 bleaching event were significantly lower than the temperatures a month before the other bleaching events. In other words, the surface temperatures heated up past the bleaching threshold faster in 1998 than in the other years that bleaching was observed. This indicates that solar radiation absorbed in the top layers of water may not have mixed down into the rest of the water column. Additionally the weather conditions observed during that period were ideal to set up thermal stratification in the water column; Mumby et al. (2001) note that the winds were unusually calm and that most days were cloudy. Wind and night-time clear skies promote mixing (the mechanisms will be described in Chapter 3); therefore, the observed calm and cloudy conditions observed indicate that temperatures in 1998 were most likely warmer on the surface than at the depth of the corals, 14 metres below.

The recommendation that temperature stratification be factored into coral bleaching studies is not intended to suggest that radiative stresses play a negligible role in coral bleaching. While biochemical mechanisms that lead to coral bleaching and mortality are still not yet completely understood, there is general agreement that both increased temperature and increased light are factors that lead to coral bleaching (e.g. Coles and Brown, 2003; Franklin et al., 2004; Hoegh-Guldberg, 1999). That said, it appears that thermal stress is the primary cause for bleaching and that solar radiation plays a secondary role. In particular, there are no cases of mass coral bleaching without the presence of elevated water temperatures, whereas there have been plenty of cases where bleaching has occurred without the presence of high irradiance (Hoegh-Guldberg, 1999).

Solar radiation plays a double role in coral bleaching; the radiation affects the coral directly as well as heating up the surrounding water. Because small changes in water temperature can have a large impact on coral stress, the only way to accurately separate the effects of solar radiation from the effects of temperature requires that the water temperature around the coral is known. Thus, there is a need in both laboratory field experiments and coral bleaching prediction for techniques that enable researches to estimate water temperature at various depths.

Physical Mechanism of Thermal Stress

Another limitation of the prediction techniques for coral bleaching is that physical mechanisms that cause anomalous temperatures are ignored. It would be useful to know the physical mechanisms which lead to water temperatures in a particular location. This knowledge could help discern whether anomalous temperatures were due to local atmospheric conditions, ocean currents, or to say, an oil rig set up near the reef.

Atmospheric events, such as wind, solar radiation, and clouds can affect temperatures in sometimes unexpected ways. Strong winds will increase surface evaporation which acts to cool the surface water in a process referred to as latent heat flux. At the same time, the wind may mix down warmer surface-water to stress bottom-dwelling corals. Cloud cover reduces the amount of solar radiation that can heat up the water, yet clouds reflect some of the longwave radiation emitted by the water back onto the water surface. Ocean currents can transport warmer water into cooler regions and therefore may also contribute to coral bleaching (e.g. Nadaoka et al., 2001). At the same time, cool water upwelled from greater depths has been identified as a mechanism that protects certain corals during bleaching-like conditions (Riegl and Piller, 2003).

Smith (2001) investigated the weather and oceanographic conditions in the Bahamas during a bleaching event in 1990. Using atmospheric observations from a local weather station, Smith estimated the local heat fluxes across the air-sea interface. His results showed that the increase in water temperature was most likely caused by a decrease in the latent heat transferred from the ocean to atmosphere. In addition, Smith found evidence that wind-driven upwelling and downwelling had an effect on shelf water temperature.

Smith's paper is novel as it may be the only study thus far that has related heat fluxes across the air-sea interface to bleaching-like conditions. However, the study falls short of actually estimating the quantitative effect of these fluxes on the water temperature. The methods developed in this thesis demonstrate that the relative importance of atmospheric conditions and thermal advection on coral bleaching can be determined at a particular site by estimating the quantitative effect of the conditions and advection on the water temperature.

Finally, predictive models can enable industries to determine how their actions affect local bleaching. If an oil company began drilling near a reef system and bleaching

followed, it would be to their benefit to know whether or not this event was caused by natural or anthropogenic processes.

Project Objectives

There are two primary objectives of this thesis. The first is to estimate from limited oceanographic and atmospheric data the vertical variation in water temperatures. The second objective is to predict regions within Scott Reef where tidal mixing may have an effect on the water temperature surrounding coral. The results will be used to hindcast the thermal environment around Scott Reef during the 1998 bleaching episode which will then be compared to coral mortality observed during that period.

Scott Reef is a 30 km-wide reef system 300 km off the northwest coast of Australia (Figure 1.2). During the 1998 mass-bleaching event, extensive coral bleaching was observed down to depths of 30 metres (Smith et al., 2003). Surveys conducted at Scott Reef over the past 10 years found a distinct drop in coral coverage due to bleaching. The mean pre-bleaching coral cover, averaged across several sites and years, was 48.4 %. Mean post-bleaching coral cover at the same sites was only 10.8% (Heyward et al., 1999). These surveys also show that the loss in coral cover between sites is not uniform. One site experienced a 60% difference in coral cover from before to after bleaching, whereas another site showed less than a 20% difference.

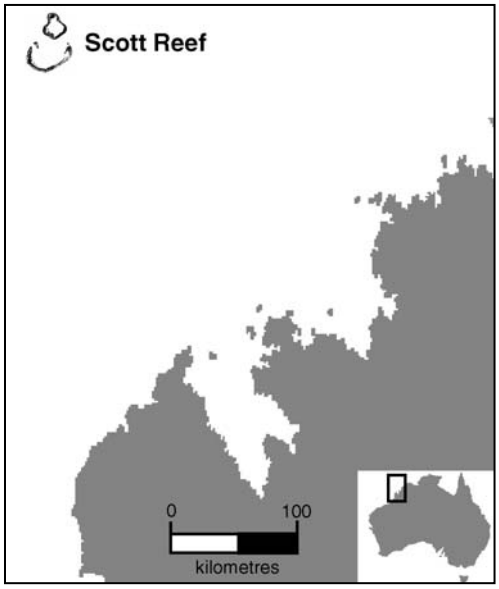

Figure 1.2 Location of Scott Reef.
Illustration from Heyward et al. 1999.

This project first involves processing and analysing extensive field data that have been collected at the Scott Reef from April to July, 2003. In addition, all available atmospheric data in the vicinity of Scott Reef during this period and in 1998 were gathered. From this atmospheric data, bulk formulas are used to estimate the heat and momentum fluxes across the air-sea interface in the waters surrounding Scott Reef. A one-dimensional water-column model is then used to relate these fluxes to vertical variation in water temperature for both 1998 and 2003. Sensitivity analysis is

performed to estimate the relative importance of wind speed, air temperature, atmospheric pressure, humidity, and cloud cover in determining vertical temperature.

In a parallel study with this thesis, Steinberg and Choukroun (in preparation) use reef-located weather stations data to estimate the water column thermal structure at several sites on the Great Barrier Reef. In this thesis, the same numerical model is applied; however, unlike Steinberg and Choukroun's study, the work in this thesis is used to hindcast a previous bleaching event in a more challenging, data-sparse location. Additionally, the temperature results are used to extend NOAA's Hot Spots and DHW products to include bleaching at depth.

The second part of this study closely follows recent work by Skirving and Steinberg (2003). These two scientists have modelled surface cooling from tidal mixing in the Great Barrier Reef and have found that their results correlate well with SST observations on a relatively coarse spatial scale. This study increases the spatial resolution, to the point where it can be shown that within the coarse resolution of observed SST there is observed (and predictable) finer-scale spatial variability of bleaching. Thus bleaching can not be predicted from SST alone, even if SST products improve in resolution.

In this thesis, cooling from tidal mixing is calculated at Scott Reef. The amount of cooling is estimated following the approach of Skirving and Steinberg (2003). The study then goes one step further and models the movement of tidally cooled patches of water during a spring tide. These modelled cooler areas are then compared with coral bleaching response observations and the observed 2003 temperature data set.

Chapter 2 – Scott Reef Oceanographic Observations

Scott Reef was chosen as the test site for the work in this thesis for a number of reasons. First and foremost, Scott Reef experienced a severe bleaching event in 1998 that was well documented (Smith et al., 2003). Next, Scott Reef ecology, oceanography, and reef bathymetry has been well documented through a joint project between AIMS and Woodside Energy Ltd., an energy company interested in exploring the area. All field measurements were taken before the start of this thesis, and my contribution is in the processing and analysing of this data. Finally, Scott Reef was chosen as a test site because it is surrounded by deep water and therefore may have access to cooler water under certain conditions.

The purpose of this section is to gain a greater insight into important oceanographic features at Scott Reef and the surrounding region. These include major currents and tidal signatures, water properties such as turbidity and salinity, and finally any internal processes which may enhance mixing or upwelling.

Insight on the oceanographic features will be gained by first recounting previous literature on field studies in the area. Then, the field data collected at Scott Reef in 2003 will be presented. The steps used to process the data from raw field measurements are described in Appendix A, as much of the time spent on this project was dedicated to that purpose though the details are not appropriate for the body of the thesis. The analysis of the processed data and the implication on the oceanography around Scott Reef will be discussed in this chapter.

Oceanographic Processes in Northwest Australia

The water clarity can have a profound effect on the heat balance in the water column. Ocean water turbidity (inverse of clarity) has been classified into fourteen categories often referred to as Jerlov Water Types (Jerlov, 1976). Five of these categories model deep ocean turbidity while the other nine model coastal turbidity. Jerlov originally classified deep water ocean into three classifications – I, II, and III – with I being the least turbid and III being the most. As more ocean water was studied, it became apparent that additional classification was needed between I and II, giving rise to the IA and IB water types.

The Jerlov water type for a region can be estimated from observations taken around the world. Jerlov configured a world map from these observations (Jerlov, 1976) and the water types surrounding Australia are shown in Figure 2.1. From this map it is difficult to estimate the class of water around Scott Reef, as nearby water ranges from class IA to class III. Additionally, this map classification assumes deep water. While Scott Reef is surrounded by deep water, it is itself a reef, and therefore might be modelled better with Jerlov's coastal water type classification.

Figure 2.1 Jerlov water types around Australia. The star denotes the location of Scott Reef.

There is strong evidence that there must be some underlying current off the northwest shelf of Australia. This evidence comes from heat balance arguments; the net heat balance measured off NW Australia indicates that there is positive yearly average heat flux into water column of about 70 W m^{-2}. To preserve the heat balance, it is believed that the excess heat is removed through ocean currents (Godfrey and Mansbridge, 2000). Namely deep cool water is advected into the region as warmer water is advected out.

The waters off northwest Australia experience two seasons, wet and dry. In the wet season the winds come from the west and are associated with high humidity and temperature. From April to October the prevailing winds change so that dry air from the land lowers the humidity. This sharp difference in the wet and dry seasons drives a seasonal oceanographic response (Holloway and Nye, 1985). Additionally, satellite altimetry has indicated that large eddies (over 100 km in diameter) are shed from the Indonesian Throughflow (Feng and Wijffels, 2002). These eddies may also play a significant role in the currents around Scott Reef.

Satellite images have not yet identified any upwelling near Scott Reef, though they have observed upwelling closer into shore on the Kimberley coast (Cresswell and Badcock, 2000). However, internal waves have been detected on the shelf near Scott Reef using ERS1&2 Active Microwave Instrumentation (Burrage et al., 1996). Field measurements taken outside of Scott Reef have indicated that internal waves are present and can have a major influence on currents and temperatures in the top 200 metres (Wolanski and Deleersnijder, 1998).

While sparse data have been collected around the reef, there have not been enough field measurements to calibrate or verify numerical models. Oceanographic field measurements are crucial as they can be used to asses the assumptions and the limitations of hydrodynamic models in the area. By noting oceanographic similarities and differences between different parts of the reef (both horizontally and vertically), the role of oceanographic processes, such as advection, on water temperatures can be assessed.

Field Sites at Scott Reef

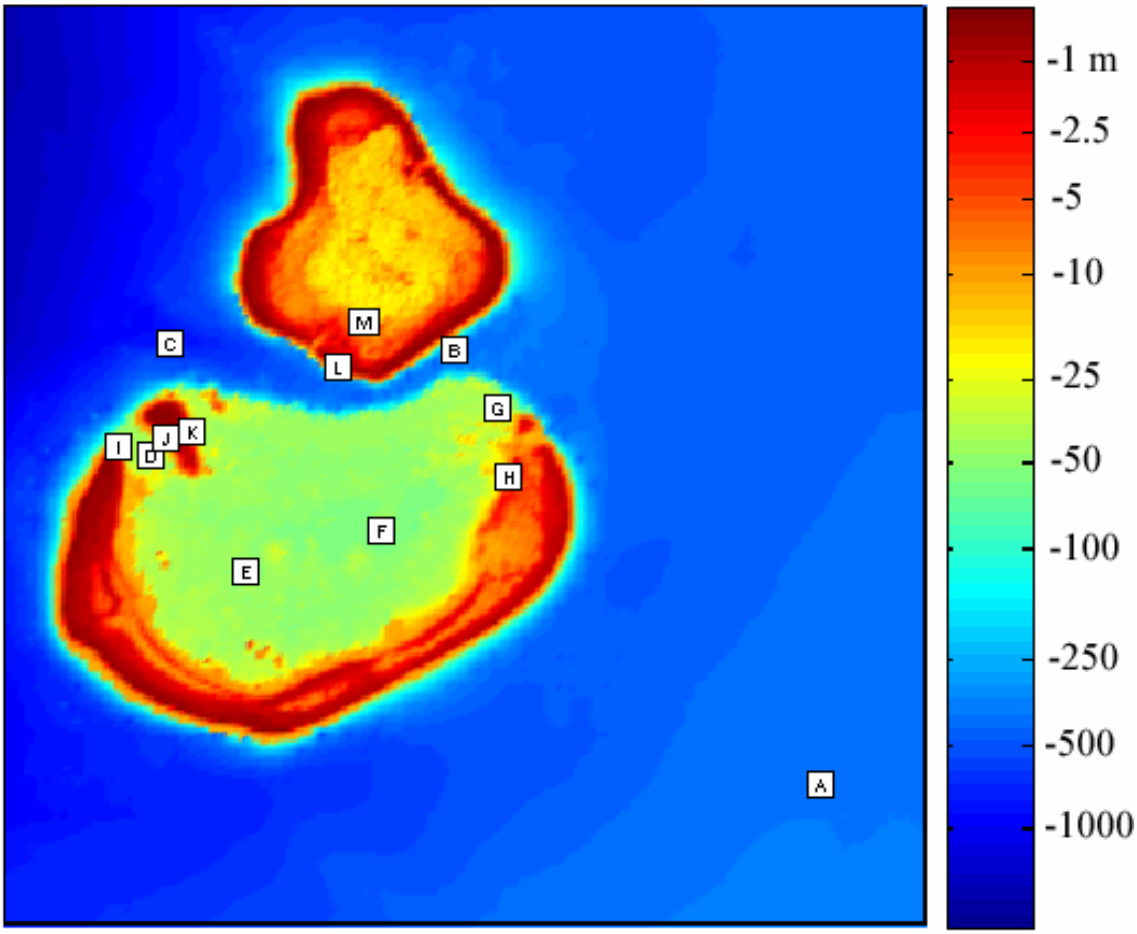

Figure 2.2 Field sites at Scott Reef during 2003 field campaign. Colour indicates depth in metres.

Extensive field measurements were obtained at Scott Reef for a 3 month period between the end of March and the end of June in 2003. Sixty-seven temperature loggers were deployed along with ten current meters (five of which were current profilers), twelve depth sensors, and three salinity loggers (see Appendix B). Measurements were taken every five or fifteen minutes depending on the type of instrument (eight different types

of instruments were deployed). Instruments were placed into one of thirteen field sites. Twelve of these sites were spread throughout the reef roughly five to ten kilometres apart. The remaining site (Site A) was located away from the reef to determine far-field conditions. The current profilers were placed around the major entrances into the lagoon so that the water flow in and out of the lagoon could be monitored. Of the 13 sites, 7 of them were moorings and 6 of them were transects (see Figure 2.3). Instruments were placed roughly 5 to 10 metres apart vertically.

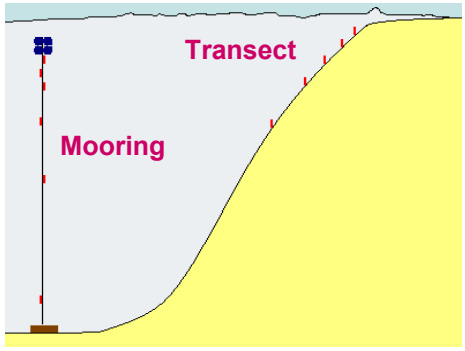

Figure 2.3 Cartoon illustrating how instruments (red lines) are arranged on a mooring and transect.

Temperature and salinity profiles were also measured by CTD (conductivity, temperature, and depth) casts. Seven casts were taken in March during the instrument deployment and five casts were taken in June during the recovery (Figure 2.4). These casts were used to help calibrate some of the instruments, act as the initial condition for some of the model runs, and provide insight into some noteworthy phenomena in the lagoon around the end of June.

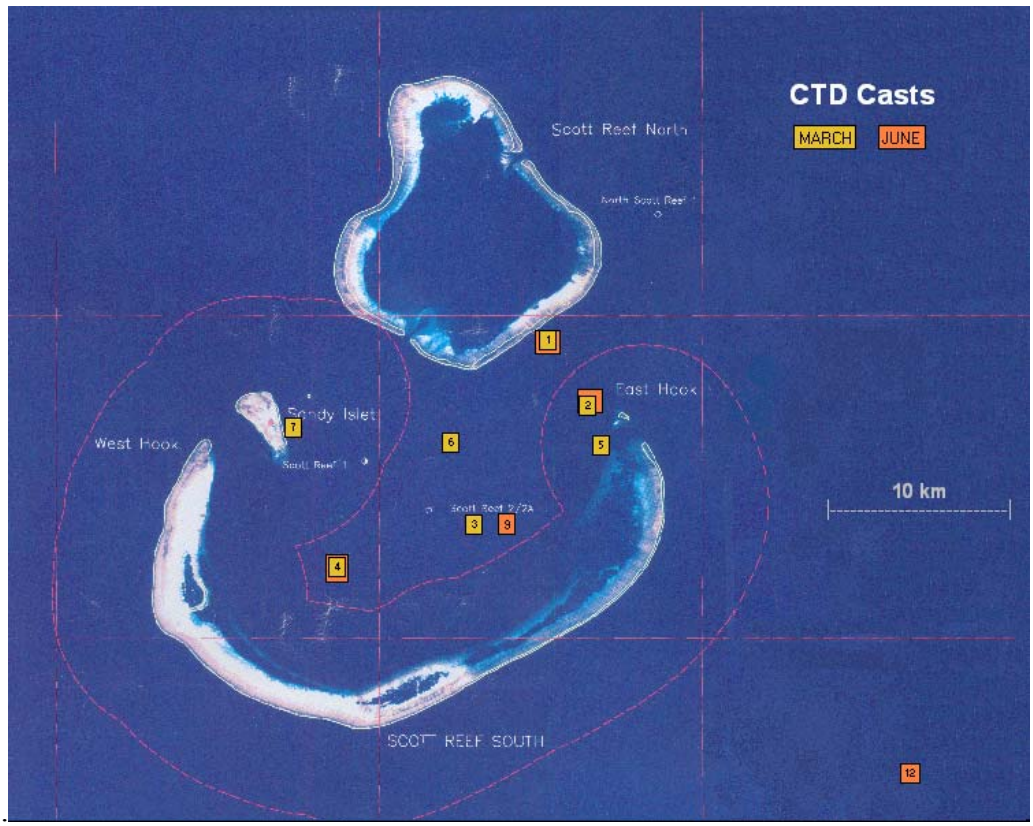

Figure 2.4 Location of Conductivity-Temperature-Depth (CTD) casts in March and June of 2003.

Data Analysis and Results

Jerlov Water Type

As mentioned earlier, water turbidity has an important role in the distribution of heat into the water column. A map of Jerlov water types around Australia (Figure 2.1) does not give enough information to adequately estimate an index value.

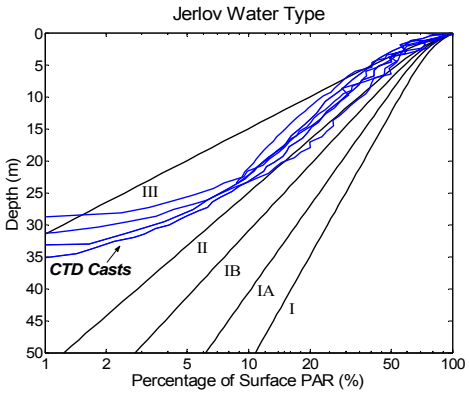

Figure 2.5 - Observed light extinction at Scott Reef.

To better estimate the water type around Scott, light extinction observations can be used. In addition to measuring conductivity, temperature, and water density, the CTD casts taken at Scott Reef also measured the Photosynthetically Active Radiation (PAR) as a function of depth. From these measurements the Jerlov water type at Scott can be estimated.

Following Jerlov, only the measurements taken near the solar zenith without the presence of clouds are used (Jerlov, 1976). These measurements are then normalized to produce the percentage of surface PAR observed at varying depths. In Figure 2.5 the observed light extinction is plotted for several CTD casts. The figure also includes the percent of surface PAR expected at different depths for each of Jerlov's ocean water types (Jerlov, 1976). The observed light extinction falls between water types II and III. The observed extinction for the first 25 metres are most similar to type II extinction; however once the percentage of surface PAR falls below 10 percent (at around 25 metres), the rate of extinction accelerates dramatically. It is possible that the noise to signal ratio increases as less light reaches the instrument, which may lead to this greater rate of extinction. Provided that the measured rate of extinction in shallower water (< 25 metres) is more accurate than in deeper water, the turbidity of water around Scott Reef should be categorized as Jerlov water type II.

Predominant Currents

The relative direction and magnitude of the measured current at Scott Reef are shown in Figure 2.6. Almost all the currents appear to be tidal, and larger flowrates are observed near the channels (Sites D and G). The currents decrease substantially in the lagoon as is expected. The currents at Site C are somewhat surprising both in the small size and the observation that the current tends to be dominated by non-tidal effects; the current maintains a relatively constant ENE direction throughout the data set.

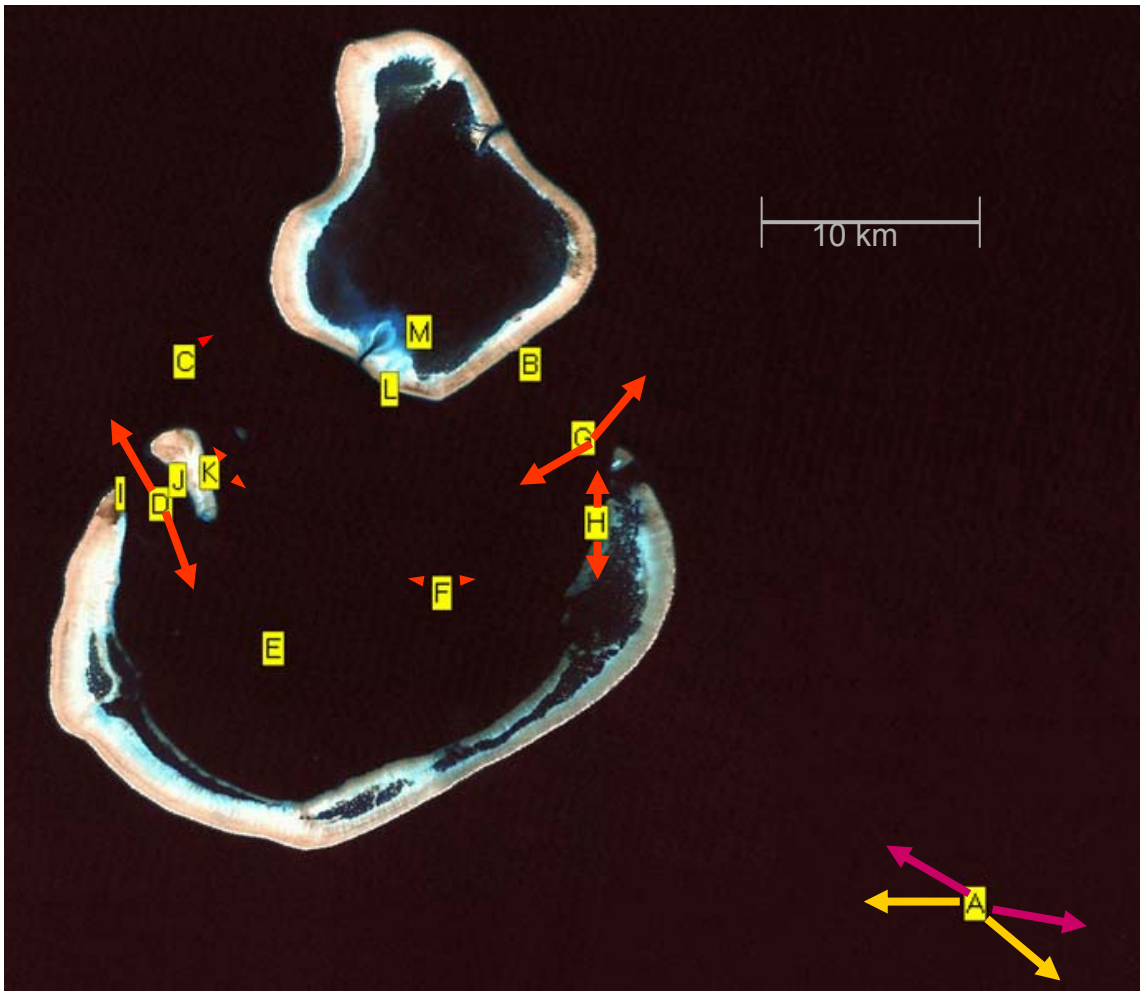

Figure 2.6 Relative magnitude and direction of observed currents (red arrows). At Site A, the currents are observed in either of two modes (denoted by yellow and purple arrows).

It is also interesting to note the currents at Site A, the far field mooring. The current is tidal; however, the direction for the ebb and the flood are not supplemental. Furthermore, the direction of these currents changes slightly at the beginning of April

(from yellow to purple in Figure 2.8). By the beginning of May the currents have returned to the original mode and a month later they have returned to the second mode for a second time. These changes in tidal direction suggest the presence of a lower frequency current oscillating between NNE and SSW. This is evidence that there may be advection through Scott Reef; however more interestingly, the observations indicate that the advection oscillates in direction.

The tidal response near the surface at Site A is illustrated below (Figure 2.7). The two tidal modes can be seen in the "direction" subplot as well as the stick plot of the currents. The low frequency changes in current direction are not correlated with the tidal spring-neap cycle which is visible in the "current speed" subplot.

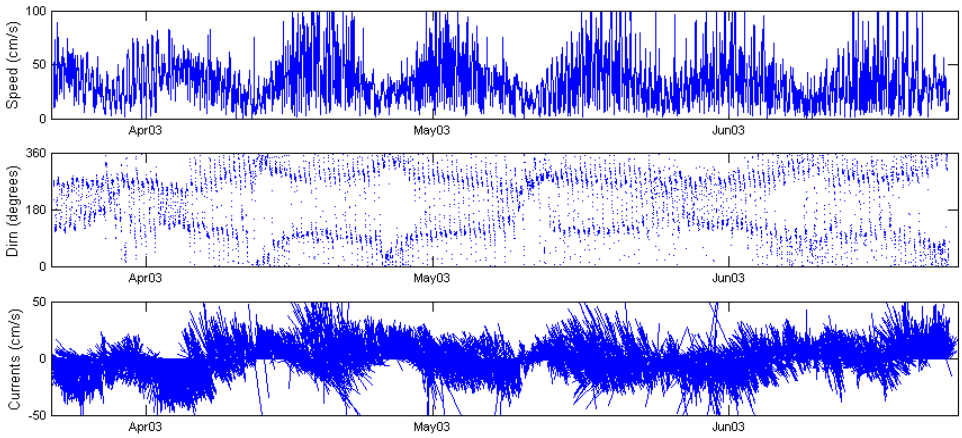

Figure 2.7 The speed and direction of current observed at Site A during three months.

Tidal Analysis

Tides are a result of astronomic orbits and thus are inherently periodic. Tidal analysis decomposes a tidal signal into each of its base frequencies, known as tidal constituents. The amplitudes and phases of these constituents can be reconstructed to predict tides for any time in the future or past.

Tidal harmonic analyses were performed for both the sea-level elevations and the current meters using a combination of MATLAB code written by Pawlowicz et al. (2002) and Fortran code written by Lou Mason of James Cook University (see Appendix D). The length of measurements needed for a tidal analysis depends on which constituents are needed. Longer periods of measurements are required to discern between similar-frequency constituents. After 90 days the major constituents can usually be extracted; however time series of over a year are necessary to extract many of the minor

components. Even longer time series may be necessary to accurately describe lower frequency terms.

Water surface elevation at Site L was measured for 395 days starting in 2002. From the tidal analysis the amplitude and phase of most of the major and minor constituents was calculated. The predicted tide from this analysis could explain 99.8% of the variance in the original data. It was found that most of the energy at Scott Reef is contained in the M2, S2, K1, and N2 constituents (in that order).

During the 2003 field campaign, sea levels were collected for only 3 months which is too short to discern between certain constituents that would be used in the hydrodynamic model. To overcome this problem, tidal analysis was run with inferences established from the year-long data set. The constituents P1, S1, and PHI1 were inferenced from K1, 2N2 was inferenced from MU2, NU2 was inferenced from N2, and T2 and K2 were inferenced from S2. The software by Pawlowicz et al. was not able to inference several component from a single component (e.g. P1 and S1 both from K1); in situations where this type of inferencing was necessary, the Fortran code written by L. Mason was used.

Tidal current can also be analysed using tidal harmonic analysis, though there is an additional degree of freedom (see Appendix D). At Site D, predictions from tidal analysis accounted for 82.1% of the variability in the 89 day current. Figure 2.8 shows the East (u) and North (v) components of the observed and predicted currents at a depth of 20 metres. There is a somewhat surprising inflection point on the incoming tide in the East current component at this site. This feature is observed throughout the measured current profile in water 4 to 34 metres below lowest astronomical tide. The inflection is detected in the analysis and most likely responsible for the relatively large MS4 and M4 constituents (3.9 and 3.6 cm s^{-1} respectively along the major axis of the respective tidal ellipse).

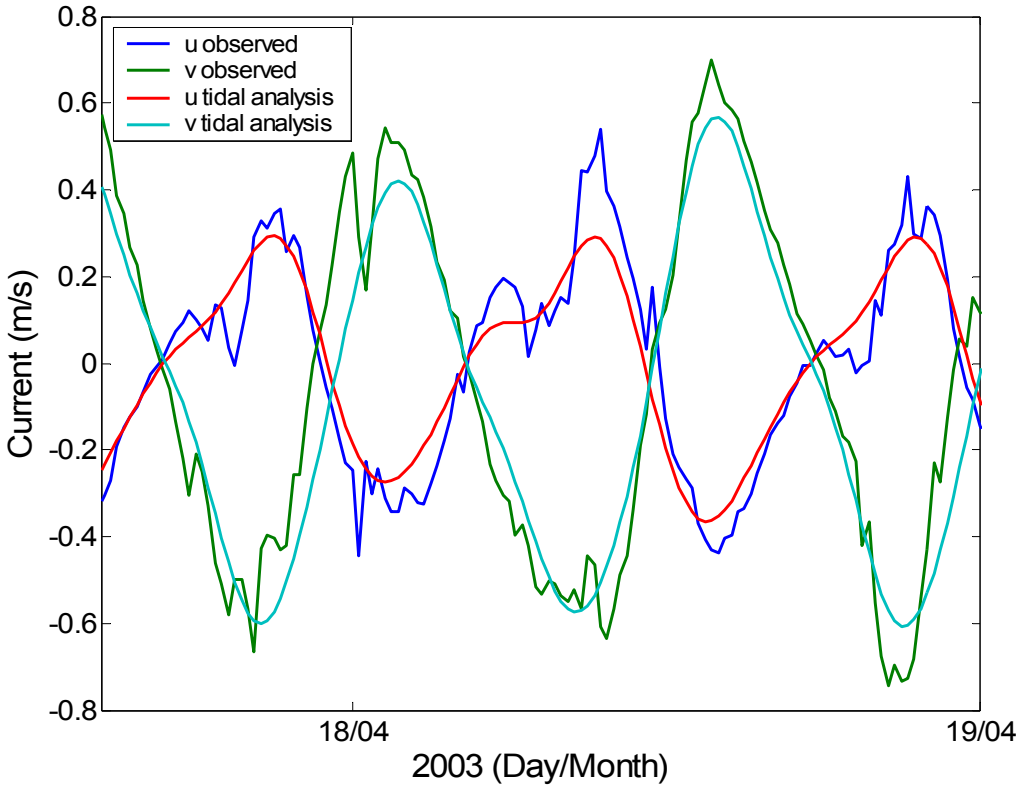

Figure 2.8 The eastward (u) and northward (v) components of observed current are compared to those predicted by tidal analysis.

By being in a channel, the currents at Site D are stronger and easier to detect than the currents in the surrounding areas. In the lagoon, only 54.3% of the variability could be explained by tidal predictions for the 89 day current at Site F. It has long been established that predicting currents is in general much more difficult than predicting sea-level (Godin, 1983) and this lower predictive capability is not surprising.

North Scott tidal asymmetry and stratification

Inside the southern channel of North Scott (Site M), the spring tides are asymmetric. Tidal analysis reveals that there is a major contribution from the MS4 and M4 constituents (13 cm and 11 cm respectively). These constituents are generally only significant in shallow water flow. While the tidal signature in North Scott is quite irregular, the tidal signature during both neap tides and high tides looks normal. When compared to the sea-level outside of North Scott, it becomes apparent that irregularities develop whenever the sea-level drops below 50 cm (Figure 2.9).

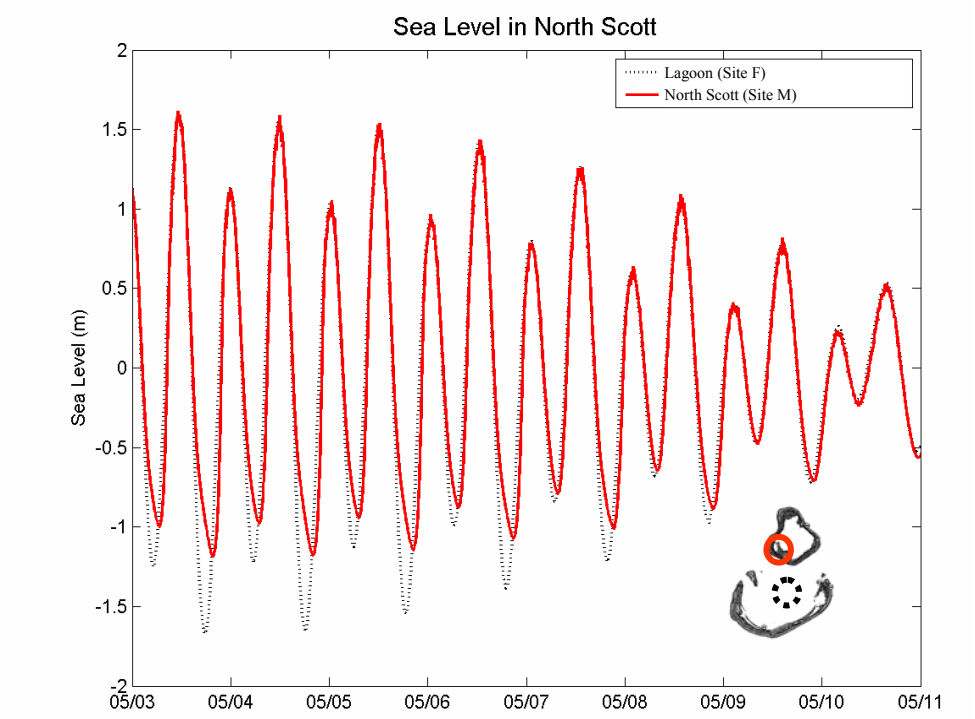

Figure 2.9 Eight days of seal levels at Site M (solid red line) are compared with sea levels in the main lagoon (dotted black line). The difference in heights illustrates the ponding effect observed in North Scott.

A theory for the tidal signature is that water can travel over the reef flat whenever the water height is above 50 cm below the mean sea-level. When the water drops below this 50 cm point, the water can only drain through the two channels that lead into North Scott. The water in North Scott can not escape fast enough through the channels to keep up with the surrounding falling water. As the water in North Scott continues to ebb, the surrounding water begins to flood. The result is a ponding effect in North Scott.

In addition to the ponding, there is an unusual temperature structure at this site. The noteworthy observation is that the two loggers (4 metres apart vertically) register the same temperature from the ebb of the higher tide to the ebb of the lower tide, and then measure significantly different temperatures from the ebb of the lower tide until to the ebb of the higher tide (Figure 2.10). This occurs only during spring tides and is phase-locked to the tide rather than the time of day. A possible explanation for these events has yet to be established.

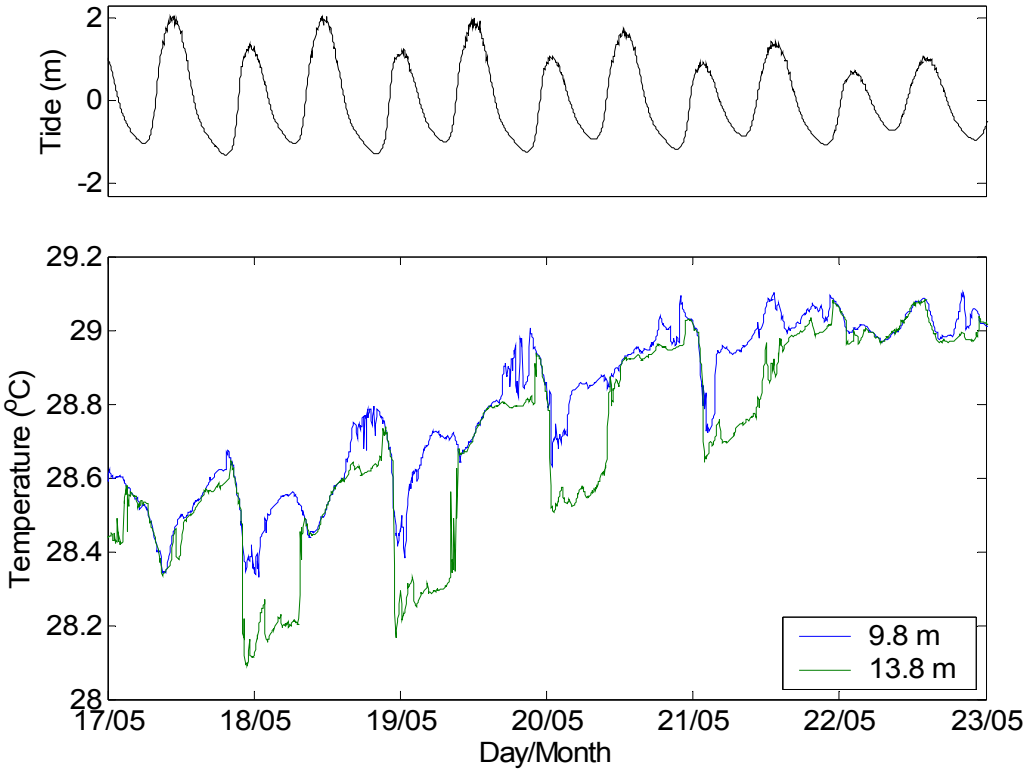

Figure 2.10 Temperature at two depths at Site M during one week of spring tides. Unusual drops in temperature are observed.

Temperature Inversion

Another unusual feature in the data is the development of an inverse temperature profile. In mid-June, temperatures on the surface of the lagoon were cooler than temperatures near the bottom. This condition is considered unusual since the cooler water would be expected to be denser and thus sink. Density depends on temperature, salinity, and depth; in this case a CTD cast shows that the temperature inversion is supported by a salinity gradient (Figure 2.11). A relatively sharp salinity gradient, known as a halocline, is present between 30 and 40 m. The word relatively is used here because the difference in salinity is only 0.2 psu. However this difference is enough to support a 0.2 degree Celsius temperature inversion. The development of the inversion can be seen through temperature and salinity time-series (Figure 2.12). The salinity (taken at 40 metres) drops suddenly a couple days before the inverse profile develops.

One question that arises is whether the drop in salinity could be caused by rain. The theory would be that the rain would add fresh water to the top layer of the water column. This freshwater would be mixed down by the same processes which mix the

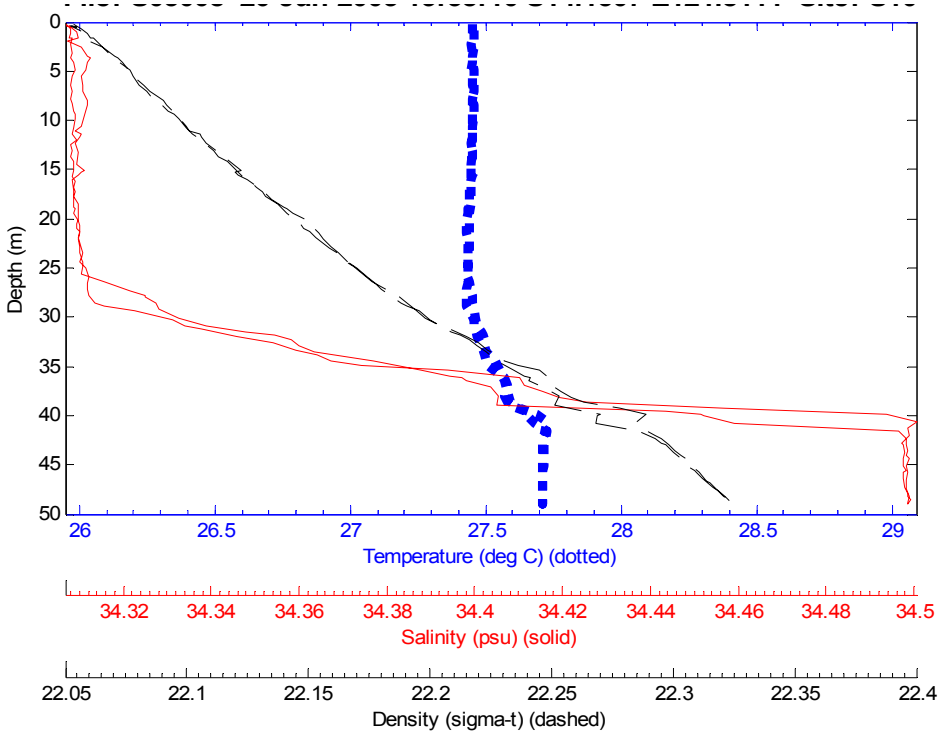

Figure 2.11 An inverse temperature profile (colder water above warmer water) is stabilized by a sharp change in salinity (halocline). Measurements were taken on the 20th of June 2004. Note the units of density are presented in sigma-t which is defined as the density in $kg/m^3 - 1000$.

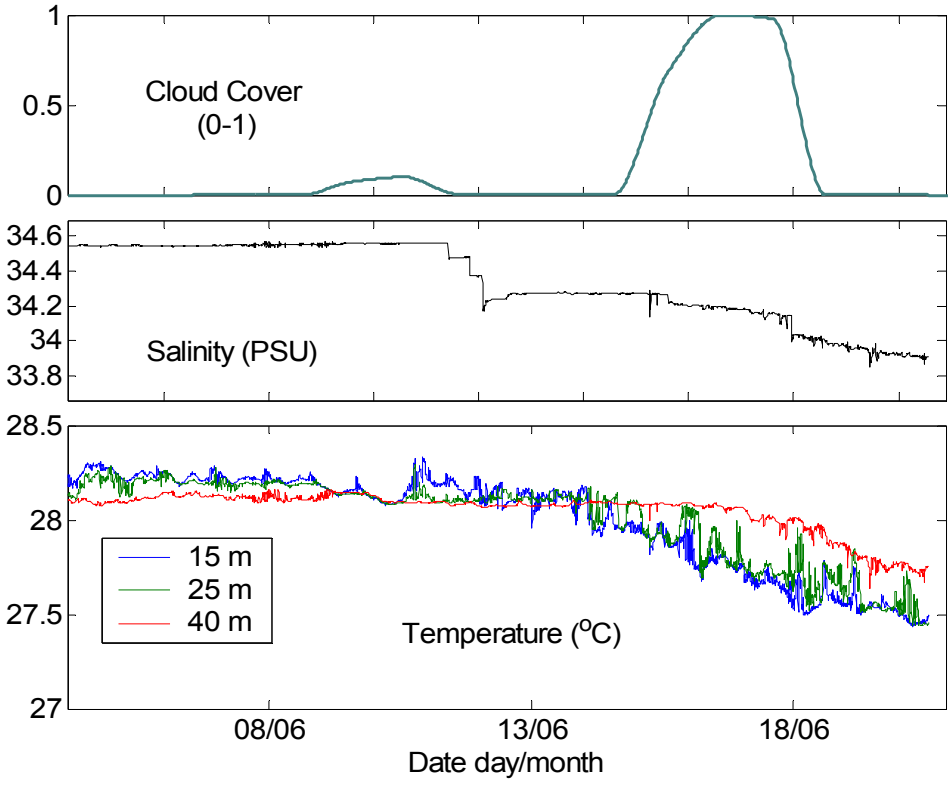

Figure 2.12 Temperature, salinity, and cloud cover time-series leading to the development of an inverse profile. Cloud cover ranges from 0 (no clouds) to 1 (complete cloud cover).

heat. If the drop of the halocline was accompanied by surface cooling, the two would act together to create a stable inverse temperature profile. A quick calculation shows that a drop of 0.2 psu in 30 metres of 34.5 psu water would require 175 mm of fresh water. 175 mm of rain is possible, though a little unlikely in northwest Australia in June. Since rainfall generally coincides with cloudy weather, it is worth noting that there is a heavily clouded period during the development of the temperature inversion (Figure 2.12). However this period falls after the salinity drops suggesting that the cloud cover is more likely responsible for the drop in temperature than the drop in salinity. The only other explanation for the development of the halocline would be through the advection of another water mass into the region.

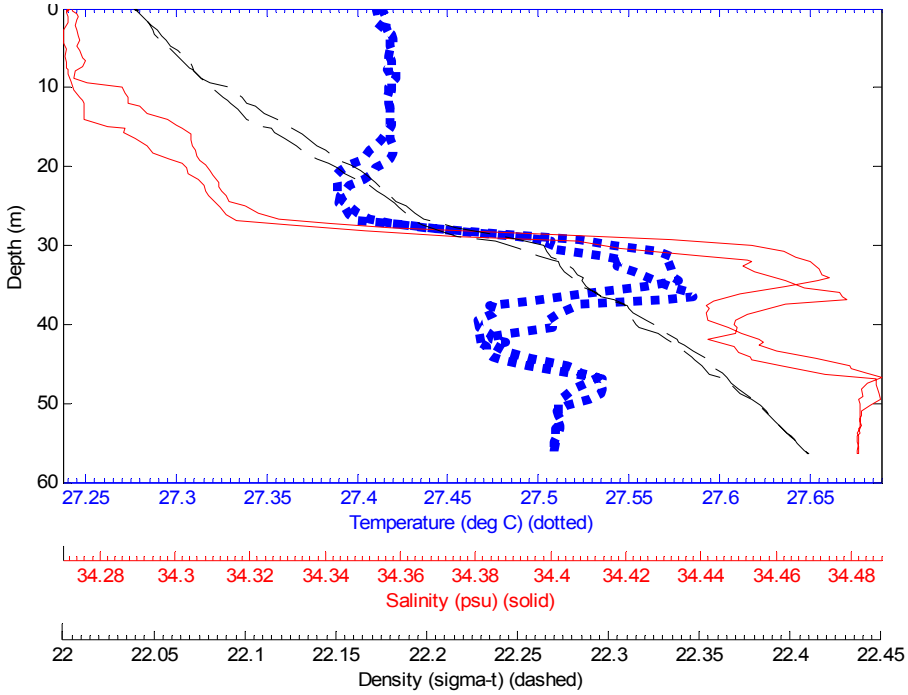

Figure 2.13 Irregular (non-monotonic) temperature and salinity profiles were observed near Site F in June. The temperature and salinity complemented each other to produce a stable density profile.

The temperature and salinity profile near Site F provides additional evidence of advection. In this profile a highly irregular (non-monotonic) temperature profile is supported by an equally irregular salinity profile. Yet both of these irregular profiles complement each other to produce a monotonic, stable density profile (Figure 2.13). While the author has no explanation on how this profile developed, it is believed that the only way such a profile could develop is through the advection of multiple water masses at differing depths.

Evidence of Benthic Advection in Lagoon

There is evidence that benthic advection can occur within the lagoon. At Site F, the temperature logger nearest the bottom (52 metres in 55 metres depth) showed that the temperature dropped to 27.5°C at the end of March (Figure 2.14). The temperature at 52 metres depth warmed back towards its initial temperature over the following week. Surprisingly the loggers at 30 and 32 metres showed no sign of cooling. Additionally, a CTD cast taken on site a few weeks earlier shows that the coolest water available was 28.2°C (Figure 2.15). This means the 27.5°C water could not have been mixed up, but rather must have come from another area.

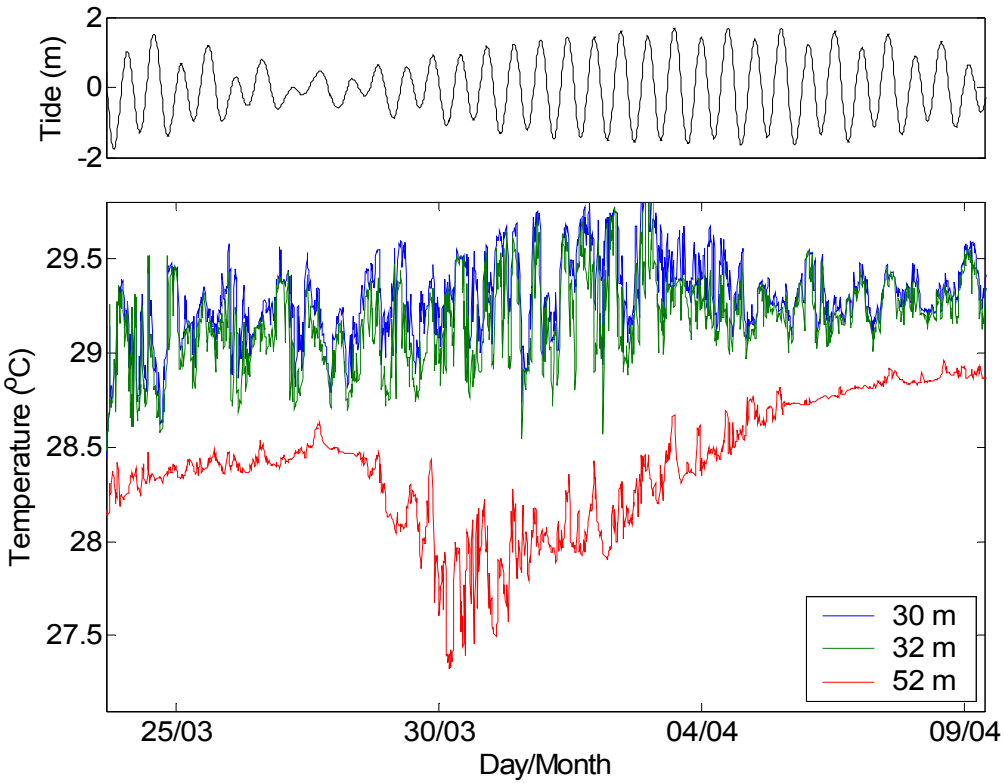

Figure 2.14 Temperatures at Site D at varying depths. The water temperature at 52 metres below sea level decreases to 27.5 ° while the temperatures in the upper layers remain relatively constant.

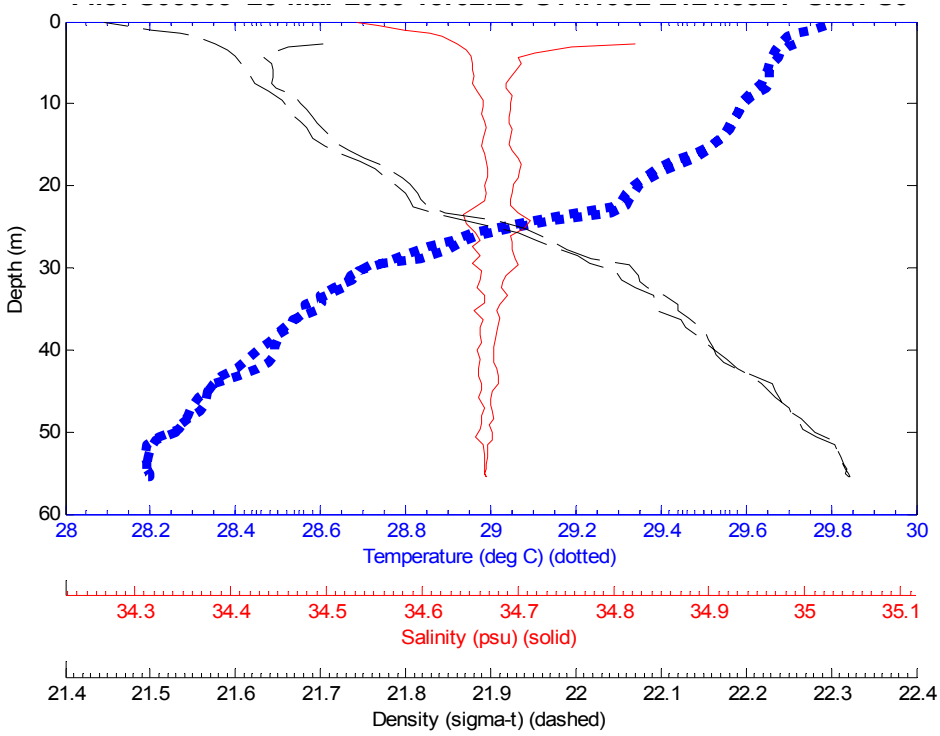

Figure 2.15 Temperature, salinity, and density profiles at Site F during mooring deployment (23-Mar-04). The minimum temperature in the water column at this point is 28.2°.

Tidal Intrusions

During spring tides, many of the temperature loggers near the edges of the reef measured cooling periods that corresponded with spring tides. The water at these sites cooled off up to 5 degrees Celsius during the flood tides and returned to their baseline temperature during the ebb tides (Figure 2.16).

This sudden temperature change suggests that deep water from outside the reef is being brought up into the channels during these peak tidal-current conditions. The temperature loggers at Site D (located in the channel between West Hook and Sandy Cay) recorded the largest tidal cooling. Figure 2.17 shows the temperature at this site for three depths during one week. Interestingly, the temperatures at all three depths measured experience this dramatic temperature decrease; however, there are instances where the two deeper loggers undergo a temperature drop while the shallower one does not. This indicates that the flow through the channel is in some cases stratified and that the cooler water may not reach the surface.

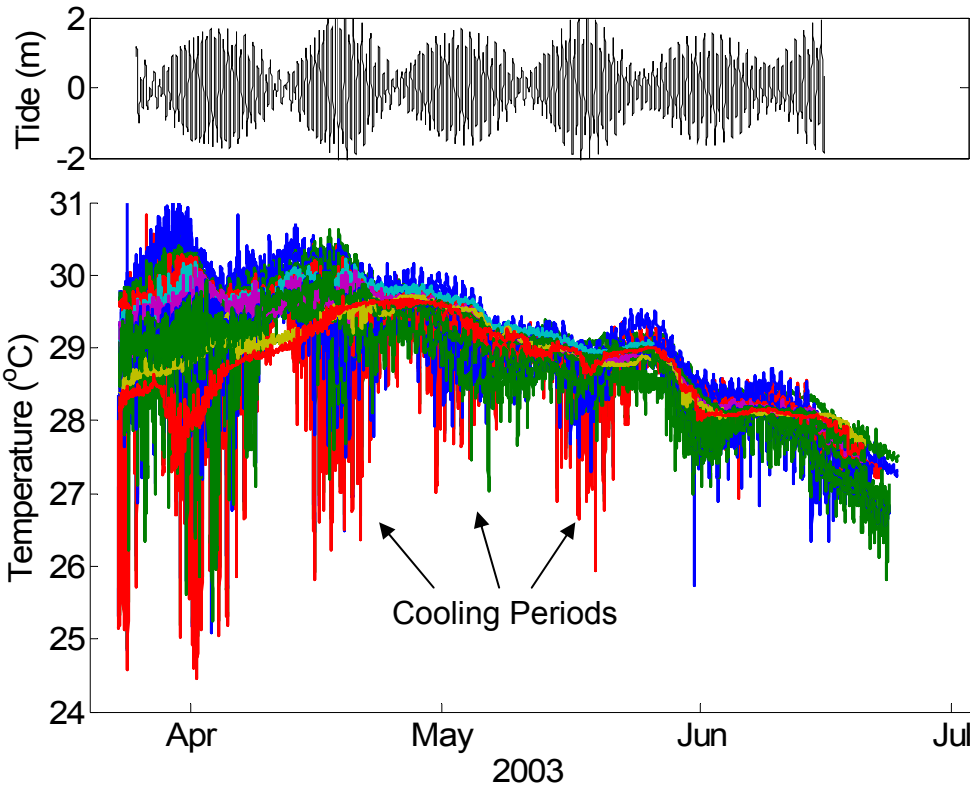

Figure 2.16 All of the temperature records plotted together (each logger corresponds to a different colour) demonstrate that there are distinct cooling periods that correlate with spring tides.

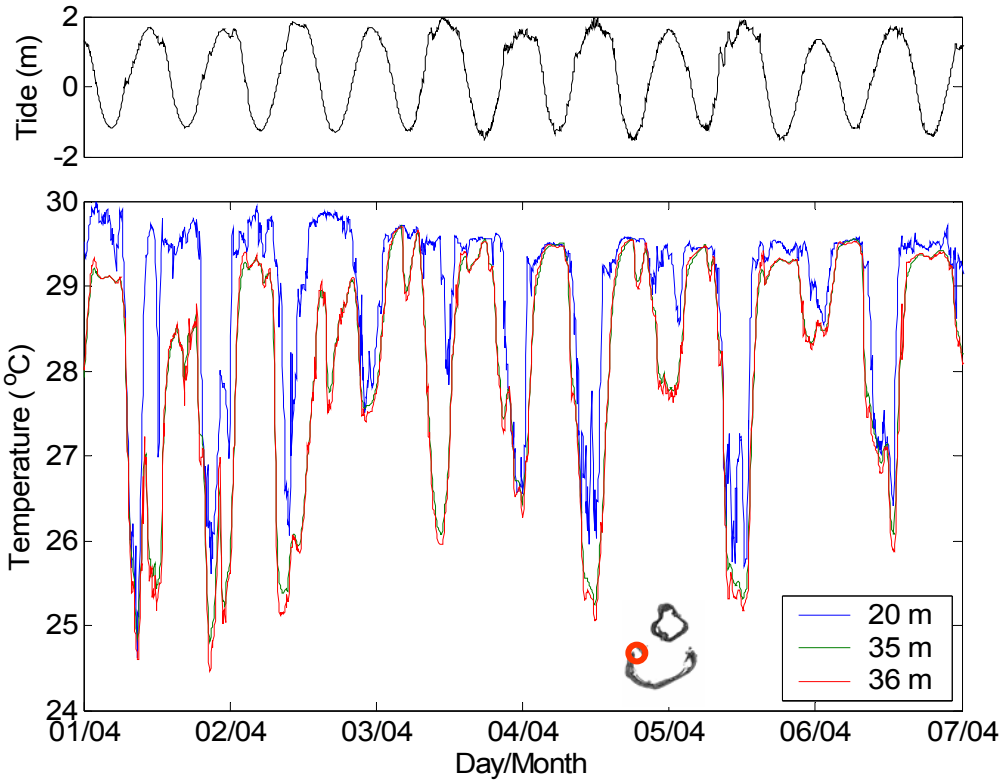

Figure 2.17 The temperatures at Site D during one week of spring tides shows that cooling occurs at varying depths (20, 35, and 36 m) during the incoming tide.

The temperature logger located at Site B gives further insight to the vertical temperature structure in deep, fast moving water. One of the buoy packs on this mooring was destroyed and the remaining floatation was insufficient to prevent the temperature logger from swinging back and forth with the current. As the temperature logger swung it dropped in depth allowing temperature to be measured as function of both time and depth (Figure 2.18). The logger measured temperatures below 10 degrees Celsius. The CTD cast taken at this site in March 2003 showed that 10 degree water was present at bottom of the channel separating North and South Scott, 300 metres deep. The depth sensor on the swinging instrument was limited to measurements of up to 160 metres and impressively continued to function after reaching far greater depths. The temperature and depth plots can be combined to form a temperature profile plot where depth is on the *y*-axis, time is on the *x*-axis, and temperature varies with colour (Figure 2.19).

Other temperature loggers around Scott Reef measured cooler water on flood tides than on ebb tides. When temperatures during the ebb and flood tides are separated for the swinging logger, it becomes apparent that warmer water penetrates deeper into the water column during spring ebb tides, and cooler water penetrates into the shallower water during the spring flood tides (Figure 2.20a and 2.20b). A thermocline is somewhat visible in Figures 2.20a and 2.20b as the transition of the temperature from red to blue. The thermocline rises up to 80 metres below the surface during spring flood tides and falls as low 140 metres below the surface during ebb tides. The 60-metre fluctuations may be due to internal tides, as internal tides have been detected on the Australian North West shelf (Holloway, 1996). It is difficult to assess the extent that cooler surface waters observed around deeper water during Spring tide floods may be due to internal tides as opposed to tidal mixing.

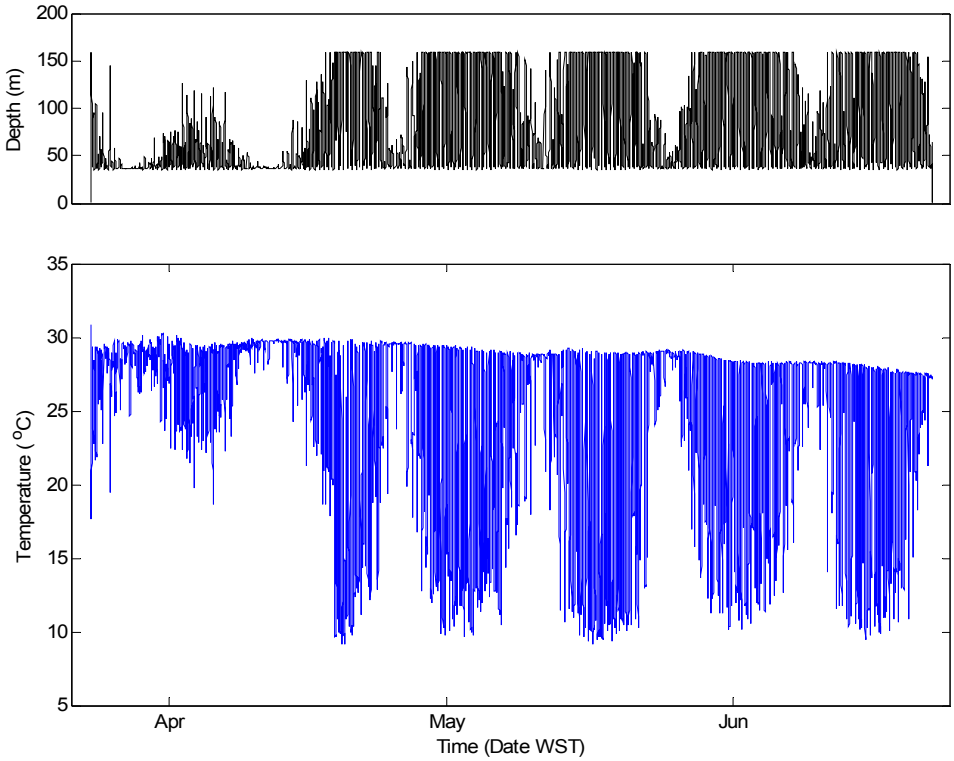

Figure 2.18 The temperature and depth record of a 'swinging' logger at Site B.

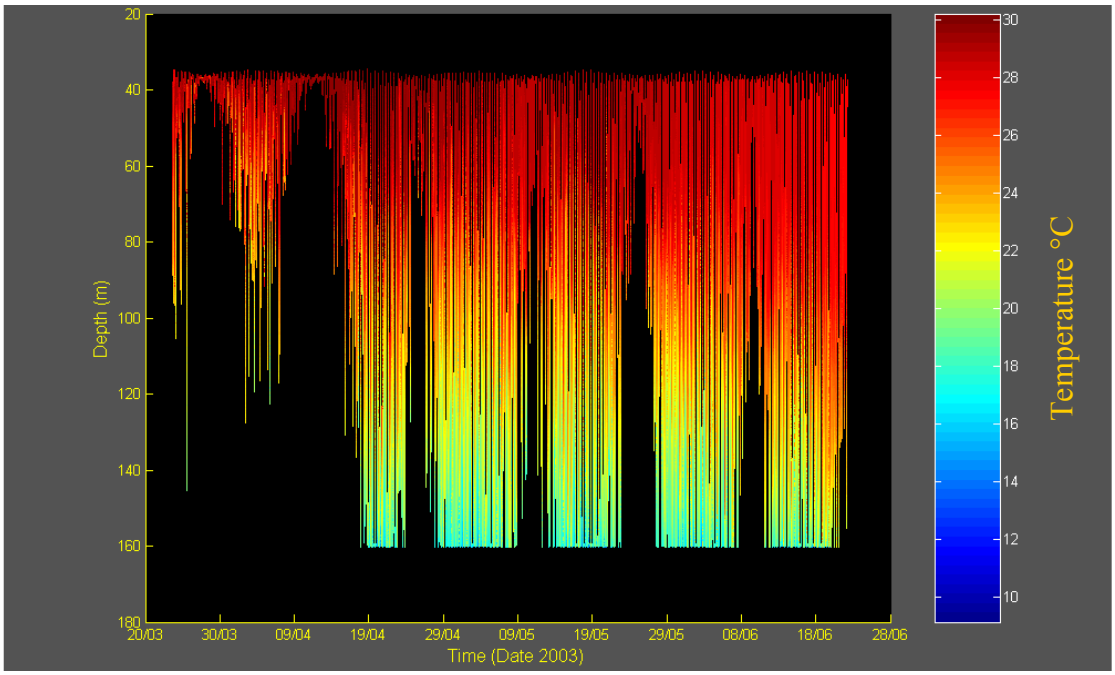

Figure 2.19 The temperature at Site B plotted as a function of depth and time. This reconstruction gives insight on vertical temperature profiles throughout the deployment period.

Flood Tides

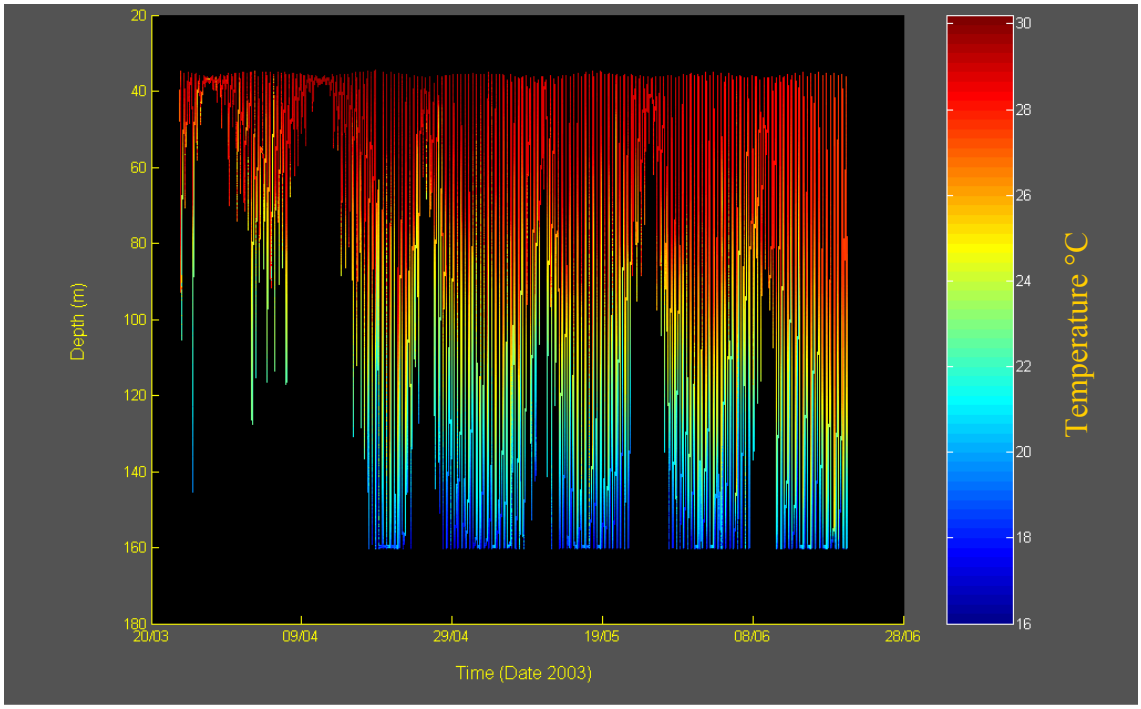

Ebb Tides

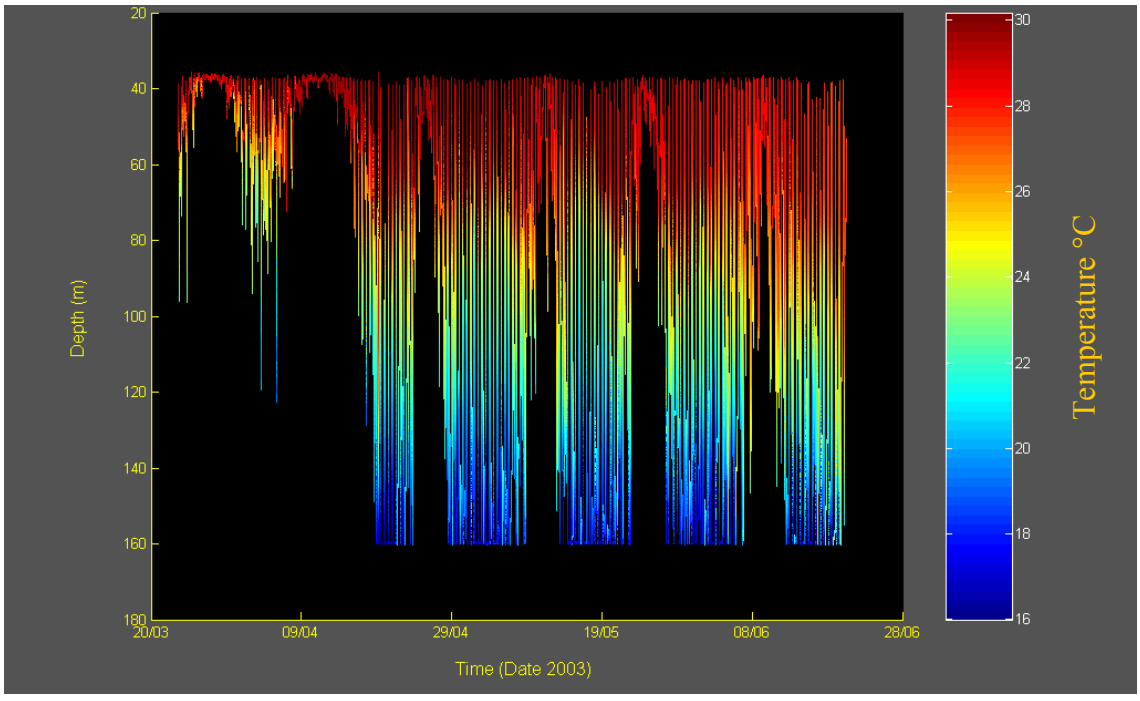

Figure 2.20 a) (top) Temperatures measured during the flood tide at Site B.
b) (bottom) Temperatures measured during the ebb tide at Site B.

Similar thermal features

While several processes have been identified in different parts of Scott Reef leading to differing thermal structures, overall all the temperature data share a common trend (illustrated by the black line in Figure 2.21). The temperatures fluctuate in April before steadily cooling into winter. It is unclear from this data set whether the similar temperature features are due to the heat balance at Scott Reef or due to advection of other water masses. The role of advection in establishing water temperatures can be evaluated by comparing the data to the results of a one-dimensional thermodynamic, water column model driven by air-sea fluxes. If the model can not identify major features in the temperature structure, then there is evidence that advection has a significant role and can not be neglected.

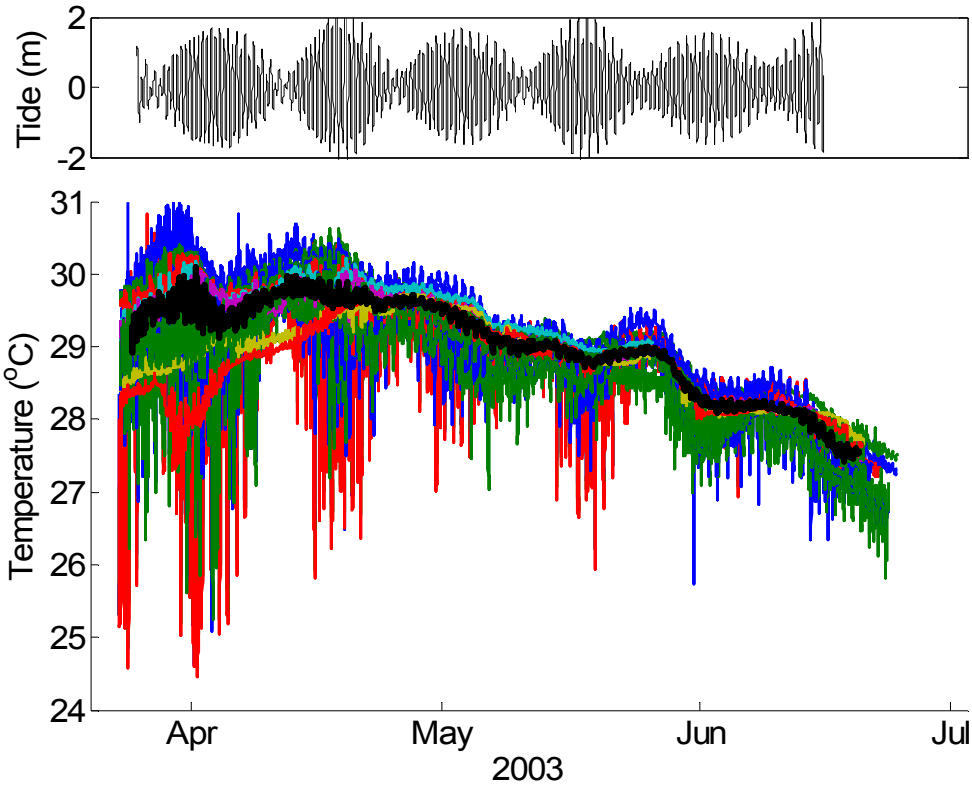

Figure 2.21 All of the temperatures measured at Scott Reef in 2003 (each logger corresponds to a different colour) share a common trend (illustrated with black line).

Summary and Concluding Remarks

The field data serves as a foundation to the other parts of this thesis and will often be referenced. It was observed that the water flow around Scott Reef is predominantly tidal, although there is evidence that slow net currents prevail throughout the region (Figures 2.6 and 2.7). There are a few instances where the field results indicated the presences of horizontal advection within the lagoon, namely the temperature inversions (Figures 2.11 and 2.13) and the period of benthic cooling at Site F (Figure 2.14). These cases of what appears to be advection in the lagoon may be linked to the larger net currents. However since the Scott Reef currents are predominantly tidal, numerical models that neglect non-tidal advection should be able to simulate the approximate oceanographic conditions.

The field data also provides insight into some of the parameters needed to model Scott Reef oceanography. For example, the Jerlov water type is a parameter in the water column model described in Chapter 4; the field results indicate that this parameter should be Type II (Figure 2.5). Similarly, the tidal constituents calculated from field observations will be used to calibrate the tidal model in Chapter 5. Once the models are running, the field data is used to verify the results. We will find that the simulations are able to reproduce the magnitude and direction of the observed currents in Figure 2.6, as well as the ponding effect illustrated in Figure 2.9.

Finally, temperature loggers around Scott Reef have indicated that some regions are cooled during strong tides (Figures 2.16–2.20). Corals living near these regions may have a better chance of surviving during a bleaching episode than coral farther away due to this tidal cooling. That said, similar features in the temperature records at different locations (Figure 2.21) are evidence that a first order temperature approximation may be attained by using a spatially invariant numerical model.

Chapter 3 – Heat Transfer at Scott Reef

The first chapter established both that coral bleaching is strongly correlated with unusually-warm water temperatures and that significant coral bleaching occurred at Scott Reef at the beginning of 1998. Therefore it should be of little surprise that water temperatures at Scott Reef were uncharacteristically warm from February to May, 1998 (Figure 3.1).

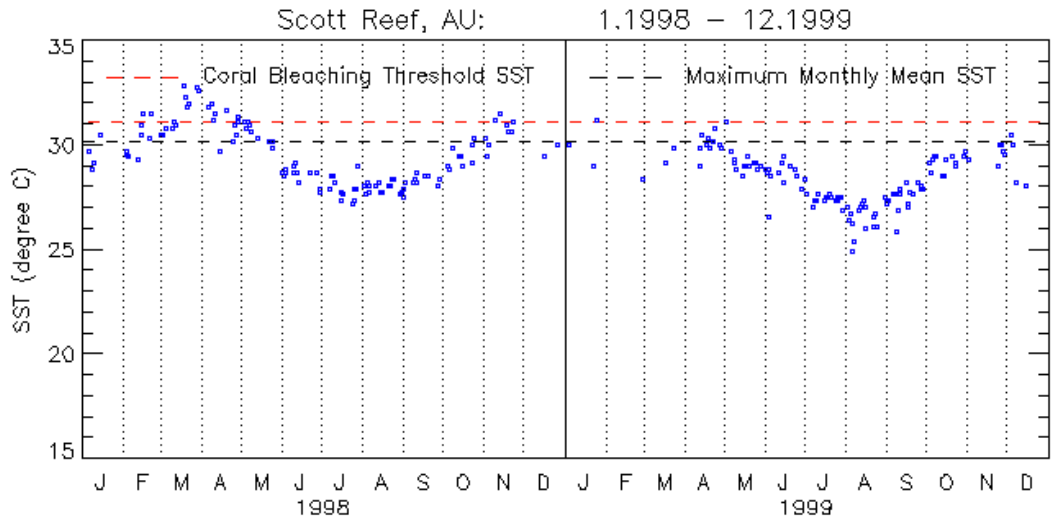

Figure 3.1 Sea Surface Temperature (SST) observed at Scott Reef from the beginning of 1998 to the end of 1999. *Picture courtesy of NOAA.*

Figure 3.1 illustrates that surface water temperatures increased steadily during February and March and then started to decrease in April. As SSTs derived from satellite images are after all only observations, they do not give any insight as to the cause of fluctuations. The goal of this chapter is to investigate how the atmospheric conditions during this period may have led to the elevated temperatures.

Heat Balance

Atmospheric conditions affect the amount of heat transferred through the air-sea interface. Heat passes through the air-sea interface through radiation, conduction, convection, and water-phase transformation. In oceanography, conduction and convection are grouped together to form a sensible heat flux. A latent heat flux is used to denote the heat transfer from a water-phase transformation, such as evaporation.

Finally, radiation is separated into shortwave and longwave components. The net daily fluxes across the air-sea interface are roughly zero; therefore the relationship between the fluxes is often referred to as the heat balance.

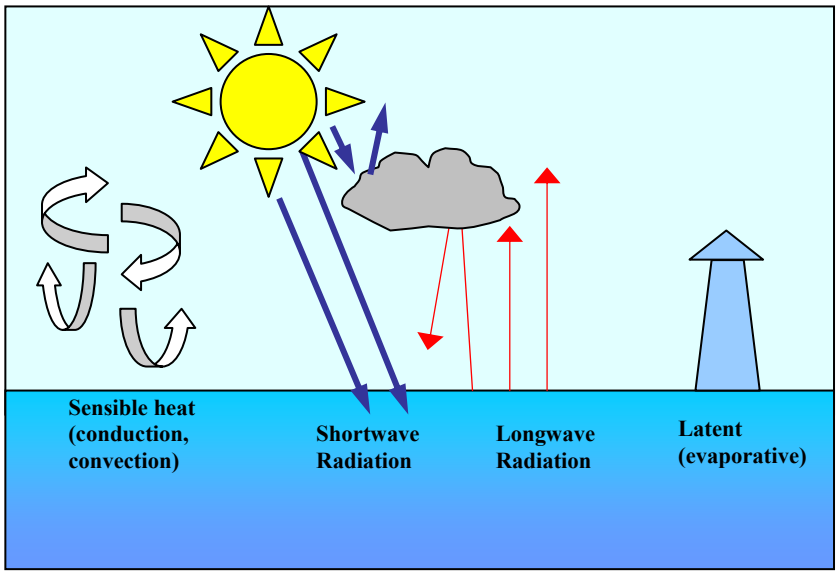

Figure 3.2 The heat balance is maintained by 4 fluxes: the sensible heat flux, the shortwave radiation flux, the longwave radiation flux, and the latent heat flux.

If the air-sea fluxes are not balanced, heat will be transferred across the interface and the surface water temperature will change. An objective of this chapter is to determine if there was a net heat flux into the water column during March 1998 at Scott Reef and if there was a significant change in any of the heat fluxes during this period.

All of the heat fluxes across the air-sea interface depend strongly on atmospheric conditions. For example, cloud cover attenuates shortwave radiation flux entering the water while wind amplifies the latent flux entering the atmosphere. Since none of the fluxes were measured directly at Scott Reef in 1998, they need to be estimated.

Estimating the air-sea interface fluxes from bulk formulas is routine. Standard formulas relate each flux to a set of atmospheric conditions, such as air temperature, sea surface temperature, humidity, atmospheric pressure, wind, and cloud cover. However, a novel aspect of this study is that there are no atmospheric records available at Scott Reef in 1998. Therefore, the meteorological data needed for the bulk formulas had to be estimated as well. A significant part of the research in this thesis involved estimating the heat balance at Scott Reef as well as the uncertainties linked with these estimates.

Methods to Determine Meteorological Conditions

This section outlines how sea surface temperature, cloud cover, solar radiation, air temperature, atmospheric pressure, wind velocity, and humidity were all estimated for Scott Reef during the 1998 bleaching period. In the ideal case, these conditions would be obtained from a nearby weather station. However since 1995, there has been no permanent weather station on Scott Reef. Therefore, it is necessary to extrapolate from nearby weather stations.

Scott Reef is in a data-sparse region; the two nearest stations, located on Browse and Adele Islands, are roughly 200 km away (Figure 3.3). These weather stations only collect air temperature, atmospheric pressure, and the wind speed. The closest weather station to Scott Reef that measured humidity in 1998 is approximately 300 km away on Kuri Bay, and the closest non-coastal humidity measurements were taken on Troughton Island, 400 km east of Scott Reef. Finally the closest station to Scott Reef that is equipped to measure solar radiation is located 450 km due south in Broome, WA.

The distances between Scott Reef and the available observations are large. Therefore it may not be appropriate to use the weather station observations as a proxy for Scott Reef conditions. Several of the following sections describe the steps taken to estimate atmospheric conditions at Scott Reef from the distant observations. Only two meteorological conditions were observed directly at Scott Reef. These are the sea surface temperature and cloud cover, both of which can be extracted from satellite imagery. The next section briefly describes this process.

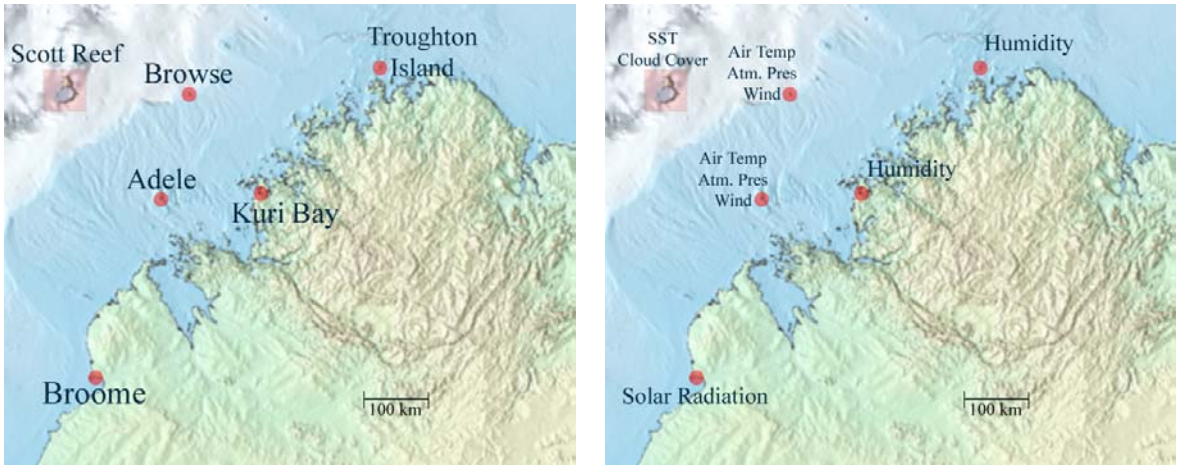

Figure 3.3 a) (left) The locations and names of the meteorological sites used in this study.
b) (right) The types of observations recorded at each site.

Satellite Images

Sea surface temperature and cloud cover are derived from one square kilometre AVHRR (Advanced Very High Resolution Radiometer) satellite imagery sourced by WASTAC (Western Australian Satellite Technology and Application Consortium) and processed by AIMS. For each pass, images of various infrared wavelengths are collected. Using conventional algorithms, cloud cover and sea-surface temperature are calculated from the infrared images.

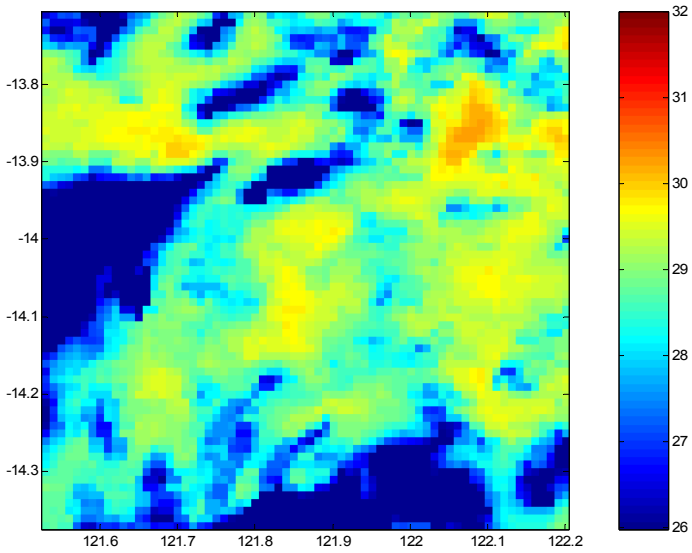

Figure 3.4 SST image around Scott Reef (colour bar is in°C). In order to interpret this image, the location of cloud cover and land mass need to be identified.

The SST image in Figure 3.4 is almost impossible to interpret as there is no information about the location of Scott Reef or of cloud cover. The precise location of Scott Reef can be identified from the visible wavelengths of the satellite images (Figure 3.5a). Relying on latitude and longitude alone to locate the reef is tedious since the satellite images use a different projection to the oceanographic maps (in this thesis, coordinates are specified in WGS-84). Figure 3.5a demonstrates that the outline of Scott Reef in Figure 3.5b (and in future figures) is correctly positioned. Using the cloud detection algorithms, a cloud mask is obtained and applied to the SST image (Figure 3.5b). From the modified image, one can reduce the SST and cloud cover to single values that are representative for those conditions during the satellite pass. The representative sea surface temperature and cloud cover can then be used in the bulk formulas needed to calculate the heat flux.

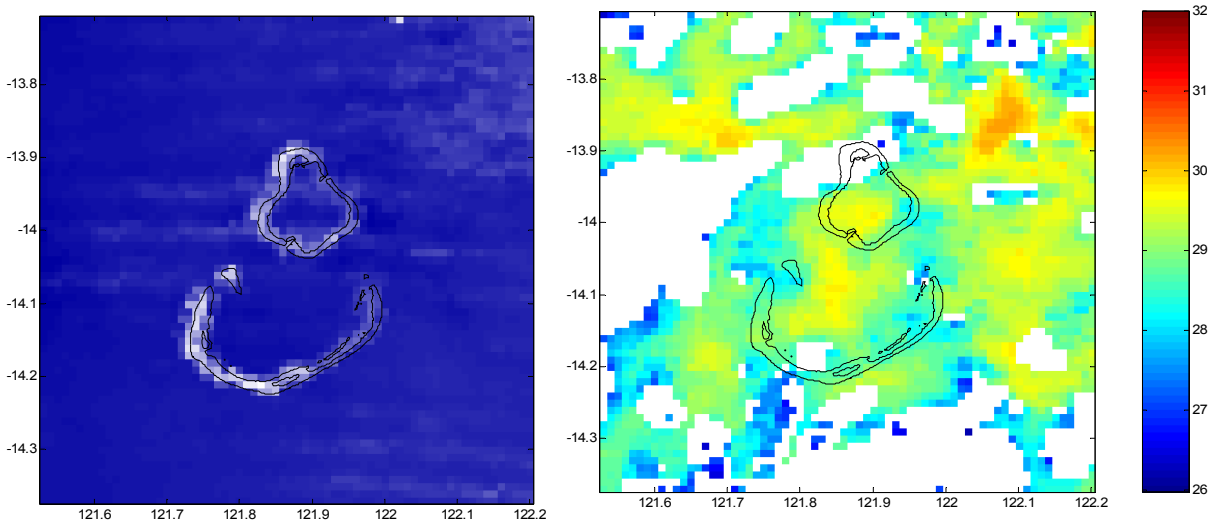

Figure 3.5 a) (left) The visible band from the satellite image (taken on a clear day) demonstrates that our outline of Scott Reef is correctly positioned. **b) (right)** This is the same image in Figure 3.4, but now with cloud cover (white pixels) and Scott Reef outline included.

SST time series

The magnitude and direction of heat fluxes depend on sea surface temperature. One approach to obtain a representative sea surface temperature is to average all the cloud-free temperature measurements during that particular satellite pass. By combining all the satellite passes, an SST time series is formed. The disadvantage of this approach is that lightly clouded areas may evade detection and lower the average temperature. Figure 3.5b shows patches of very cool water (blue pixels) near and within detected clouds (white pixels). Because cloud cover only leads to cooler detected temperatures, it is common practice to take the maximum temperature within a region as the representative SST. The likelihood of the maximum temperature being biased by cloud cover increases with cloudiness. Therefore, I have chosen not to include any SST measurements that occurred when 90% of the region was covered by clouds.

Maximum night-time sea surface temperature is measured by NOAA at Scott Reef. The NOAA night-time SST and the AIMS-processed daytime SST are plotted in Figure 3.6 for beginning months in the first half of 1998 and 2003. The 1998 data sets are sparser than those of 2003 because of the unusually high cloud cover over Scott Reef in 1998.

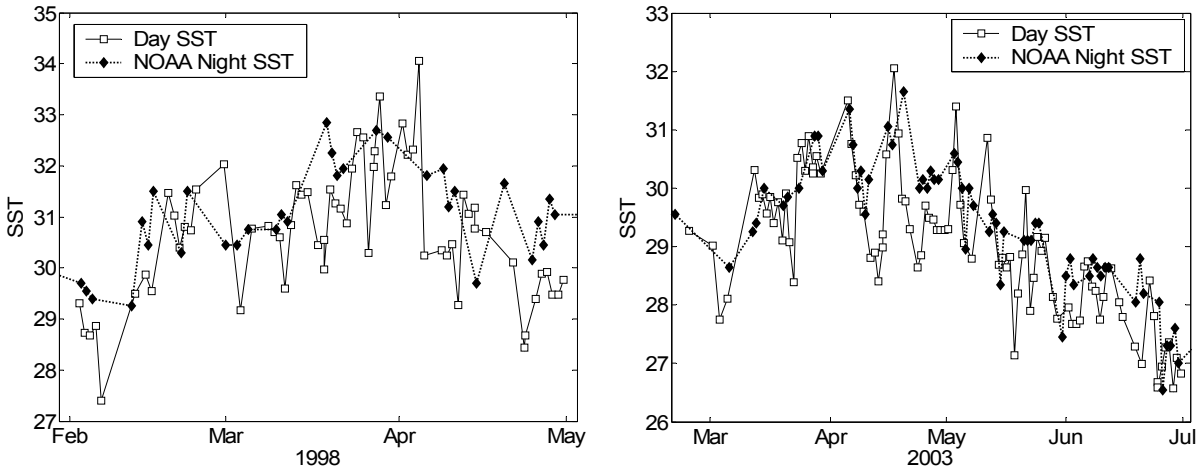

Figure 3.6 Sea Surface Temperature (SST) observed at Scott Reef from February to May 1998 and from March to July 2003 (note the different temperature axes). The white squares mark the temperatures observed during the day using analysis techniques described in this chapter. The night SST data were collected and processed by NOAA.

The plots show that the day and night SSTs are in agreement; however, it should also be noted that the variability within the data sets is quite high. This variability is a problem to model calculations that rely solely on the SST measurements.

Cloud Cover

Cloud cover directly affects the heat budget in two ways; it attenuates the downward shortwave radiation and reflects the upward longwave radiation back into the water column. No cloud cover observations were taken at Scott Reef, or at any weather station nearby. However as mentioned earlier, clouds can be detected in satellite imagery (Figure 3.5b). The cloud-cover fraction (0 to 1) over Scott Reef was determined by calculating the ratio of the number of square kilometre pixels covered by cloud in a 90 by 90 kilometre area, to the total number of pixels in that area.

A satellite image is taken in the form of a swath; when these swaths are geo-referenced, any area beyond the swath is wrongly interpreted as cloud by the cloud mask. Therefore special care was taken to filter out any images in which the Scott Reef region was not completely observed.

Cloud cover was only detected when satellite images were taken (once a day); therefore to get half-hour cloud fraction values the results were interpolated using the "pchip" method. The pchip method was chosen over linear and spline interpolation techniques because of the large fluctuations in the data; linear interpolation was not smooth, and spline interpolation produced cloud cover fractions outside the zero to one range.

Shortwave Radiation

Solar exposure (J m^{-2}) is collected at Broome every half-hour and is available during both the 1998 bleaching period and the 2003 field campaign (Chapter 2). The average radiation for each sample period (W m^{-2}) is obtained by simply dividing the measured solar exposure by the exposure time.

Broome is close enough to Scott Reef that the difference in latitude will have a minor effect on the short wave flux entering the atmosphere. However, differences in cloud cover between Broome and Scott can lead to large flux differences between the sites at the sea surface. This section outlines a technique developed to estimate the half-hour shortwave radiation at Scott Reef. This estimation combines the Scott Reef cloud fraction with the shortwave radiation measurements from Broome.

The theoretical daily-averaged shortwave radiation in the absence of clouds can be calculated using a bulk formula developed by Seckel and Beaudry (described in Reed, 1977),

$$Q_0 = A_0 + A_1 \cos\phi + B_1 \sin\phi + A_2 \cos 2\phi + B_2 \sin 2\phi \qquad (3.1)$$

Here $\phi = (t-21)\left({}^{360}\!/_{365}\right)$ where t is the time (day) of the year. For latitudes from 20S to 40N, Seckel and Beaudry found that the coefficients in 3.1 are the following functions of latitude, L.

$$\begin{aligned} A_0 &= -15.82 + 326.87\cos L \\ A_1 &= 9.63 + 192.44\cos(L+90) \\ B_1 &= -3.27 + 108.70\sin L \\ A_2 &= -0.64 + 7.80\sin\left[2(L-45)\right] \\ B_2 &= -0.50 + 14.42\cos\left[2(L-5)\right] \end{aligned} \qquad (3.2)$$

Reed (1977) demonstrated that the daily-averaged, cloud-attenuated shortwave radiation, Q_s, can be related to the theoretical cloud-free radiation Q_o, (calculated in 3.1), the daily averaged cloud cover, C, (measured in tenths) and the noon solar altitude, α, through the following bulk formula.

$$Q_s / Q_0 = 1 - 0.62C + 0.0019\alpha \tag{3.3}$$

Quick inspection of Equation 3.3 shows that certain cloud fraction values, such as C = 0, will predict a shortwave radiation, Q_s, greater than the corresponding cloud-free radiation. Therefore in cases when $Q_s / Q_0 > 1$ (which occurs when C is less than approximately 0.3), the cloud-free shortwave radiation value is used.

Thus far the technique to estimate the shortwave radiation reaching the sea surface is completely independent of the measurements taken at Broome. Therefore if this technique is applied to Broome instead of Scott, the predicted values can be compared to the Broome observations. Figure 3.7 compares both the observed and estimated daily average solar radiation for March to June 2003.

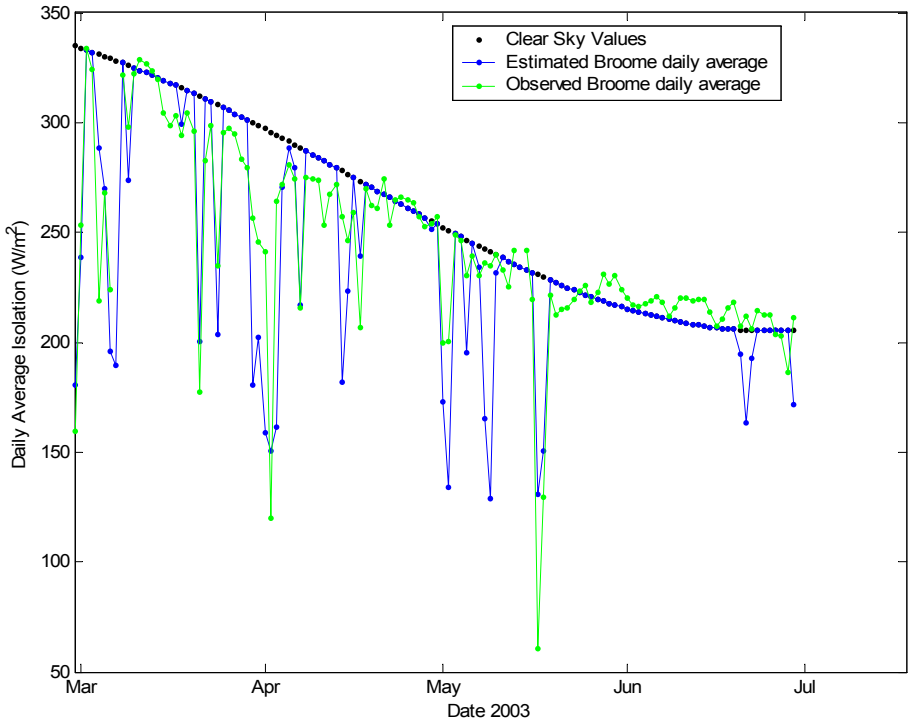

Figure 3.7 Daily average shortwave radiation at Broome is estimated from satellite-derived cloud cover data from March to July 2003 (blue). This estimation is compared to the radiation measured at Broome weather station during those months (green).

Figure 3.7 illustrates that the predicted solar radiation matches the observed values fairly well in low cloud conditions. During cloudy conditions, both the estimated and observed values show attenuation; however the difference between the attenuation of the two signals can be quite large. The reason for the difference in attenuation is most likely a consequence of the cloud cover being characterized by a cloud fraction rather than an optical thickness. A cloud fraction describes how much of the sky is covered by clouds but does offer insight into the thickness or altitude of the measured cloud cover. While an optical thickness parameter adds this useful information, the additional information is eventually lost as bulk formulas tend to be restricted to only incorporating cloud data through the cloud fraction.

When the shortwave radiation is estimated for Scott Reef using satellite-derived cloud fraction data, it is apparent that there is a marked difference from the measurements collected at Broome (Figure 3.8). First, the cloud-free shortwave radiation daily

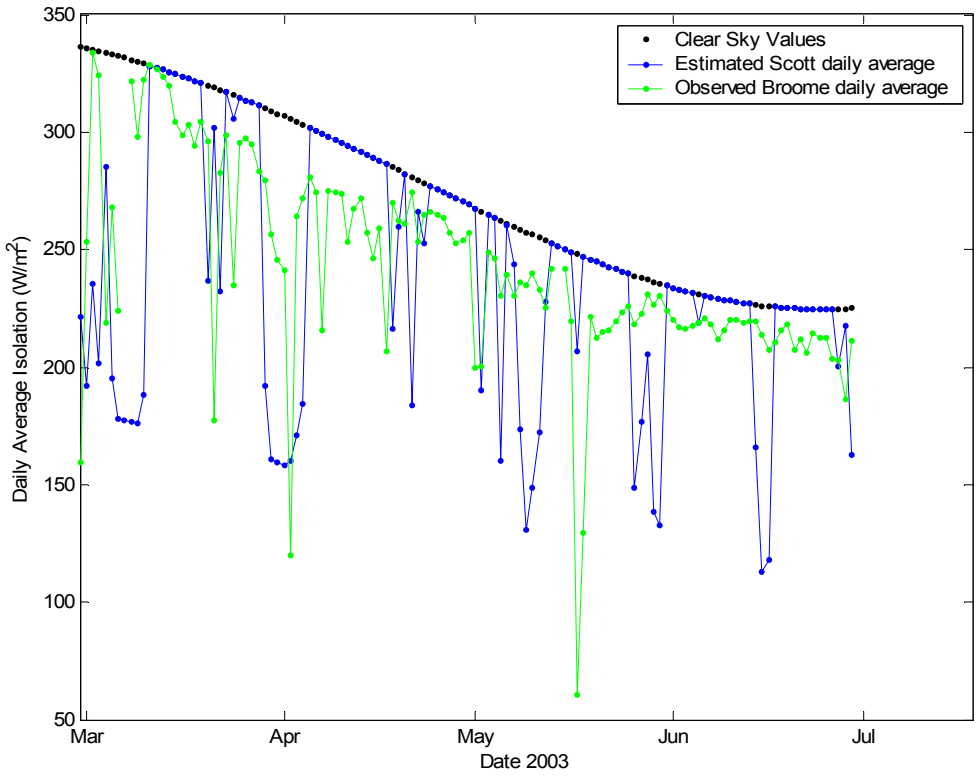

Figure 3.8 Daily average shortwave radiation at Scott Reef is estimated from satellite-derived cloud cover data from March to July 2003 (blue). As expected, this estimation is less correlated with the radiation measured at Broome (green) than the estimation in Figure 3.7.

average is slightly higher for Scott than it is for Broome. This increase is expected, due to the difference in latitude between the two sites. Additionally, the observed Broome average radiation correlates better with the estimated Broome radiation than with the estimated Scott radiation. While it may come as no surprise that Broome observations correlate better with Broome than with Scott predictions, the degree of difference in the correlations illustrates that the difference in cloud fraction between the sites is significant and should be incorporated in radiation estimates.

The bulk formulas used to estimate the shortwave radiation can at best produce daily averages. Unfortunately, daily averages smooth out the characteristic diurnal component of the shortwave radiation signal. In this study, the diurnal aspect of the radiation flux needs to be considered as it may enhance surface mixing.

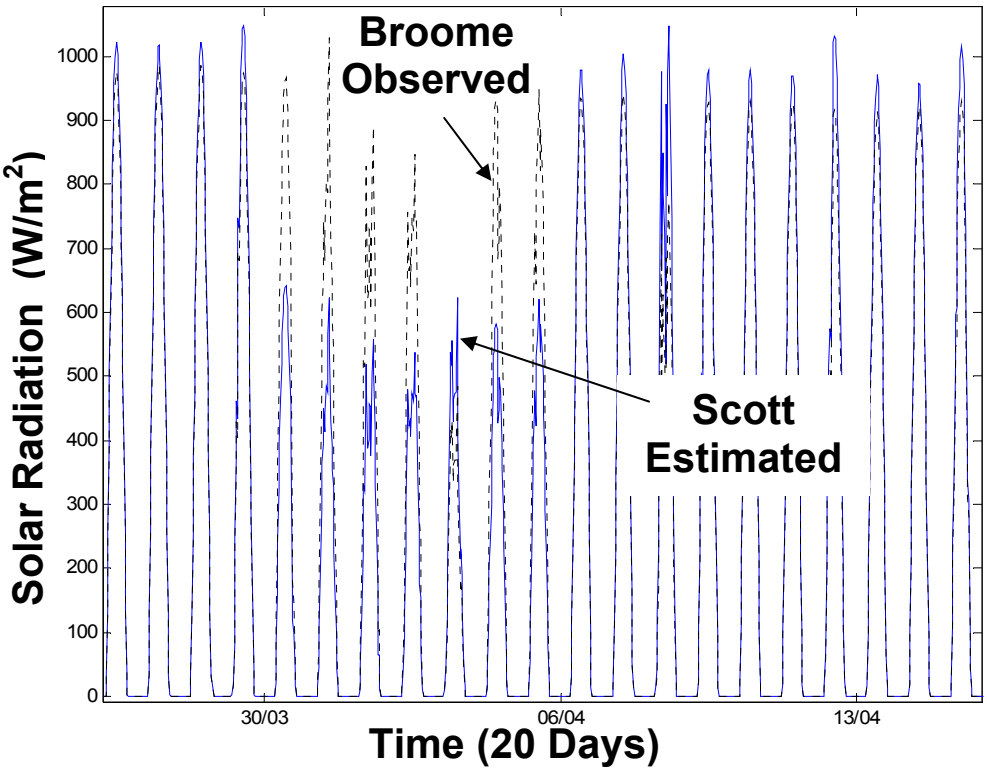

Figure 3.9 The radiation is estimated at Scott Reef (solid line) by amplifying or attenuating the measurements directly observed at Broom (dotted line). The average daily radiation from this estimation is the same as that calculated for Scott Reef in Equation 3.3.

Since shortwave radiation was measured at half-hour intervals at Broome, the Broome observations can be used to estimate the diurnal radiation signal at Scott Reef. Scott Reef and Broome are located at roughly the same latitude, so that one would expect the

shortwave radiation would exhibit roughly the same shape and phase for the two sites. The largest difference between the two signals will occur when the cloud cover over the two regions is different. The Broome shortwave radiation measurements can be amplified or attenuated during each day so that estimated daily average radiation is equal to that of Scott Reef, derived in Equation 3.3.

Figure 3.9 shows the solar radiation in a three week period in 2003 measured at Broome (dotted black line) and estimated at Scott Reef (solid blue line). The half-hourly estimated signal captures the diurnal envelope characteristic of solar radiation while maintaining the appropriate daily energy estimated from latitude and satellite-derived cloud fraction data.

Uncertainty in Cloud Fraction & Shortwave Radiation

Estimating the uncertainty in Scott Reef cloud fraction data is not immediately intuitive. Error will result from detecting cloud where there was none and vice versa. Even if the cloud fraction was detected perfectly, it was only collected once daily; as clouds can develop and pass through the region at hourly time-scales, there is a sampling error associated with only using a daily snapshot. Finally, with this technique a thin, high cirrus cloud has the same effect as a low, optically-thick stratonimbus cloud. While these two types of clouds will have a significantly different effect on the heat-budget, the bulk formula used to predict heat fluxes do not account for cloud type. Therefore when cloud is used in bulk formulas, cloud height and optical thickness are inferred from the cloud fraction.

Using Reed's (1977) bulk formula (Equation 3.3), the cloud fraction over Broome can be estimated from the observed solar radiation. This empirical cloud fraction is based on cloud height and optical thickness rather than cloud cover; additionally it is based on half-hour measurements taken throughout each day rather than daily measurements.

Cloud cover is also collected at Broome through daily satellite images using the same technique used to estimate the fraction of sky covered by clouds at Scott Reef. By comparing the two independent approaches used to determine cloud fraction, we can estimate the uncertainty in the results obtained. For each day, cloud fractions are determined by shortwave radiation and by satellite imagery (Figure 3.10).

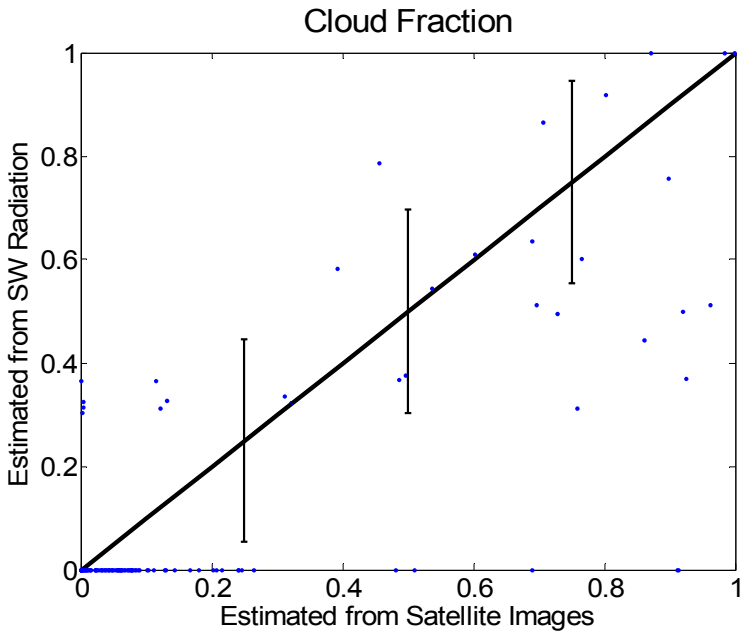

Figure 3.10 Cloud fraction is independently estimated from shortwave radiation and satellite images. When the values for these two methods are compared, the spread of the points gives insight into the certainty of the measurements. The points in this plot represent the cloud fraction at Broome, WA using each method. If the two methods were perfectly correlated, the points would all lie on the solid line. The error bars indicate that the points have a standard deviation of about 0.2 from that line.

Part of the large error is due to a subtle breakdown in Reed's (1977) bulk formula. The formula was designed for cloudy skies and therefore considers any cloud fraction less than approximately 0.3 to be cloud-free. At the same time, the spread of the points in Figure 3.10 may appear larger than is the case: there are several points at (0,0) and (1,1) which are plotted on top of each other and hence do not appear in the figure.

Air Temperature, Pressure, and Wind

Air temperature, atmospheric pressure and wind velocity are measured every 3 hours at Browse and Adele Islands (Figure 3.3). Even though the Browse and Adele Island sites are roughly the same distance from Scott Reef, the Browse Island site is farther offshore and thus is assumed to have atmospheric conditions more similar to Scott Reef. Therefore whenever possible the Browse Island data sets are used to estimate the air temperature, pressure and wind at Scott Reef. However due to large gaps in the Browse Island data set, it was useful to incorporate some of the data from Adele Island as well.

As is the problem with automatic weather station data in general, there are large gaps in the meteorological data sets with missing data spanning periods of months and even

years. Additionally, in the last few years most of night-time data from Browse Island have not been recorded. It was discovered that at night there was significant interference within the cable attaching the weather station to the satellite transmitter and the signal became corrupted (Australian Bureau of Meteorology, personal communication). Fortunately no corrupt data went into the database since the data could not be interpreted in the first place. However because the data loss occurred every night, there is no diurnal variation in the data.

Diurnal variation is quite significant in the air temperature data, and at Scott Reef the air temperature can drop a few degrees Celsius during the night. Without any indication of the night-time temperature, heat fluxes during the night would have to be inferred from the day-time temperatures, which potentially might lead to significant error. To avoid these errors, Browse Island data are used for calculations in 1998 when the daily record is available, while Adele Island is used for calculations in 2003.

The weather stations on Browse and Adele are roughly 200 km away from Scott Reef (Figure 3.3). Therefore, it would be unwise to immediately assume that weather station data measured at Browse or Adele are directly transferable to Scott Reef. In other words, there may be significant variation in air temperature, atmospheric pressure, and wind velocity between Scott Reef and the other sites.

Prior to 1996, the Australian Bureau of Meteorology operated an automatic weather station on Scott Reef. While the archived data can not directly determine the conditions at Scott Reef for 1998 and 2003, the data can be compared to data simultaneously recorded at the other weather stations. From these comparisons, we construct a linear transfer function to relate the other weather stations to Scott Reef and estimate the uncertainty in the measurements.

The weather station data recorded between 1993 and 1996 at Adele, Browse, and Scott Reef was analysed to find all of the measurements that were observed simultaneously between stations. This was not a trivial task as the records are filled with gaps and the sampling times between stations have changed over the years. Over this period there were 5,736 measurements taken simultaneously at Scott Reef and Browse, and 12,589 simultaneous measurements between Scott Reef and Adele.

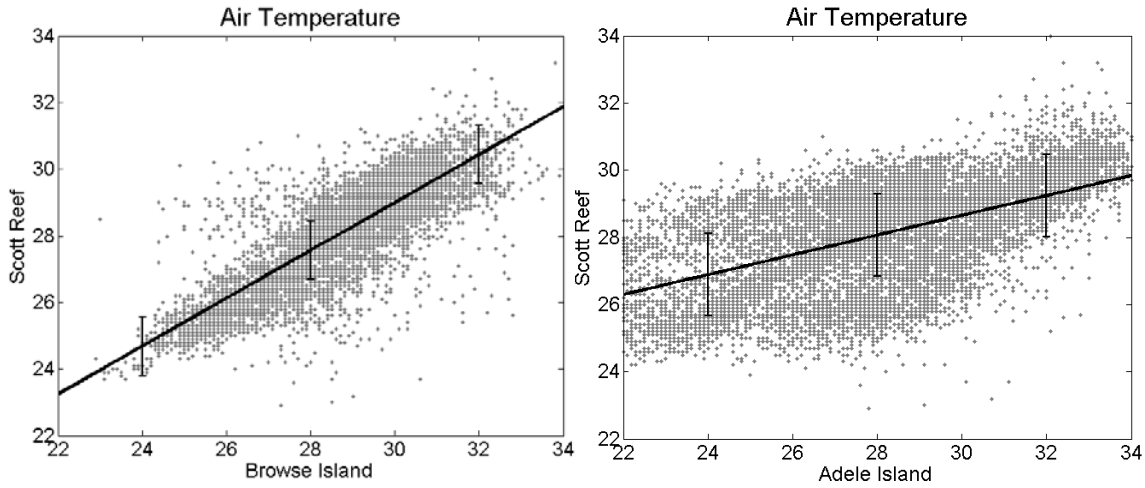

Figure 3.11 Air temperature was recorded simultaneously at Browse Island, Adele Island, and Scott Reef prior to 1996. The scatter plots show a general relationship between Scott Reef and the other stations. The linear regressions (black solid lines) are used to transfer the 1998 and 2003 measurements from the other stations into Scott Reef air-temperature estimations.

Figure 3.11 shows both the relationship between air temperatures collected simultaneously at Scott and Browse and the air temperature collected simultaneously at Scott and Adele during 1993 to 1996. The least squares regression line is plotted along with the corresponding standard deviation.

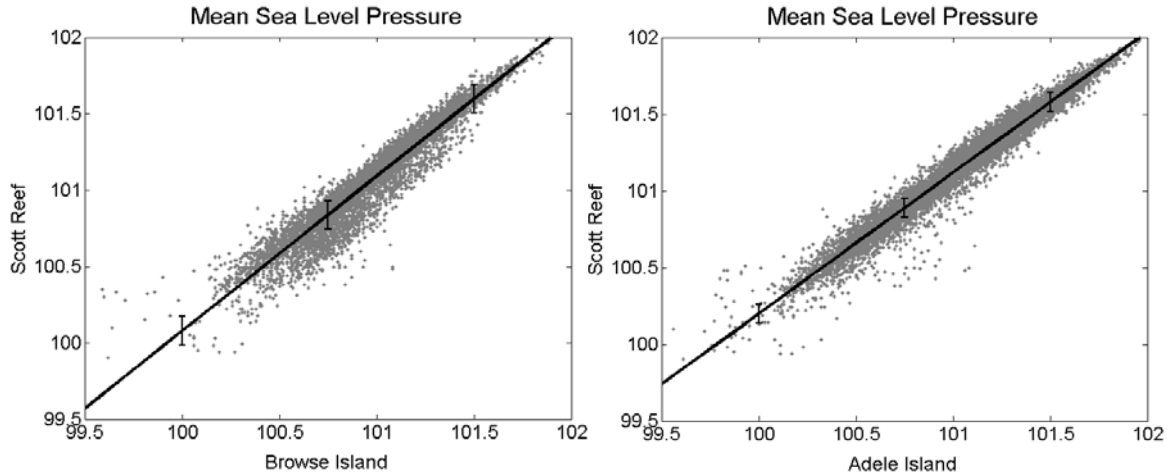

Figure 3.12 Atmospheric pressure scatter plot and best-fit linear relationship between Browse Island and Scott Reef (left) and between Adele Island and Scott Reef (right) prior to 1996.

The pressure and wind data measured simultaneously at Scott Reef and the other weather stations are plotted against each other in a similar fashion (Figures 3.12 and 3.13). The measured east and north components of the wind are converted into a wind magnitude and direction. The wind magnitude has a much greater effect on mixing than

does the wind direction. Therefore, standard error is only calculated from the wind magnitude between Browse and Scott.

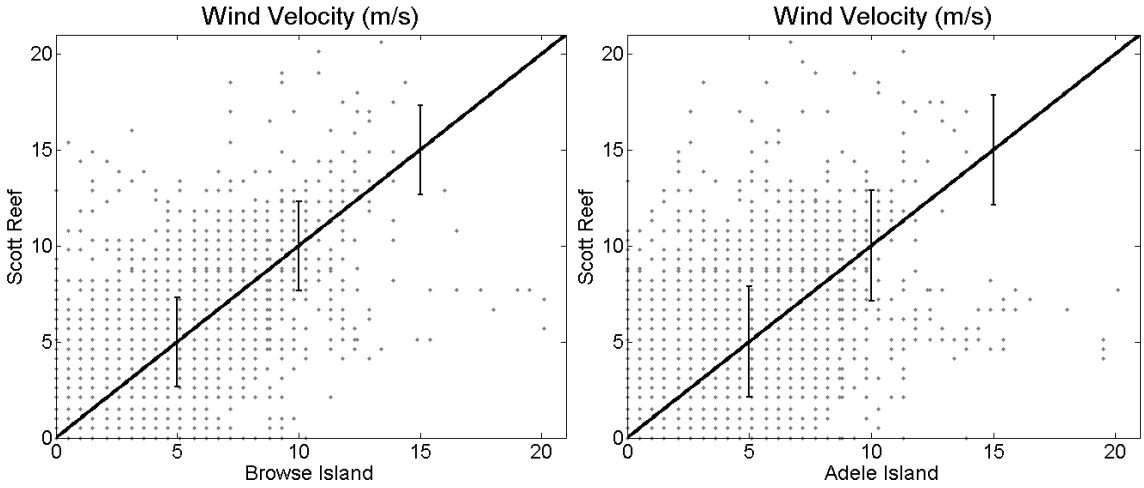

Figure 3.13 Wind speed scatter plot and best-fit linear relationship between Browse Island and Scott Reef (left) and between Adele Island and Scott Reef (right) prior to 1996. The discreteness of the recorded measurements obscures points that coincident with each other.

The relations illustrated in Figures 3.11 to 3.13 are noteworthy for three reasons. First, they show that the meteorology is strongly correlated between Scott Reef and the other sites. Next, the figures demonstrate that linear transformations provide a better estimation of Scott Reef conditions than a direct substitution from the neighbouring weather stations. For example the linear regressions show that if the temperature was measured to be 28°C on Browse Island or Adele Island, it is most probable that the temperature on Scott Reef was also 28°C. However if it was 22°C on Browse Island, most likely it would be around 23°C on Scott Reef; likewise, a temperature of 22°C on Adele Island corresponds to a temperature of 26°C on Scott Reef. Finally, the relations provide an estimation of the uncertainty corresponding to the transformation denoted by the error bars. The goal of calculating the least-square fit line between the data measured from the two sites is that it allows us to estimate the conditions at Scott Reef in 1998 directly from observations recorded at Browse Island during that period. Likewise, the linear relationship between Scott and Adele is used to estimate Scott Reef conditions from Adele data in 2003 when measurements from Browse Island are not available. The uncertainty bars give us an indication of error in these transfers.

As an aside, the linear regression for the wind magnitude was not computed; instead the wind magnitude is modelled to be the same as from the other stations. This was done because the linear regression computed for Scott Reef as the dependent variable was significantly different from the correlation for Scott Reef as the independent variable. The error in this case becomes the standard deviation of the differences in wind measured between Browse and Scott at a particular time. The wind records are discreet causing several points coincide with each other in Figure 3.13. This can help explain the scattered appearance of the data.

Because Adele is so much closer to the Australian coast, one would expect to see an increased diurnal effect in data such as wind velocity. In fact since air temperature, wind, and pressure are largely driven by cyclic events, one would expect that changes in location would affect the data at certain frequencies more than others. Future studies may wish to determine if estimations can be improved by calculating transfer functions based on frequency response.

Estimating Humidity

Humidity is an important factor in calculating both the longwave and latent heat fluxes. Unfortunately, the weather stations at Browse and Adele are not equipped to measure humidity. The nearest humidity-measuring station is located at Kuri Bay (see Figure 3.3) which samples humidity every three hours. However, unlike Browse and Adele Island, Kuri Bay is located on the coast and therefore may contain coastal effects in its humidity signature. While the long-term humidity may be accurate for the region, directly substituting the humidity at Kuri Bay for the humidity at Scott Reef is difficult to justify. The nearest island where humidity data is collected is at Troughton Island (see Figure 3.3), 450 km East of Scott Reef. It is not immediately clear which data set (Troughton Island or the Kuri Bay) better represents the humidity at Scott Reef. Both stations are probably ill-suited to predict short-term humidity values at Scott Reef, both because of the significant distance from Scott Reef and the proximity to the coast. However when examining several years of humidity data, it becomes clear that Kuri Bay and Troughton Island have roughly the same annual signal – higher humidity in February and lower humidity around July.

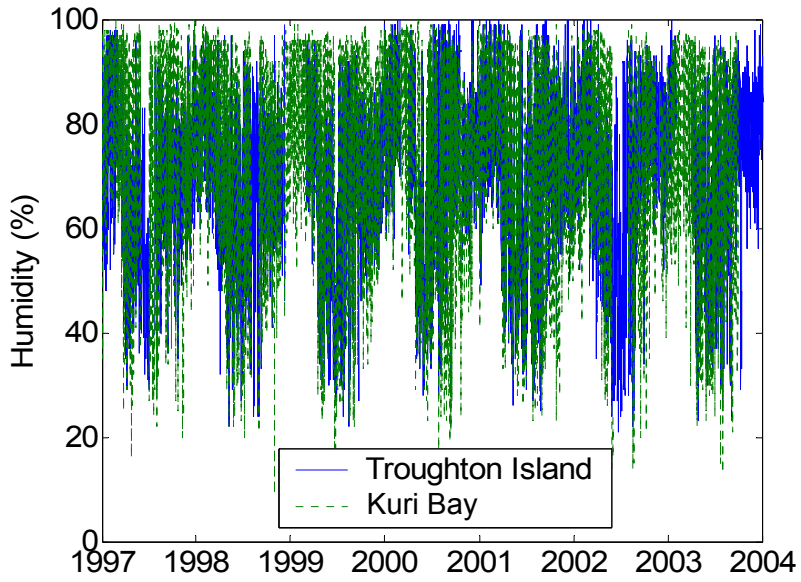

Figure 3.14 Relative humidity (100% being the most humid) measurements for seven years at Troughton Island and Kuri Bay. Both sites exhibit nearly identical seasonal variations in humidity.

It is nearly impossible to estimate the humidity at Scott Reef from a particular humidity value at Kuri Bay or Troughton Island; however, the seasonal variation observed in the humidity data (Figure 3.14) suggests that the humidity in the region can be estimated, based on the time of year. The first step is to calculate a climatological humidity curve by taking weekly averages from the humidity observed at both sites during 1997 to 2004. The second step is to smooth the data by lowpassing the weekly averages with a Butterworth filter (Figure 3.15). The seasonal humidity relation captures the high humidity found in summer and the lower humidity found in winter, both of which were apparent from the raw data (Figure 3.14).

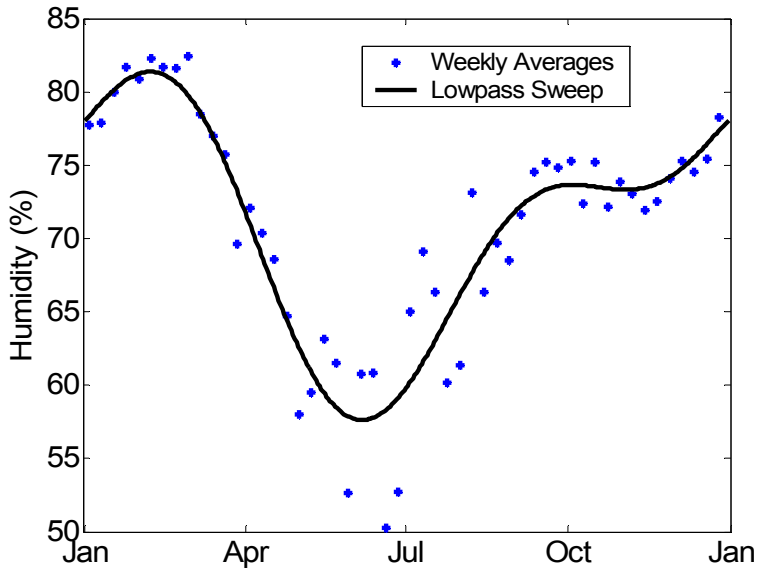

Figure 3.15 A climatological humidity curve calculated from the weekly averages of the measurements taken at Troughton Island and Kuri Bay (Figure 3.14).

Before assuming that the humidity at Scott Reef follows the above curve, it would be best to compare the estimated humidity function with actual Scott Reef humidity data. Presently, the best method to estimate humidity at a remote location out at sea is from ship measurements. Another method with much potential is SSM satellite imagery, which uses algorithms based on microwave images to estimate the vapour content in the atmosphere. At the time of writing, this approach is still in the research and development stages and no commercial products that estimate near-surface humidity have been released. However, mention of this approach is warranted as future investigators may gain more accurate results from humidity remote sensing. Nevertheless, no ship data or SSM satellite imagery are available for 1998 or 2003. However, humidity observations were collected by the *Franklin* as it passed by Scott Reef in 1995, 1999, and 2000 (data used with permission from CSIRO). The exact location that each observation was taken is illustrated in Figure 3.16. The humidity measurements are plotted in Figure 3.17 and show good agreement with the seasonal humidity estimate obtained above.

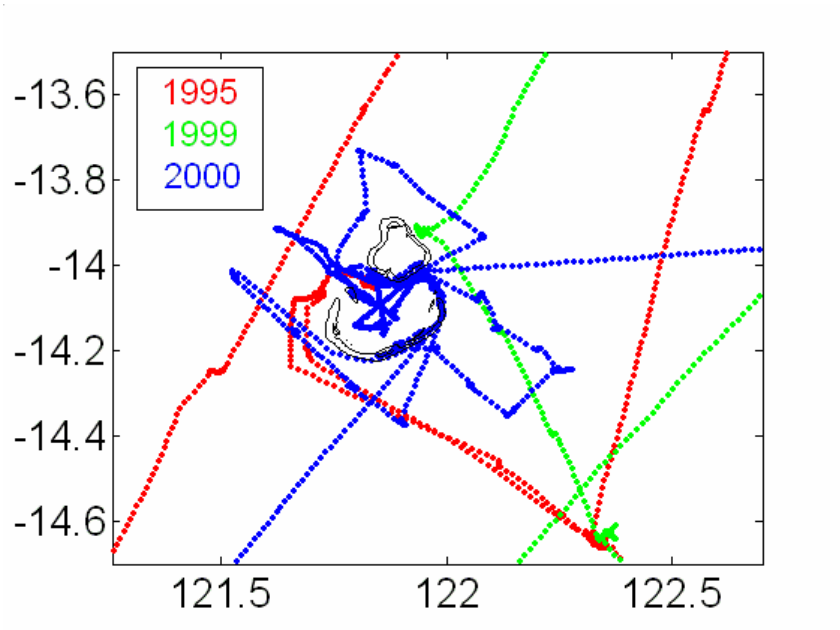

Figure 3.16 The locations of individual humidity measurements collected by the *Franklin* as it passed Scott Reef in 1995, 1999, and 2000.

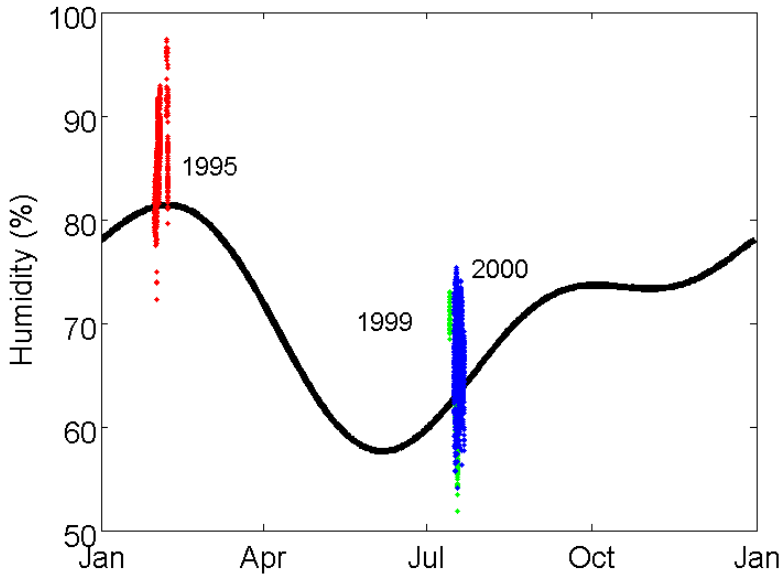

Figure 3.17 The relative humidity measured at Scott Reef by ship in 1995, 1999, and 2000 supports the use of the climatological humidity curve at Scott Reef. Note that the humidity scale is from 50% to 100%.

The Scott Reef ship measurements also give insight to the daily humidity signature. Both the humidity measured at Kuri Bay and at Troughton Island exhibit a strong diurnal fluctuation (Figure 3.18). It is not immediately obvious whether this fluctuation is driven by coastal effects or by some other means. Since the diurnal fluctuations are

not present in the humidity at Scott Reef (Figure 3.18), it is believed that they are in fact due to coastal effects. This finding suggests that the smoothed out, seven-year average humidity is even more appropriately used for out-at-sea locations, such as Scott Reef, than for coastal regions.

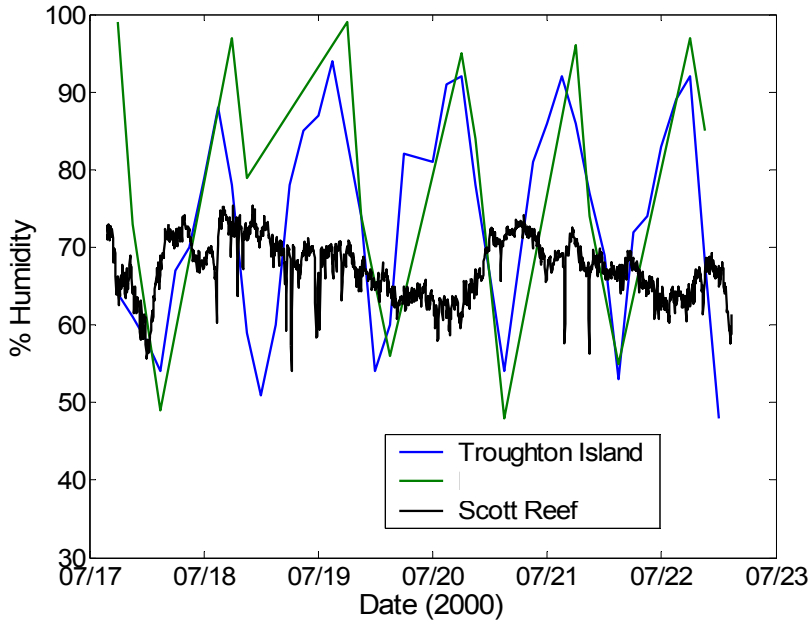

Figure 3.18 Relative humidity measured at Scott Reef by ship for a week in July of 2000 is compared with measurements observed at Kuri Bay and Troughton Island during this period. Note that the humidity scale is from 30% to 100%.

Uncertainty in Humidity

To estimate the confidence in the humidity approximation, the 68% confidence intervals were measured at each month. The monthly standard deviation for the seven-year Kuri Bay and Troughton Island humidity data is plotted in Figure 3.19. The humidity variation appears seasonal; it is least in the summer (November to March) and greatest in the winter (May to September). It is not immediately apparent whether the humidity at Scott Reef would fall within these confidence intervals. Air masses from land tend to bring with them lower humidity; therefore it seems more likely that Scott Reef would have a higher humidity than the coastal stations. At the same time the relatively large variability in Figure 3.19 accounts for the diurnal fluctuations present at the near-coastal stations, which were not seen in the Scott Reef signal. Therefore it is expected that the standard deviation of Scott Reef humidity would be smaller than those in Figure 3.19.

Thus, while the uncertainties in Figure 3.19 were calculated from Kuri Bay and Troughton Island data, it is believed that Scott Reef humidity is adequately expressed by these points.

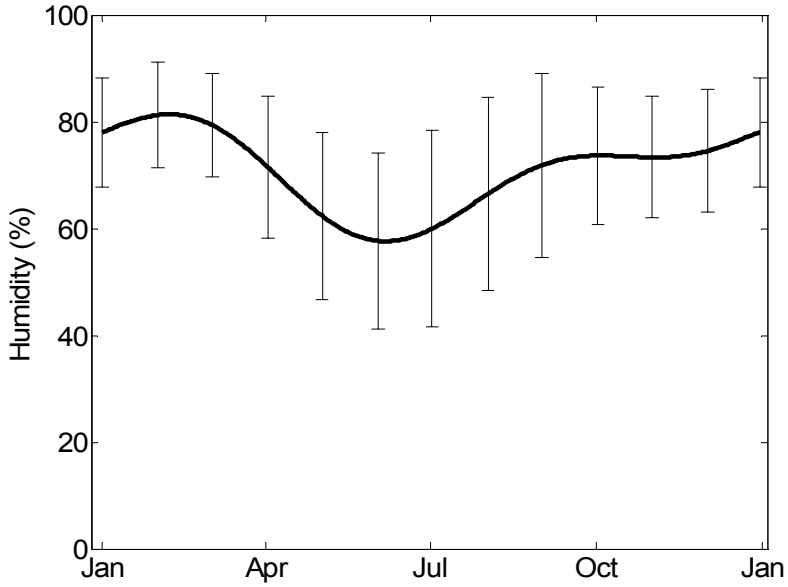

Figure 3.19 The 68% confidence intervals are calculated for the climatological humidity curve. The variability in the humidity (size of the fluctuations) appears to be seasonal.

Bulk Formulas

Once all of the meteorological conditions have been estimated for Scott Reef, the next step is to convert them into heat fluxes using bulk formulas. Figure 3.20 outlines how each of the bulk formulas (illustrated as light-blue boxes in Figure 3.20) relates the meteorological conditions to the heat and momentum fluxes. The rest of this chapter discusses the need, selection, and use of these bulk formulas.

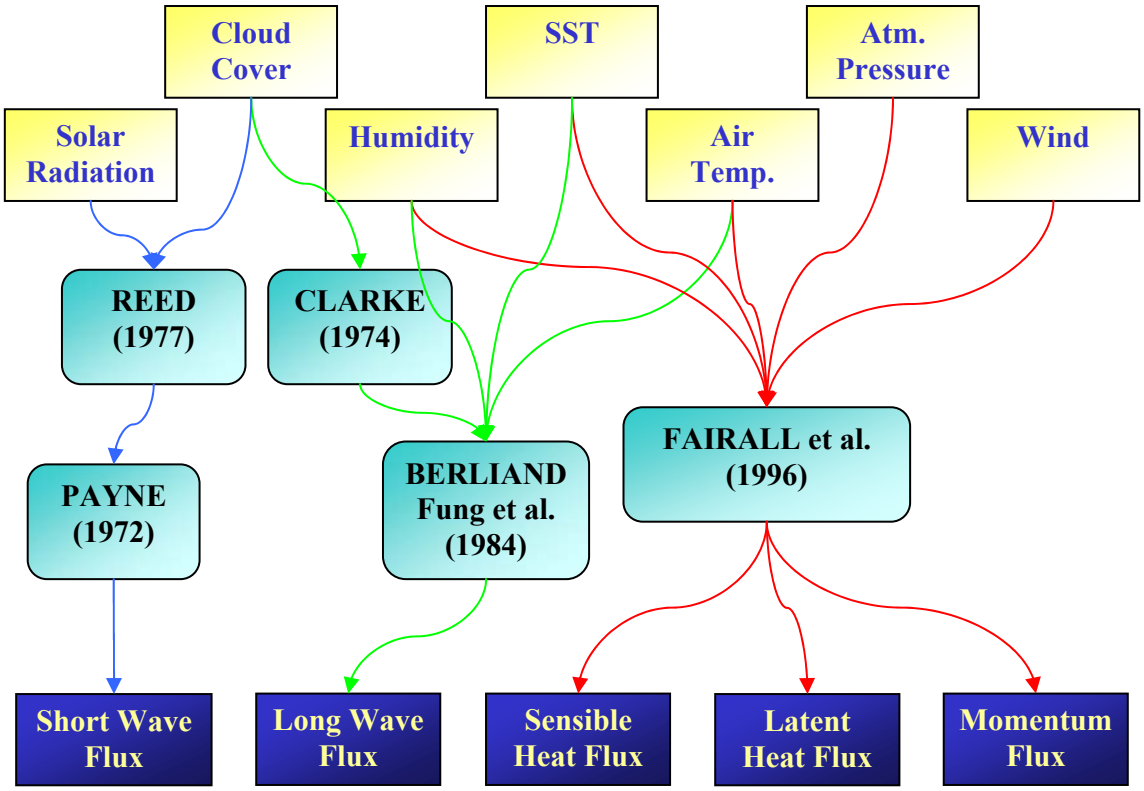

Figure 3.20 The meteorological conditions are converted in to heat and momentum flux estimations using appropriate bulk formula. The bulk formulas are illustrated as light-blue boxes with labels that reference the author and source paper.

Shortwave Flux

In the previous section, the shortwave radiation was estimated at Scott Reef by using a bulk formula (Reed, 1977) to account for the observed cloud cover. It is important to note that this shortwave radiation represents the radiation flux incident on the ocean, not the radiation flux *penetrating* the ocean. A significant percentage of the radiation hitting the ocean is reflected and is known as the albedo. In this study, the albedo is estimated using tabulated results from Payne (1972). The albedo and the resulting

shortwave flux into the ocean are calculated for half-hour intervals with the help of a MATLAB script written by Pawlowicz et al. (2001). The script relates the shortwave radiation, position on the earth, and the position of the earth relative to the sun to the bulk formula documented by Payne (1972).

Longwave Flux

A review of longwave radiation flux bulk formulas can be found in Fung et al. (1984). Fung et al. (1984) compared the net longwave radiation flux of several bulk formulas with computational results carried out with the full radiative transfer equation. For tropical conditions, they found that 3 formulas attributed to Berliand, Bunker, and Anderson respectively best replicated the full radiative transfer equation results.

The longwave radiation flux is generally estimated from the sea surface temperature, air temperature, cloud cover, and humidity; however there have been attempts to implicitly relate humidity to air temperature, thus generating a bulk formula that is independent of humidity. Because of the uncertainty in the humidity measurements at Scott Reef, it is tempting to use one of these humidity-independent bulk formulas, such as the relation developed by Swinbank (described in Fung et. al 1984). However in their paper, Fung et al. (1984) advise against such approaches, noting that in almost all cases a rough estimate of the humidity can be made, and in these cases the formulas of Berliand, Bunker, and Anderson perform better.

Cloud correction factors are often used to improve performance of the bulk long-wave flux by incorporating latitude into the corrected cloud fraction. The correction determined by Clarke (described in Pawlowicz et al., 2001) is used in this study as the other correction factors described by Pawlowicz et al. are restricted to the Atlantic. MATLAB scripts written by Pawlowicz et al. (2001) are used to calculate the longwave radiation from the Berliand bulk formula with the Clarke cloud correction factor.

Latent & Sensible Heat Flux

Latent and sensible heat fluxes depend on wind speed, air temperature, atmospheric pressure, humidity, and sea surface temperature. Additionally, knowledge of the altitude that these measurements were taken from the sea surface is necessary.

Traditionally the Kondo bulk formula (Kondo, 1975) is used to calculate these fluxes. However recent work by Fairall et al. (1996) has almost completely replaced the use of the older formulas. The Kondo formulas are worthwhile to note as they are still found in many flux calculations. In this report, the latent and sensible heat fluxes were calculated using the Fairall et al. bulk formulas (via MATLAB scripts by Pawlowicz et al., 2001).

Summary and Concluding Remarks

The SSTs around Scott Reef were unusually hot during March and April of 1998. It is unlikely that the warm water was advected into the region since the net currents are relatively small. Instead, the elevated SSTs were more likely due to atmospheric conditions (low wind, warm air temperature, etc.) that lead to a net heat flux into the water column. Atmospheric conditions are collected from weather stations and satellite images. Since the weather stations are spread over a considerable distance (up to 450 km from Scott Reef), considerable care has been taken to make sure that the measurements are representative of the Scott Reef region.

In order to estimate how the atmospheric conditions affected the temperatures in the water column (as will be done in Chapter 4), the atmospheric conditions need to be converted into heat fluxes. The heat flux across the air-sea interface is comprised of four components: sensible heat flux, latent heat flux, longwave radiation, and shortwave radiation. Using standard bulk formulas, each of these components are estimated from the meteorological conditions.

Chapter 4 – Modelling Vertical Temperature Structure

In the previous chapter the different processes that comprise the heat balance were discussed and estimated from meteorological conditions around Scott Reef. Estimating the heat fluxes into the water column during a particular period can provide insight into how much heat is being transferred into the water column. However to more accurately predict water temperatures, mixing processes need to be considered along with heat fluxes. Additionally, Chapter 3 neglects any vertical variation in the water temperature.

The goal of this chapter is to apply a numerical model to calculate the water temperature at various depths during a bleaching episode. The first sections in this chapter describe the numerical model that was used and how the heat fluxes and mixing processes specify the boundary conditions. The following sections discuss how the numerical model was calibrated and validated using atmospheric and oceanographic conditions during the 2003 field campaign and temperature observations taken during this period. In the final sections of the chapter, the model is used to calculate the temperature profiles during the 1998 bleaching episode at Scott Reef: these temperature profiles are then compared with coral bleaching records.

The Water-Column Numerical Model

The General Ocean Turbulence Model (GOTM) written by Burchard et al. (2001) was used to calculate the vertical temperature distributions at Scott Reef. GOTM simulates the small-scale thermodynamics and hydrodynamics in a water column as generally as possible and is therefore not restricted to a particular site or application (a disadvantage with empirical models).

GOTM is a one-dimensional, hydrostatic water column model. The fact that GOTM only models vertical mixing requires that horizontal gradients are either neglected or else prognostically prescribed. One of the distinct advantages of GOTM over other water column models is its large selection of state-of-the-art turbulence closure schemes. A dimensionless stability function, a turbulent velocity scale, and turbulent macro length scale are all needed to calculate the Kolmogorov-Prandtl relations. Several zero-, one-, and two-equation models used to calculate the turbulent velocity

and macro length scales, as well as various stability functions, are available in GOTM. For a review of turbulence modelling and detail on the particular turbulence schemes available in GOTM, the reader is referred to Burchard (2002).

The model results in this thesis were carried out using the same second moment closure scheme and the k-ε model used by Burchard (2002) to verify GOTM against field data. Model runs using other turbulence schemes were carried out as well, and it was found that these differences had little effect on the model results.

Temperature Boundary Conditions

In the modelled system, heat only enters the system through the air-sea interface. However when running the model, both a net surface heat flux and a radiation heat flux are specified at the air-sea interface for each point in time. The net surface heat flux is the sum of the sensible heat flux, Q_H, latent heat flux, Q_E, and longwave radiation flux, Q_{LW}, as all the heat transfer from these fluxes occurs at the sea-surface. At equilibrium, the surface fluxes are related to the temperature by the following differential equation evaluated at the air-sea interface:

$$\left(\alpha_t + \alpha\right)\partial_z T = \left.\frac{-Q_H - Q_E - Q_{LW}}{C_p \rho_0}\right|_{z=\zeta} \tag{4.1}$$

where α and α_t are the molecular and eddy diffusivity respectively.

Shortwave radiation, however, does not transfer all of its energy at the air-sea interface. Instead, the shortwave radiation penetrates into the water column and heats the water column as it is absorbed. Thus the shortwave radiation flux needs to be specified as an additional boundary condition. The shortwave radiation absorption, $R(T)$ is given by

$$R(T) = \frac{\partial_z I}{C_p \rho_0}. \tag{4.2}$$

Here C_p is the specific heat, ρ_0 is the relative density and I is the shortwave radiation intensity. A fraction of the radiation is absorbed for each metre passed through the water column; thus in theory the intensity will drop exponentially with depth. The radiation intensity can be expressed by using

$$I(z) = I_0\left(ae^{-\eta_1 z} + (1-a)e^{-\eta_2 z}\right) \tag{4.3}$$

where I_0 is the intensity of shortwave radiation entering into the water, a is a weight factor, and η_1 and η_2 are the attenuation lengths for the longer and shorter-wavelength shortwave radiation respectively. The values of a, η_1, and η_2 depend on the water clarity and have been classified into Jerlov Water Type categories (Jerlov, 1976).

Processes that contribute to vertical mixing

Additional boundary conditions and internal forcing are required to model the processes that contribute to vertical mixing. In this study, three mechanisms were included in the numerical model: wind stress, tidal currents, and internal mixing.

Wind Stress

Wind velocity creates a stress on the sea surface. This stress causes surface mixing and can mix heat down into the water column. The wind velocity estimated from weather station data was converted into wind stress using the Fairall et al. (1996) bulk formulas (see Chapter 3).

Tidal Currents / Bottom Friction

Tidal currents interact with the sea floor in a similar way to the interaction of wind with the sea surface. Bottom friction transfers energy in the tidal current to tidal dissipation which creates bottom-up mixing. Measurements from the current meters deployed during the 2003 field campaign are used directly in calculations during that period. In other periods, such as 1998, current predictions derived from the current tidal analysis (see Chapter 2) are used.

Internal Mixing

An additional source of mixing can occur within the water column, as oppose to the top-down wind mixing and the bottom-up tidal mixing discussed above. Internal mixing is far more elusive than the other sources and is quite difficult to parameterize, as it acts

along all 3 dimensions. Internal mixing occurs along a pycnocline when either internal waves break or when vertical shear overcomes the stratification and becomes unstable through the Kelvin-Helmholtz instability mechanism. The stability of each layer of water depends on the ratio of stratification to vertical shear. This ratio is known as the Richardson number and defined as

$$Ri = \frac{N^2}{\left(du/dz\right)^2} \tag{4.4}$$

where u(z,t) is magnitude of the horizontal velocity, z is the water depth, and N^2 is the Brunt-Vaisaila frequency (also known as the buoyancy frequency). The Richardson number is calculated by GOTM at each time step for each vertical level.

Model Setup

GOTM is run from between 2 to 4 months with one-minute time steps. The model is driven by heat and momentum fluxes across the sea surface estimated in Chapter 3, as well as tidal currents observed in the field (Chapter 2) in a process described briefly in the last few sections. Internal wave mixing can be controlled by one of the modules within GOTM. When internal wave mixing is included, the eddy viscosity and thermal diffusion rates (ν_t and α_t respectively) are estimated following Large et al. (Burchard, 2002; Large et al., 1994). In this estimation, the internal wave breaking and shear instability mechanisms are separated. The diffusion rates from the internal wave breaking are approximated as

$$\begin{aligned} \left(\nu_t\right)^{IW} &= 10^{-4}\ m^2 s^{-1} \\ \left(\alpha_t\right)^{IW} &= 10^{-5}\ m^2 s^{-1} \end{aligned} \tag{4.5}$$

whereas the shear instabilities are estimated as a function of Richardson number as follows:

$$\left(\nu_t\right)^{SI} = \left(\alpha_t\right)^{SI} = \begin{cases} 0\big|_{Ri>0.7} \\ 5\times10^{-3}\left(1-\left(\dfrac{Ri}{0.7}\right)^2\right)^3\ m^2 s^{-1}\Big|_{0<Ri<0.7} \\ 5\times10^{-3}\ m^2 s^{-1}\Big|_{Ri<0} \end{cases} \tag{4.6}$$

Internal waves are known to exist around Scott Reef (Holloway, 1996). By including the internal wave mixing parameterization in the GOTM runs, the significance of this mixing relative to other sources can be investigated.

When verifying GOTM with the 2003 field measurements, the model simulated a site (Site E) that had a depth of 50 metres. For these runs, 100 vertical levels are computed. Since the largest flux gradients are near the surface, the 100 levels are spaced non-uniformly. The distance between levels ranges from 1.5 cm for the top-most layers to 1.5 metres for the bottom-most layers. In more general simulations, the top 100 metres of deep water is modelled. In these cases, GOTM is run with 200 levels with a distance of again 1.5 cm between the top-most layers and 1.5 metres between the bottom-most layers.

Model Results

Building up the Model: Effect of Mixing Processes

Wind stress, tidal currents, and internal waves all contribute to vertical mixing. By introducing each of the mechanisms into the model one at a time, the effect that each has on the water column at Scott Reef can be determined. The temperatures throughout the water column are compared to those measured at Site E, which is located within the lagoon (Figure 2.2). There were six temperature loggers at this site during the 2003 field campaign. The loggers were located at 5, 7.5, 15, 20, 25, and 40 metres and took readings every 5 minutes from the end of March to the end of June. The logger at 20 metres stoped recording temperatures in mid-May.

Convection only from surface cooling

Figure 4.1 shows the evolution of the vertical temperature profile simulated by GOTM. The water column depth is on the ordinate with the top of the plot being the sea-surface. Time is on the abscissa and ranges from when the instruments were deployed (23 March, 2003) to the recovery date (20 June, 2003). The colour represents the temperature at the particular depth and time. The temperature scale ranges from 26.5°C (dark blue) to 32.5°C (dark red). Instrument observations are superimposed over modelled temperatures and use the same temperature-colour scheme. The instrument bands give an indication of the similarity between the model predictions and actual observations.

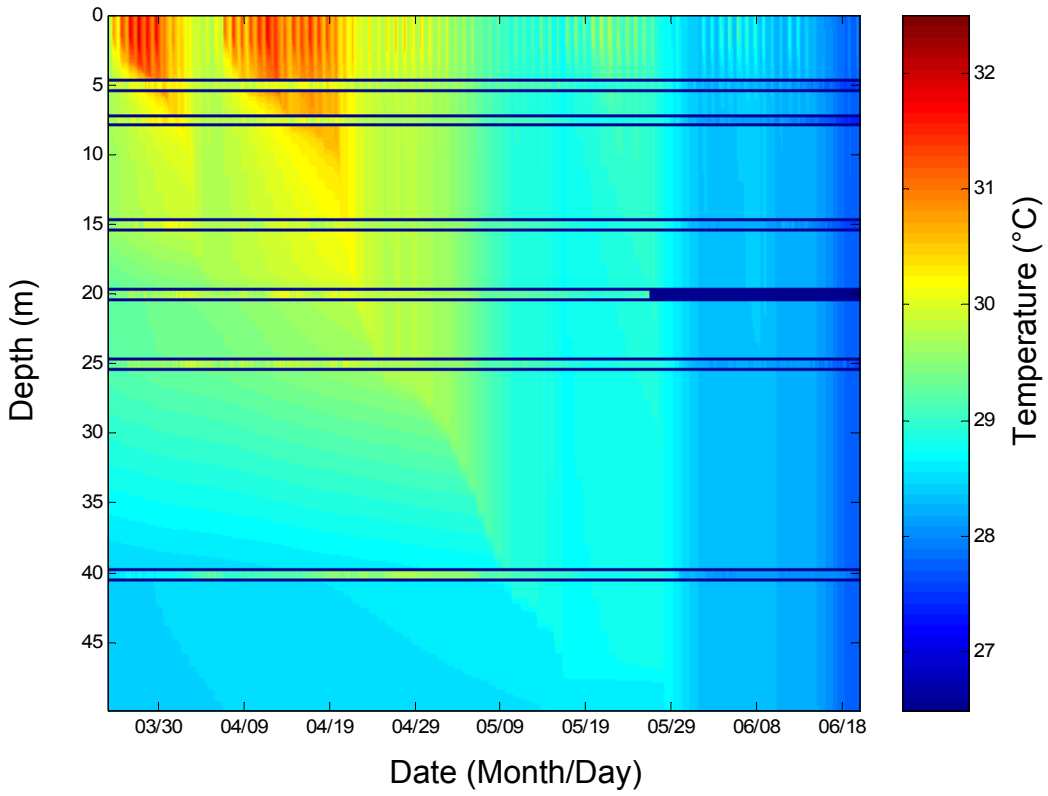

Figure 4.1 Temperature profiles (from the surface to 50 metres deep) numerically calculated at Scott Reef from the end of February to mid-June. These profiles neglect any mixing due to wind, currents and internal processes. The bars at 5, 7.5, 15, 20, 25, and 40 metres indicate actual temperature observations at this site.

The results shown in Figure 4.1 are temperatures simulated solely by heat fluxes. The fluxes were calculated using the atmospheric conditions approximated in Chapter 3, relying on the SST iteration procedure discussed in Appendix C. The initial profile and water turbidity estimate were taken from field data (Chapter 2). Substantial mixing is achieved by surface cooling alone. It should be noted that the surface mixing is strongly correlated with wind velocity. While wind stresses have not been included in the surface mixing, the wind velocity has a dramatic effect on the latent heat flux and thus on surface cooling.

The observations show that the temperatures at 5 and 10 metres are overestimated, especially during the first month. However, the loggers located 15 metres and below show that the temperatures during the first month are underestimated by the model. When the water column becomes well-mixed starting in mid-May, the temperatures predicted by the model compare well with the field observations.

Addition of wind stresses

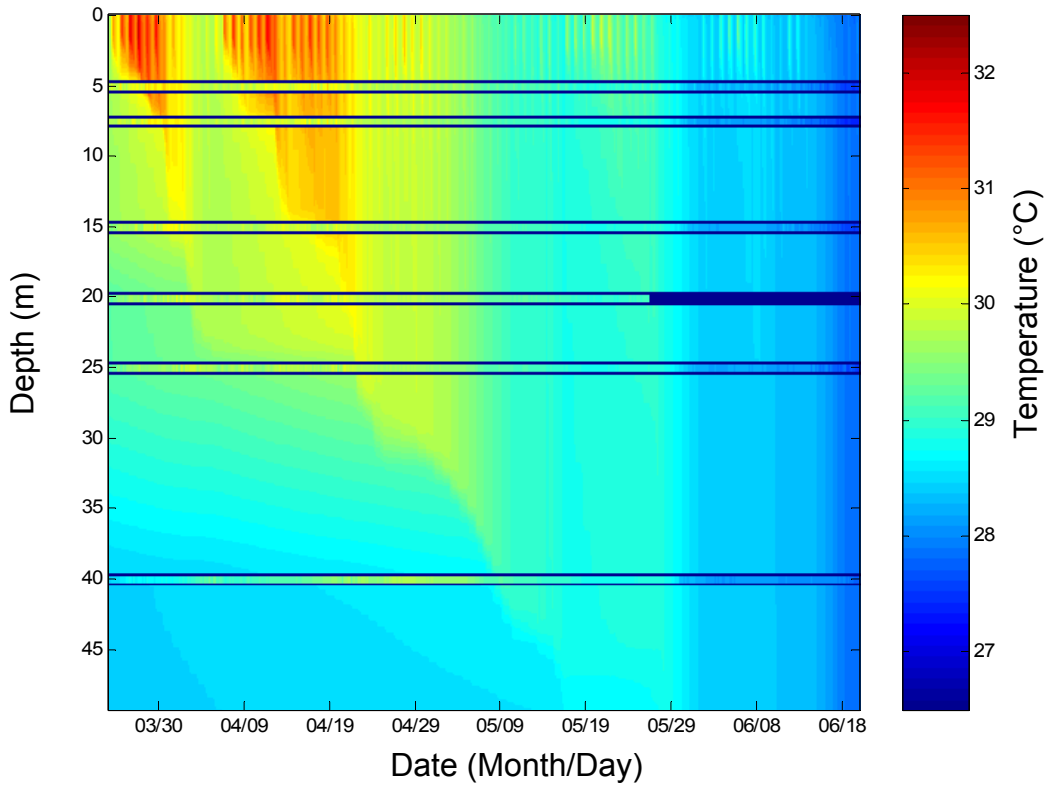

Figure 4.2 By including the effects of wind stress, vertical mixing is enhanced.

As identified earlier, wind stresses can cause top-down mixing. When these stresses are included with the heat fluxes in the numerical model, more mixing occurs in the top layer (Figure 4.2). The addition of wind stresses appears to lower the mixed layer depth by about 5 metres. However, the field observations indicate that the mixed layer depth is still too high. It is a somewhat surprising finding that the majority of the surface-down mixing seems to be caused by heating fluxes rather than momentum fluxes.

Addition of Tidal Currents

Tidal currents interact with the bottom through friction to create bottom-up mixing. The current meter at Site E malfunctioned so there were no current measurements taken at that location. Current measurements were successfully measured at Site F, also in the lagoon (see Figure 2.2), so these measurements can be used to calculate tidal mixing. Figure 4.3 shows the temperature distribution predicted from the model when heat fluxes, wind stress, and tidal currents are all included.

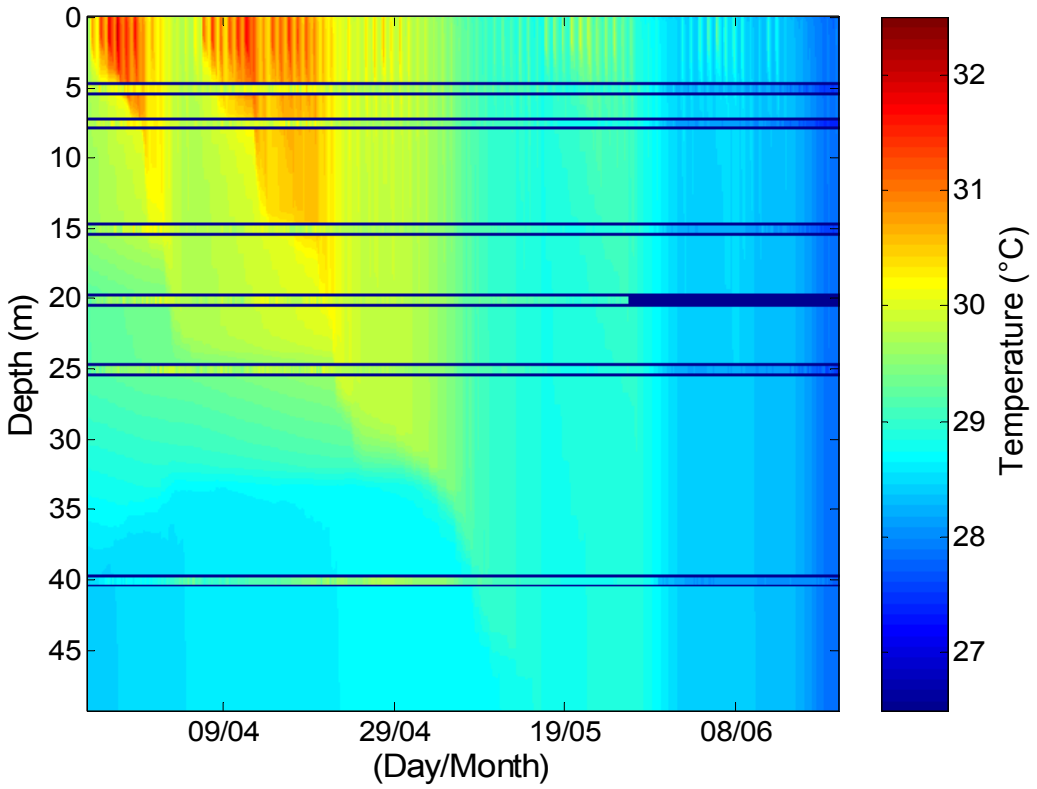

Figure 4.3 Temperature profiles that include both bottom friction and wind stress. Bottom friction mixes bottom-up and wind friction mixes the water column from the top down.

The tidal mixing at this site only affects the bottom 20 metres. The bottom 10 metres became well-mixed throughout the duration of the field campaign, except for slight stratification occurring around 10 May during neap tides. The addition of tidal currents does not lower the mixed layer in the model. During the first month, the temperatures observed near the surface are cooler than those simulated, while the temperatures observed at 40 metres depth are warmer than the simulated temperatures.

Addition of Internal Waves

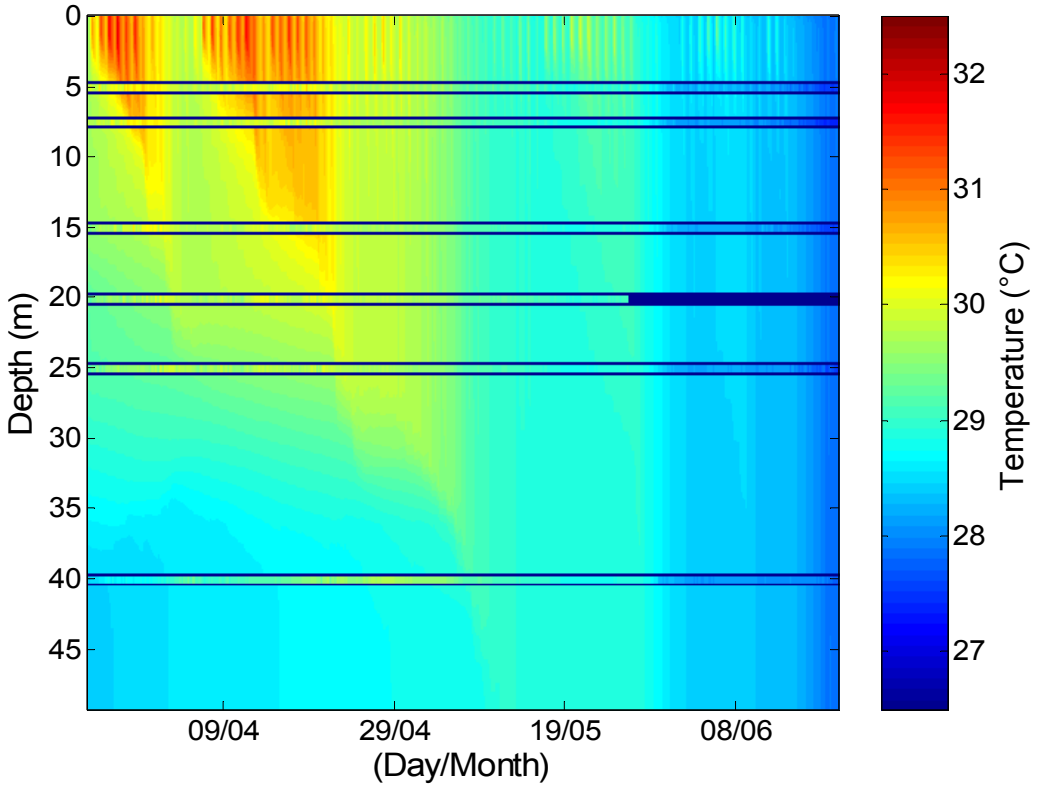

Figure 4.4 Temperature profiles that include the effects of internal waves, bottom friction and wind stress. Internal mixing smooths the transition between the stratified layers.

The final simulated mixing process is internal mixing from shear instability and internal wave breaking. These processes target the middle of the water column, specifically the thermocline. The resulting temperature distribution is shown in Figure 4.4. The effect of internal mixing is not immediately obvious, as Figure 4.3 and Figure 4.4 appear nearly identical. Figure 4.5 shows the difference between Figure 4.3 and Figure 4.4. In Figure 4.5, the x-axis is time and the y-axis is again depth; however the colour in this plot represents the change in water temperature due to internal mixing at a given depth and time. The addition of internal mixing changes some temperatures by as much as 0.5°C and lowers the mixed layer depth by a couple of metres (Figure 4.5). However, the overall impact is small. While the addition of internal mixing as parameterized by Large et al. (1994) does mix down warmer surface temperatures slightly, the field observations still indicate that more vertical mixing is required during the first month.

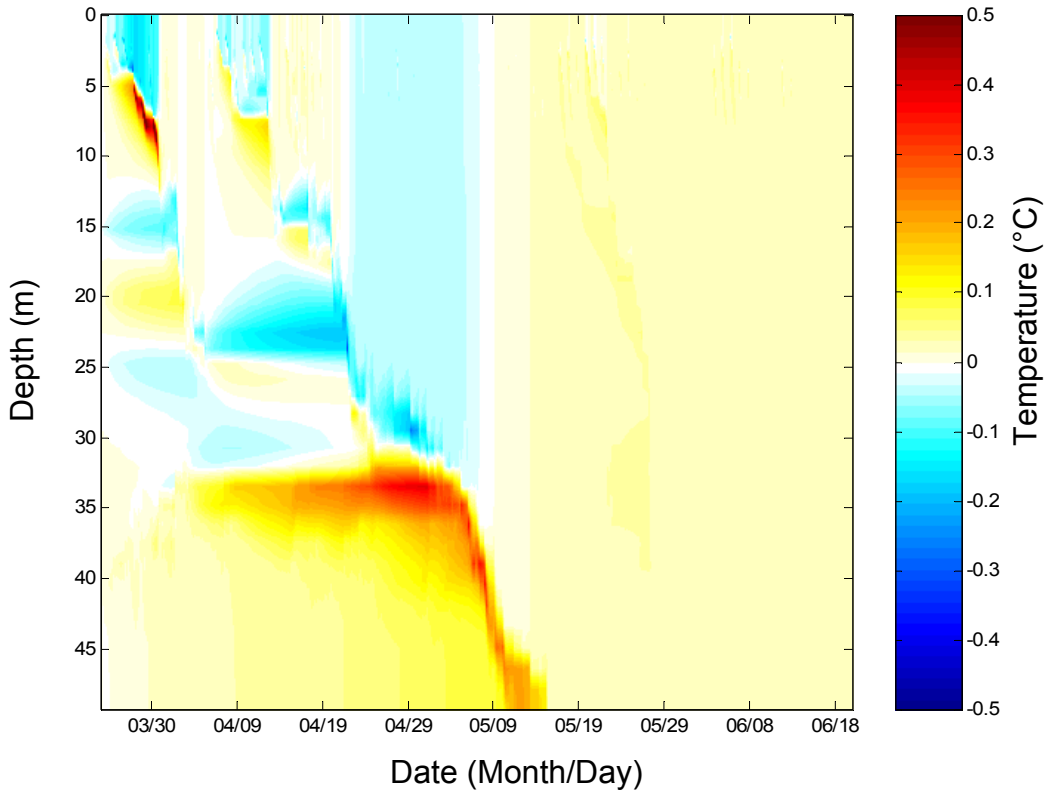

Figure 4.5 Difference in the temperatures in Figures 4.3 and 4.4 as a function of depth and time. The internal mixing has the largest effect on the stratification boundary and lowers the mixed layer slightly.

Comparison with observed SST and XBT Profile

The surface temperature layer in the model can be compared to the SST processed from satellite images over the same period (Figure 4.6). The model results and the observed SST agree well, though there are periods, such as mid-to-late April and the beginning of June, when the model over-predicts the observed temperatures.

The model can also be run in deeper water. Outside Scott Reef depths range from 500 metres to almost 2 kilometres. As demonstrated earlier, the tidal currents provide bottom-up mixing. In the deeper water where tidal currents are not strong, the effect of tidal currents on the top 100 metres is negligible. Tidal current is the only mixing parameter modelled that varies with location around Scott Reef. In other words, the heat and momentum fluxes across the air-sea interface, the water turbidity, and the effect of internal waves is assumed to be spatially invariant around Scott Reef. Therefore, the near-surface (top 100 metres) temperatures simulated in the model should be essentially the same for all the deep-water regions around Scott Reef.

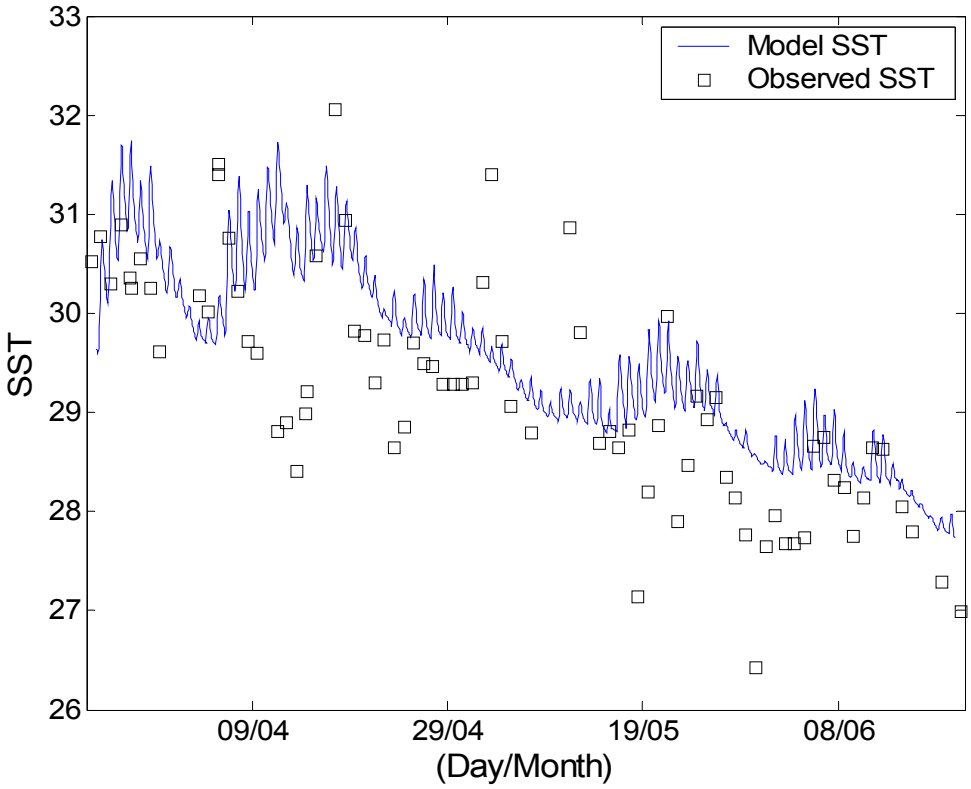

Figure 4.6 Modelled sea surface temperature compares well with the observed sea surface temperature (°C) during the field campaign (end of March to end of June, 2003). However, on average, the modelled temperatures are slightly warmer than those observed.

The temperature profiles in deep water can be compared with expendable bathythermograph (XBT) data collected near Scott Reef. Processed XBT records for all of northwest Australia were supplied by the CSIRO Marine Research Data Centre in Hobart. Of the hundreds of casts supplied, one XBT cast was taken within a degree of Scott Reef during the 2003 deployment period. This temperature profile was collected by a passing ship at 1 a.m. on 13 April. The top 100 metres of this XBT cast is plotted along with the corresponding temperature profile from the numerical model (Figure 4.7). At this particular point in time, the model overestimates the temperature in the top 30 metres and underestimates the temperature in the bottom 50 metres.

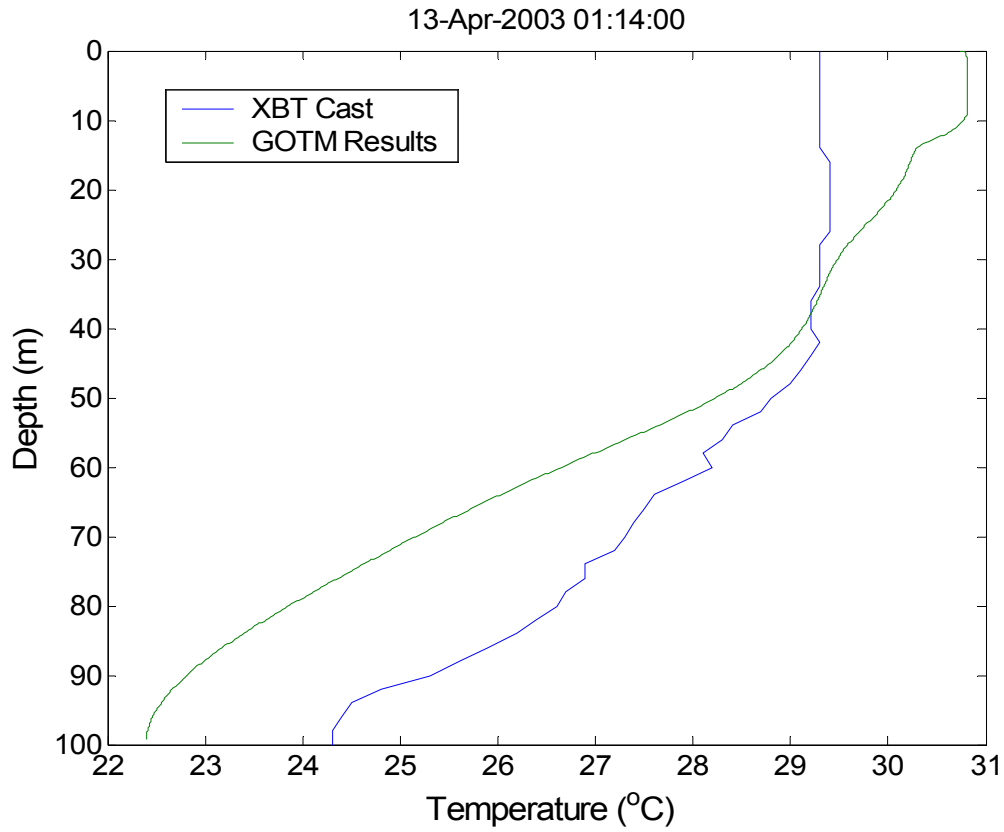

Figure 4.7 Model results are compared with an observed temperature profile collected near Scott Reef on the 13th of April. The observations suggest that the mixed layer depth is deeper than that calculated by the model.

The temperature disparity in the XBT cast is similar to the discrepancy noted earlier between the model results and temperature loggers within the lagoon. However in the deep water case, tidal currents have been removed from the model, indicating that they are not responsible for the temperature differences. The temperature differences appear to be caused by mixing rather than by an error in the fluxes across the air-sea interface; if the fluxes were incorrect, then the temperature of the fully-mixed water column starting in mid-May would deviate from the observed temperatures rather than align with it. Increased wind velocity would provide bottom-down mixing needed to better align the modelled and observed temperatures; however, the increased wind would remove energy from the water column through an increase in the latent heat flux. The overall result would be cooler-than-observed temperatures from mid-May onward.

Internal mixing can also be increased to lower the mixed layer depth. Kantha and Clayson used Large et al.'s (1994) internal mixing parameterization in the Northern Pacific Ocean and found that they needed to increase the suggested diffusivities by a factor of 5 (Kantha and Clayson, 1994, reported in Buchard 2001). However when the

Scott Reef model is run with increased internal wave diffusivities, the difference between the modelled and observed temperatures does not decrease significantly.

Effect of Turbidity on Water Temperatures

The simulated temperatures can be calibrated to field observations by varying the water turbidity in the model. The water turbidity dictates the rate at which shortwave radiation is absorbed. In turbid water, shortwave radiation will be absorbed in the first several metres, whereas shortwave radiation can penetrate to greater depths in clearer water. Since the radiation energy is transformed to heat, water turbidity has a significant effect on the vertical temperature distribution. In March 2003, the turbidity at Scott Reef was measured to be Jerlov water type II (Chapter 2). However, in this section it is shown that the observed water temperatures are closest to the modelled water temperatures when the turbidity is modelled as Jerlov type I.

There are two possibilities for this difference in turbidity. The first is that the observed water turbidity was not representative of Scott Reef during the modelled periods. The turbidity was estimated using only four CTD casts (twice down and up) as shown in Figure 2.5. Additionally these casts were taken close together and only hours apart. Turbidity can fluctuate seasonally and can vary dramatically in response to strong winds or storms. Water types IA and IB have been reported to the West and North of Scott Reef respectively (see Figure 2.1). Thus there is reason to believe that the measured turbidity may not be representative of the area.

Another possibility for the discrepancy in the turbidity is that there is another mechanism that is not accounted for in the model. It is possible that there is a physical process that is causing significant vertical mixing and is not accounted for in the model. Alternatively, numerical error or other computational artefacts of the vertical model could dampen the computed vertical mixing. Regardless of the reason for the discrepancy, the temperatures are best modelled when the water clarity is Jerlov type I.

The rest of this section describes the effects of turbidity on the water column temperatures. Figure 4.8 compares the modelled water temperatures (with Jerlov-type-I turbidity) with water temperatures collected in the field from the end of March to the end June, 2003. The modelled temperatures shown in Figure 4.8 are much closer to the field measurements than when the turbidity is modelled as Jerlov type II (Figure 4.4).

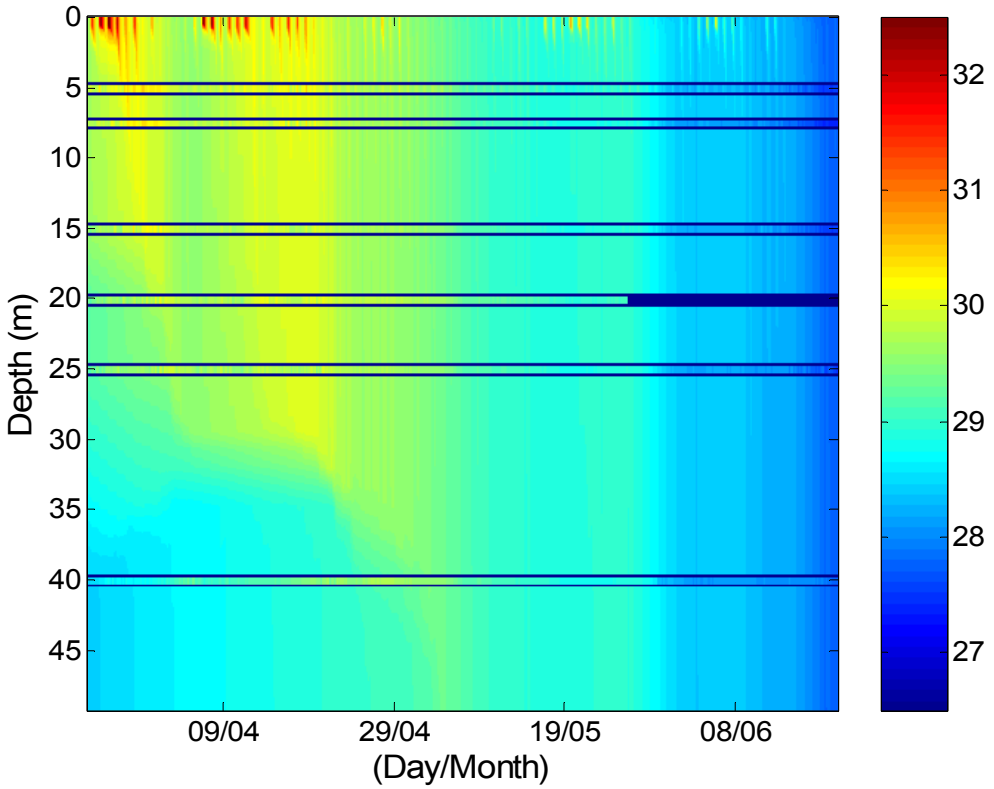

Figure 4.8 Temperature profiles (from the surface to 50 metres deep) numerically calculated at Scott Reef with water clarity modelled as Jerlov type I. The temperature profiles include the effects of internal waves, bottom friction and wind stress estimated for Scott Reef from the end of February to mid-June, 2003. The bars at 5, 7.5, 15, 20, 25, and 40 metres indicate actual temperature observations at this site.

Different water types do not have a substantial effect on the sea surface temperature (Figure 4.9). The only difference is the daily range of SST, with clearest water (type I) almost doubling the range of the most turbid water (type II). The daily average of the SSTs does not change much because of the feedback through the air-sea heat fluxes. This can be explained as follows. The top layer of turbid water absorbs more energy than clearer water, causing it to rise in temperature. As the sea surface temperature rises, the fluxes respond by providing less heat slowing down and potentially stopping the SST increase. For clearer water, less energy is absorbed by the top layer so that the fluxes continue to provide heat to the water column. This suggests that the overall energy transferred into the water column is greater for clearer water than turbid water. However if the water column eventually becomes well-mixed, any temperature increase will dissipate through the balance of heat fluxes, using the same arguments as just presented.

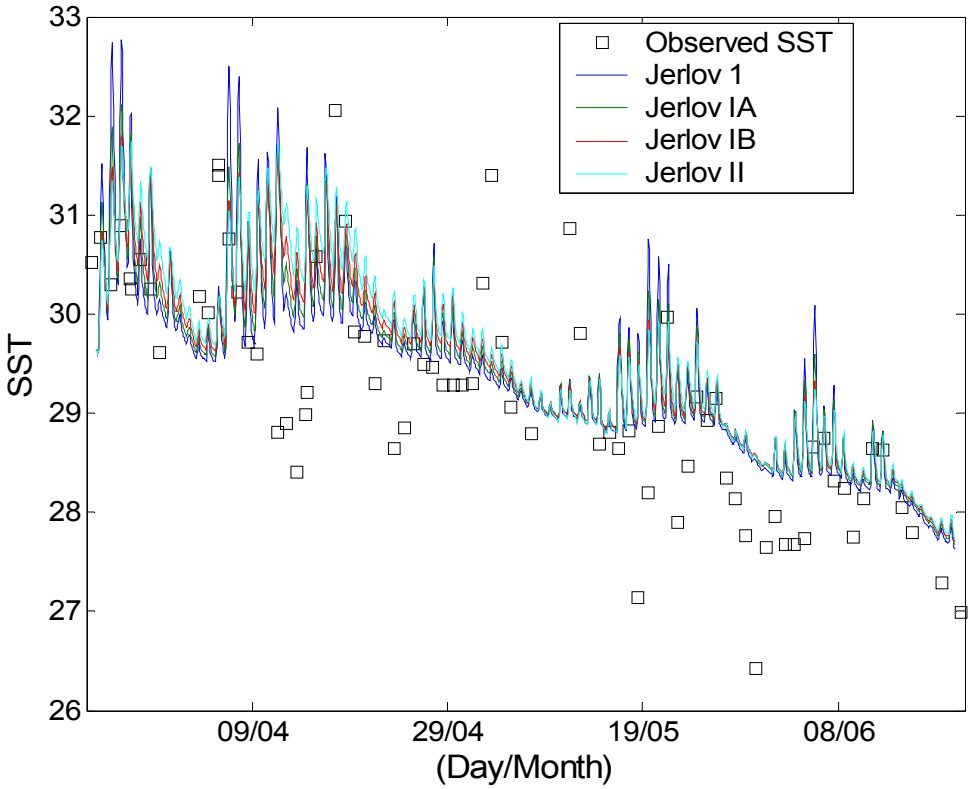

Figure 4.9 Sea surface temperature (°C) for various water clarities are compared to observations during the field campaign (end of March to end of June, 2003). Altering the Jerlov water type in the model does not significantly change the modelled sea surface temperature. The only noticeable effect is that clearer water creates larger diurnal fluctuations.

The effects of turbidity can also be compared to the deep-water temperature profile from the XBT data (Figure 4.10). The profiles from model runs with water types IA and II are omitted from Figure 4.10 for clarity, and lie between the other model curves. The figure illustrates how increasing the water clarity has a similar effect to mixing the top layers of water. Below 50 metres, the water clarity has little effect on the temperature distribution. The XBT record indicates that even with the clearest water type, the model is over predicting temperatures in the top 30 metres by about 1°C. This finding is in marked contrast to the lagoon field observations. The observed temperatures in the lagoon (Figures 4.8) agree for the most part with those of the model to within a small fraction of a degree. Surprisingly, the XBT record also shows that water 100 metres deep is being heated substantially more than the model predicts. This heating is an indication that a deeper water mixing mechanism is not being taken into account. It is important to note that the XBT cast was taken only once and therefore may not be representative of the overall temperature distribution, especially since internal waves can distort the temperature profile results.

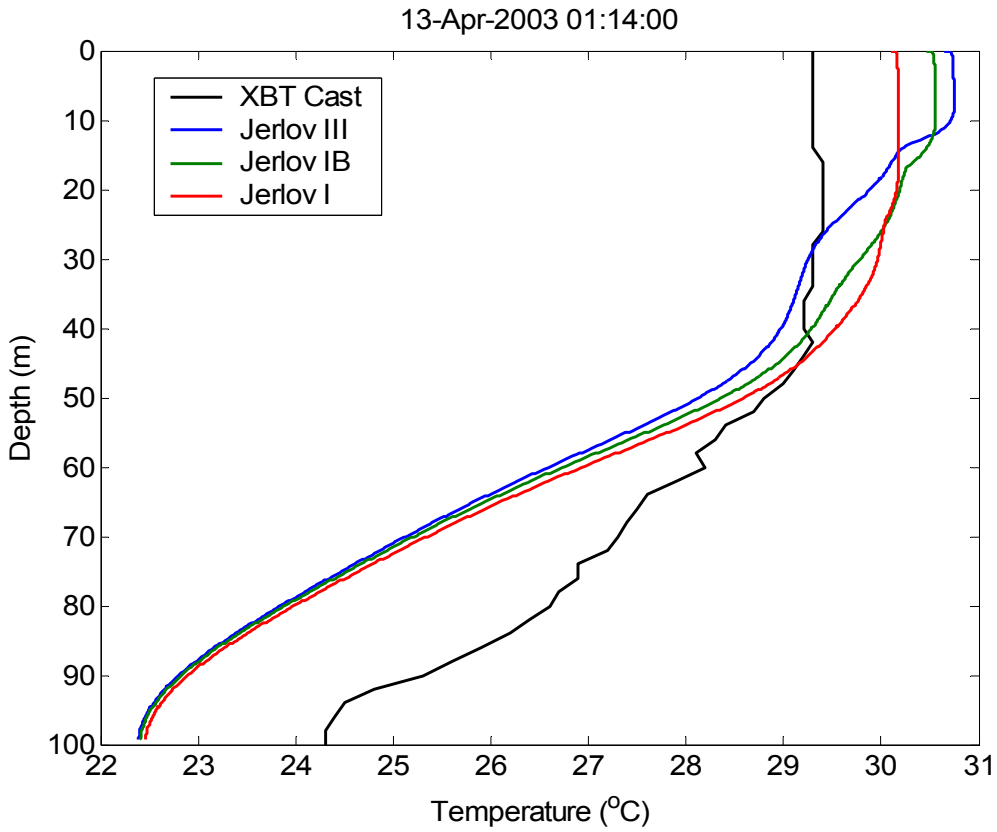

Figure 4.10 Model results for various water clarities are compared with an observed temperature profile collected near Scott Reef on the 13th of April. Lowering the turbidity has the effect of lowering the mixed layer depth.

There are two main processes influencing vertical temperatures that the water column model does not take into account. The first is mixing due to salinity gradients formed by precipitation and evaporation. As discussed briefly in Chapter 3, precipitation rates are nearly impossible to estimate with the accuracy required to include them in the model, as no precipitation measurements were taken near Scott Reef. For this reason, the model has been driven solely by tidal currents, wind stress, and heat fluxes across the air-sea interface. The model also neglects water advection. The field observations in Chapter 2 provide evidence that there may be slow-moving net currents passing through the region. However, the ability of the numerical model to predict temperatures illustrates that water advected into the region is roughly the same temperature. The meteorological data acquired and processed in Chapter 3 did not vary substantially between stations. Thus, while the heat and fluxes were estimated for Scott Reef, they are more or less applicable to the entire Timor Sea (the waters off northwest Australia). Therefore, any advected water should have roughly the same energy content. However,

the distribution of this energy throughout the water column can potentially change, based on location. Shallower water on the inner shelf may mix before being advected into deeper water, producing a well-mixed upper layer. Water in less productive areas may be clearer and absorb the shortwave energy deeper in the water column. If these waters advect over Scott Reef, a deeper mixed layer will be observed. While the model may ignore advection, there are some parameters that can be tweaked, such as water turbidity, to indirectly include these advection effects. Thus for the rest of this study water turbidity will be modelled as type I.

Linking water temperature features with atmospheric conditions

One of the key aspects of using a thermodynamic model to estimate water temperature is that there are physical explanations for any noteworthy result. Any distinctive features in the field observations that are also produced in the thermodynamic model must result from fluxes across the air-sea interface, rather than the advection of cold water, as the latter can not be simulated by the model. One striking example is the sharp cooling at the end of May (Figure 4.11). To add context to the physical nature of the model, the actual driving forces causing the sharp cooling will now be identified.

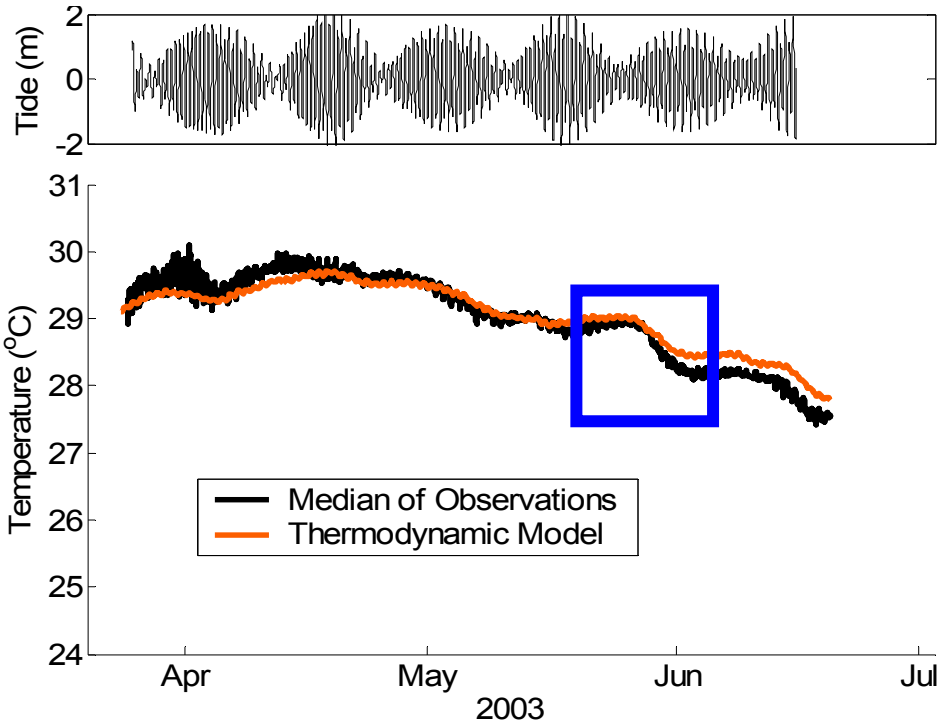

Figure 4.11 Meteorological conditions cause the modelled temperatures to sharply cool at the end of May. A similar cooling is observed in the water temperature records.

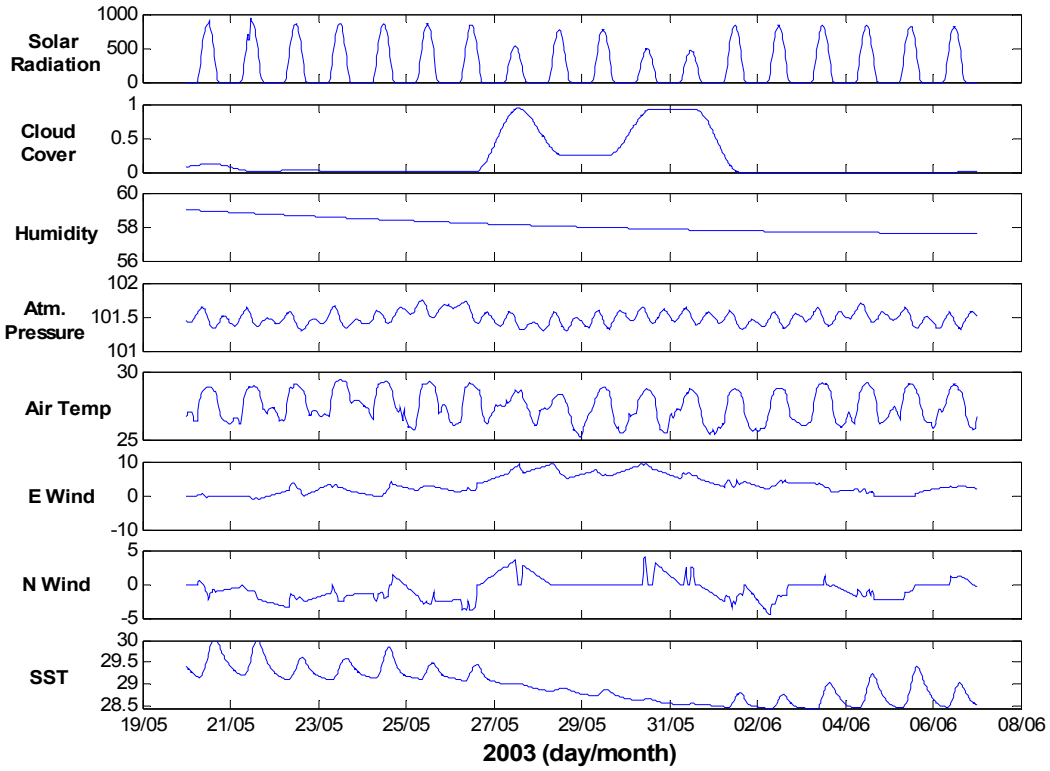

Figure 4.12 Meteorological conditions for the 20 days surrounding the distinctive cooling period in water temperatures at Scott Reef in May 2003.

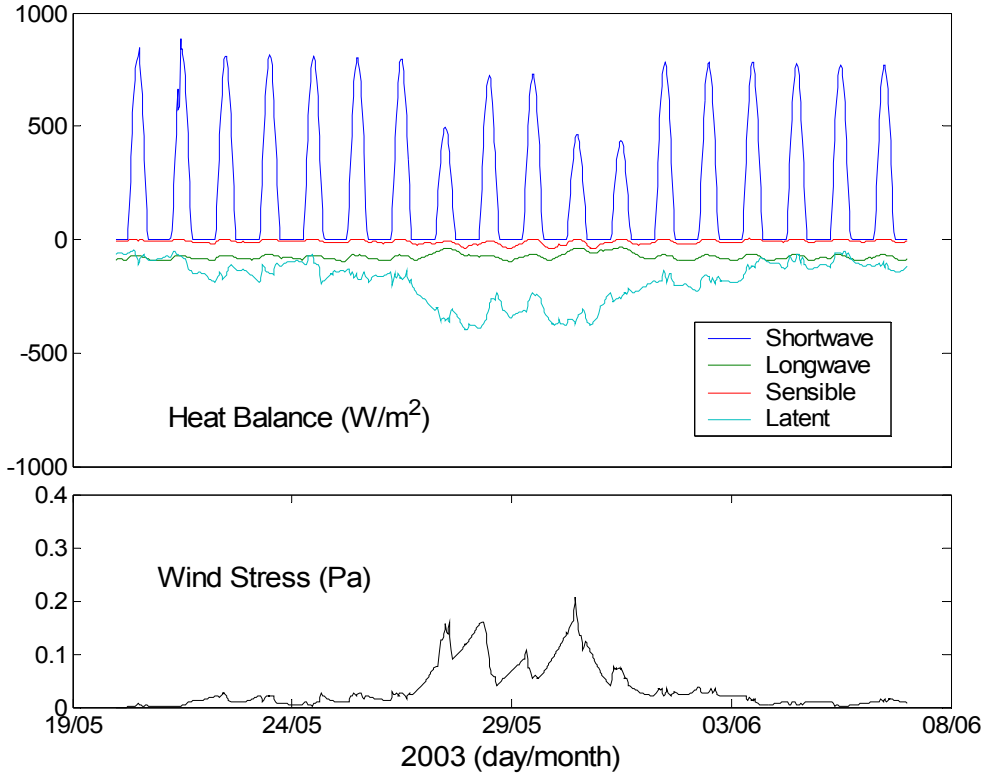

Figure 4.13 The heat fluxes and wind stress associated with the meteorological conditions in Figure 4.12 are calculated for the 20 days surrounding the distinctive cooling period. A combination of decreased shortwave radiation into the water column and increased latent flux out of the water column is responsible for the cooling.

The meteorological data for the 20 days surrounding the cooling episode are plotted in Figure 4.12. Moving from the bottom of the plot to the top, the sea surface temperatures undergo a quick drop from the 27th of May to the 2nd of June. This is accompanied by an increase in the easterly component of the wind during that period. The air temperatures drop slightly and the atmospheric pressure and humidity remain fairly constant. Cloud cover increases from the 27th to the 2nd, and as a result solar radiation drops. Overall it is difficult to ascertain the degree to which the different measurements affect the heat balance. Using the bulk formulas identified in Chapter 3, the wind stress and each component of the heat balance can be calculated (Figure 4.13).

During the cooling event, the shortwave radiation dropped due to the cloud cover. The cloud cover also increased the net longwave radiation back into the water column while the cooler temperatures and higher winds increased the sensible heat flux out of the water column. However the longwave and sensible heats fluxes were minor compared to the large latent flux (evaporation), due to the strong winds and relatively low humidity. The atmospheric conditions were able to cool the water column quickly, in part because of the increased mixing due to the night-time surface cooling and increased wind stress.

Sensitivity Analysis

Determining the effect of each component of the meteorological data (for example cloud cover and humidity) has on the water column temperature is not trivial as all the components interact nonlinearly with each other and the water column to form the net heat fluxes. However such knowledge would enable future work to concentrate effort on accurately estimating certain key components, rather than using resources to improve the accuracy for less important factors.

The thermodynamic model was run under varying conditions to provide a sensitivity analysis for the meteorological components. Table 4.1 lists the changes in the water temperature based on changes in the source condition by a prescribed amount (the uncertainty). For example, the effect of wind was found by running the model three times. The first simulation is run with the "true" wind velocities. The second and third simulations are run using wind velocities that are consistently 2.9 m s^{-1} higher and lower

respectively than the "true" wind velocities. It was found that offsetting the wind velocities by 2.9 m s^{-1} raised or lowered the simulated temperature by about 2.0°C.

The uncertainty values were chosen as the estimated standard deviation of the field measurements in Chapter 2 and thus reflect the uncertainty in the meteorological data in this study. The effect on temperature should be interpreted as purely as a relative quantity, and not the actual uncertainty for the numerical results presented throughout this thesis.

Source	**Uncertainty**	**Effect**
Wind	2.9 m s^{-1}	2.0°C
Humidity	15%	1.0°C
Air Temp	1.2°C	0.5°C
Cloud Cover	20%	0.1°C
Atm. Pressure	0.1 hPa	0.0001°C

Table 4.1 The relative effect of the uncertainties in the meteorological conditions on the water temperature.

The sensitivity analysis demonstrates that the present uncertainty in wind and humidity measurements have the largest effect on the water column temperatures. Future work should address the accuracy of these measurements before improving the cloud cover estimation techniques.

Hindcast of 1998 bleaching conditions

A major goal of this project is to model the water temperature profiles during the 1998 bleaching event. In fact, the main point in calibrating and verifying the model with 2003 data was to confirm that the method presented thus far would be appropriate to model the 1998 event.

Atmospheric data and satellite images recorded in 1998 are available to derive air-sea fluxes, and one XBT cast was taken near Scott Reef in April. However, an initial profile will have to be estimated as no temperature profiles were measured in the period leading up to the bleaching event. In cases where the initial condition needs to be estimated, it is best to start experimental runs when the water column is well-mixed (Martin, 1985), which generally occurs in winter. Unfortunately, this is not an option in 1998 due to gaps in the meteorological measurements. Nearly continuous meteorological records are available from the 13th of February 1998 through the bleaching event. SST from satellite images indicated that the surface temperatures were below bleaching thresholds in February 1998, rose to record temperatures at the end of March, and then dropped to "safe" temperatures by the end of April. In this study, temperatures are modelled from the 14th of February until the 30th of April, 1998.

Estimation and Effect of Initial Profile

The initial profile for the 1998 model runs was estimated from the CSIRO Atlas of Regional Seas (CARS), as it provides an interpolated grid of water properties for each day over a standard climatological year (Ridgway and Dunn, 2002). CARS temperature profiles consist of mean, annual, and semi-annual signals for temperatures around the Australian seas, to depths of 1000 metres (the mean is supplied for even greater depths). These profiles are derived from a combination of NODC (National Oceanographic Data Center) World Ocean Atlas 1998 hydrographic data and Australian hydrographic data from the CSIRO archive. A reconstruction of the top 50 metres of climatological water temperatures at Scott Reef is shown in Figure 4.14. Two years are given to illustrate the cyclic nature of the data. The warmest water occurs in January when the top 20 metres reaches 30°C. However, the water at 30 metres and below continues to warm until

May. The top 50 metres, stratified in January, becomes well-mixed in April and continues to cool until September.

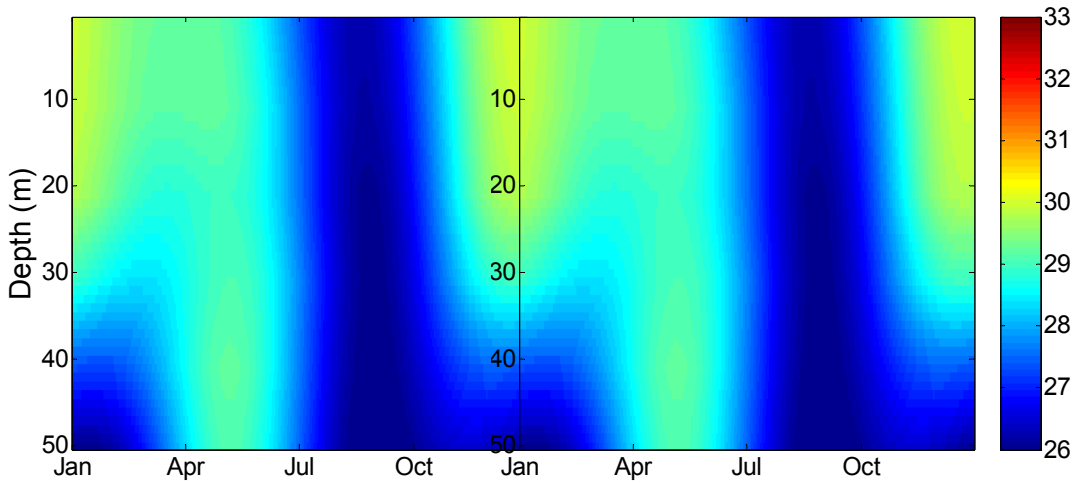

Figure 4.14 CARS temperature profile data in the vicinity of Scott Reef over two climatological years. Two years are shown to illustrate the seasonal cycle.

From the CARS data (Figure 4.14), it would seem that the ideal time to start the thermodynamic model would be between September and October, as the water column is mixed the most during this period. However since gaps in available data force the starting time to be in mid-February, it becomes crucial to estimate how sensitive the temperature profiles are to the initial condition. This sensitivity is estimated by comparing two model runs, one using a measured initial profile and the other using an initial profile from the climatological data. An XBT cast was taken by a ship passing near Scott Reef on the 24th of February, 2003. This profile measured 30°C water down to 40 metres, at which point there was a sharp thermocline. CARS data from the same climatological day indicate that the 24th of February is typically cooler, with the top 30 metres being well-mixed at around 29°C. The thermodynamic model was run once for each profile using the fluxes calculated in Chapter 3 and a water turbidity of Jerlov type I. Figure 4.15 shows the vertical temperatures in the top 60 metres for the 4 month period. Even with significantly different initial profiles, the modelled temperatures share the same features. Furthermore, the difference in temperature between the two runs decreases over time. The two profiles are initially different by about 1°C; however by the end of the first month, the top 10 metres are within 0.3°C. The initial profile has less of an effect on areas where heating and mixing occur; the difference in temperature in 2003 between the two runs is least in the sections exposed to heating at the beginning

and middle of April. This observation is evidence that using a climatological initial profile in 1998 will have an even less effect than doing so in 2003, as the period of interest in 1998 was marked by excessive heating.

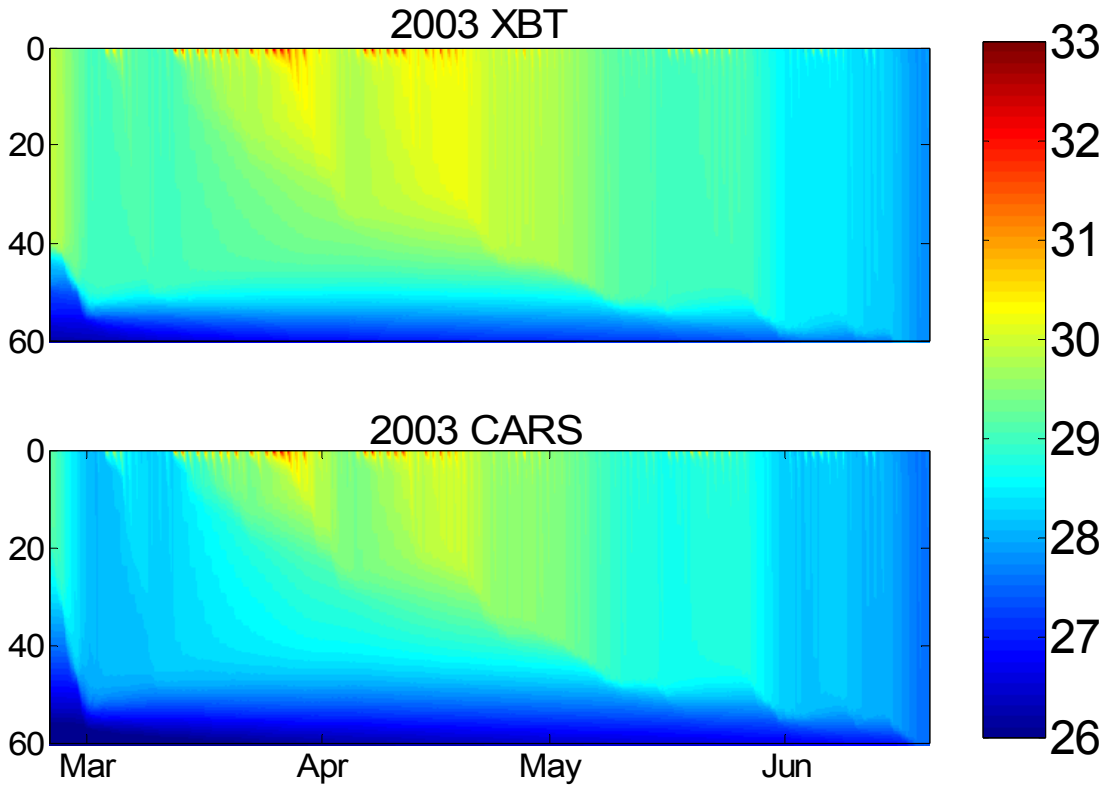

Figure 4.15 Modelled water temperature profiles (°C) from surface to 60 metres from March to the end of June 2003. The top graph shows the evolution of temperatures when started with an observed initial profile (from an XBT cast). The bottom graph depicts the evolution of temperatures when started with an climatological initial profile.

1998 Temperature Profile

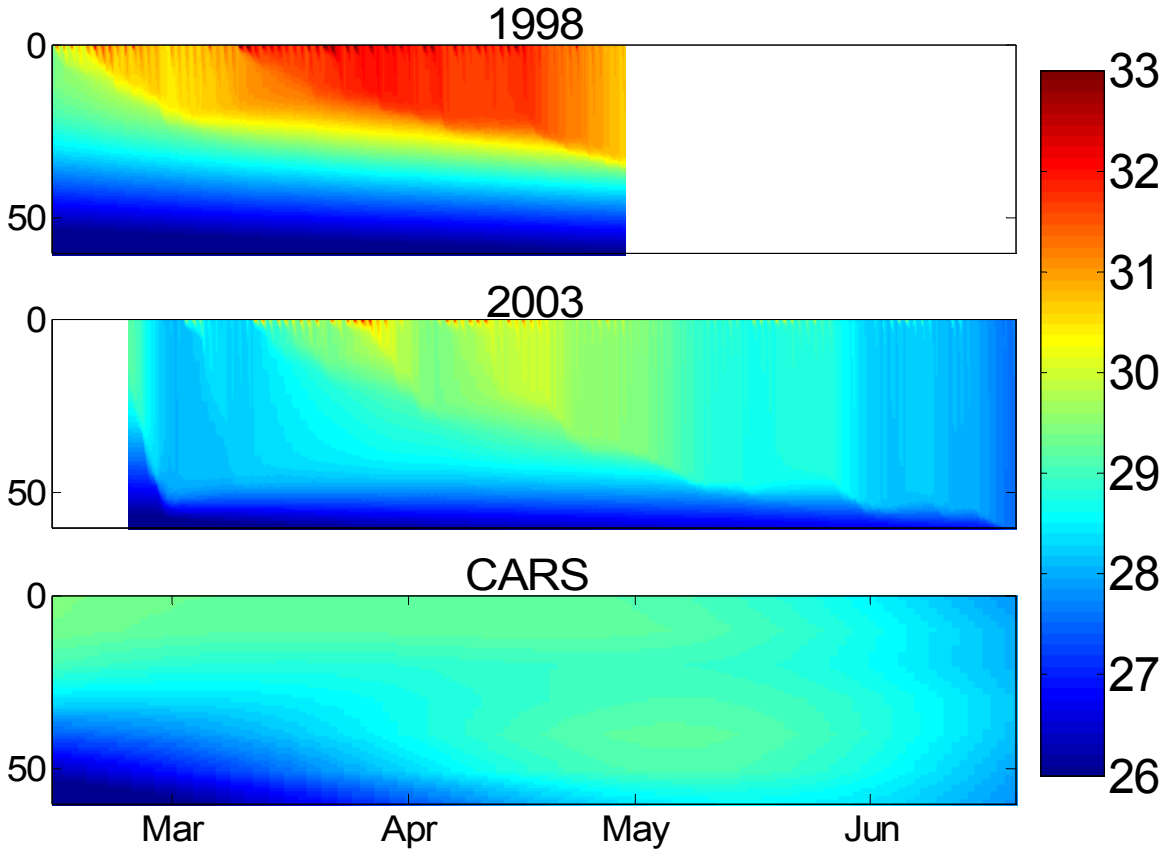

Figure 4.16 Modelled water temperature profiles (°C) from surface to 60 metres are compared, showing 1998 (top), 2003 (middle), and the climatological average (bottom). The model is able to hindcast a water temperature anomaly for the Scott Reef region in 1998.

GOTM hindcasts water temperatures in 1998 that far exceed the 2003 results and climatological average (Figure 4.16). The temperatures remain stratified throughout the period modelled. Temperatures of up to 34°C were hindcast near the water surface (Figure 4.17) and temperatures exceeding 30°C were present down to 35 metres. The model results depict the time evolution of the thermal structure. Interestingly, it appears that the bulk of the heating started after the first week of March. However, the temperatures were able to increase markedly partly because of an earlier heating period at the end of February. The late February heating was mixed downwards by the strong winds at the beginning of March, and as a consequence warmed the top 20 metres.

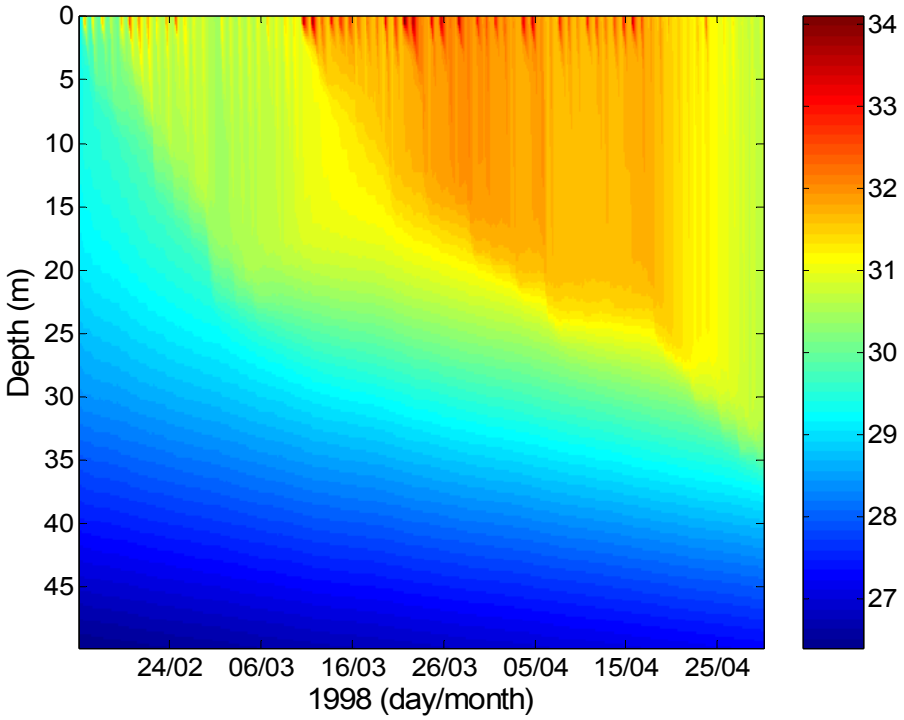

Figure 4.17 Modelled water temperature profile at Scott Reef for the period February to April 1998. The temperature scale is slightly different from that in Figure 4.16, in order to depict temperature variations in the near-surface waters.

Comparison with observed SST and XBT Profile

The only temperature data collected near Scott Reef during the bleaching period were from satellite images and a single XBT cast taken on the 19th of April. These measurements are compared to model results in Figures 4.18. Both sets of measurements confirm that the model hindcast is realistic. The observed SST tends to be lower than the model prediction; this is especially evident in periods when the observed SST quickly cools. Nevertheless, the relation between the two is good, considering that the fluxes driving the model are calculated in a data-sparse area and some mixing mechanisms (e.g. precipitation) are not included. Additionally, the 1998 period was unusually cloudy, leading to the underestimation of the observed SST.

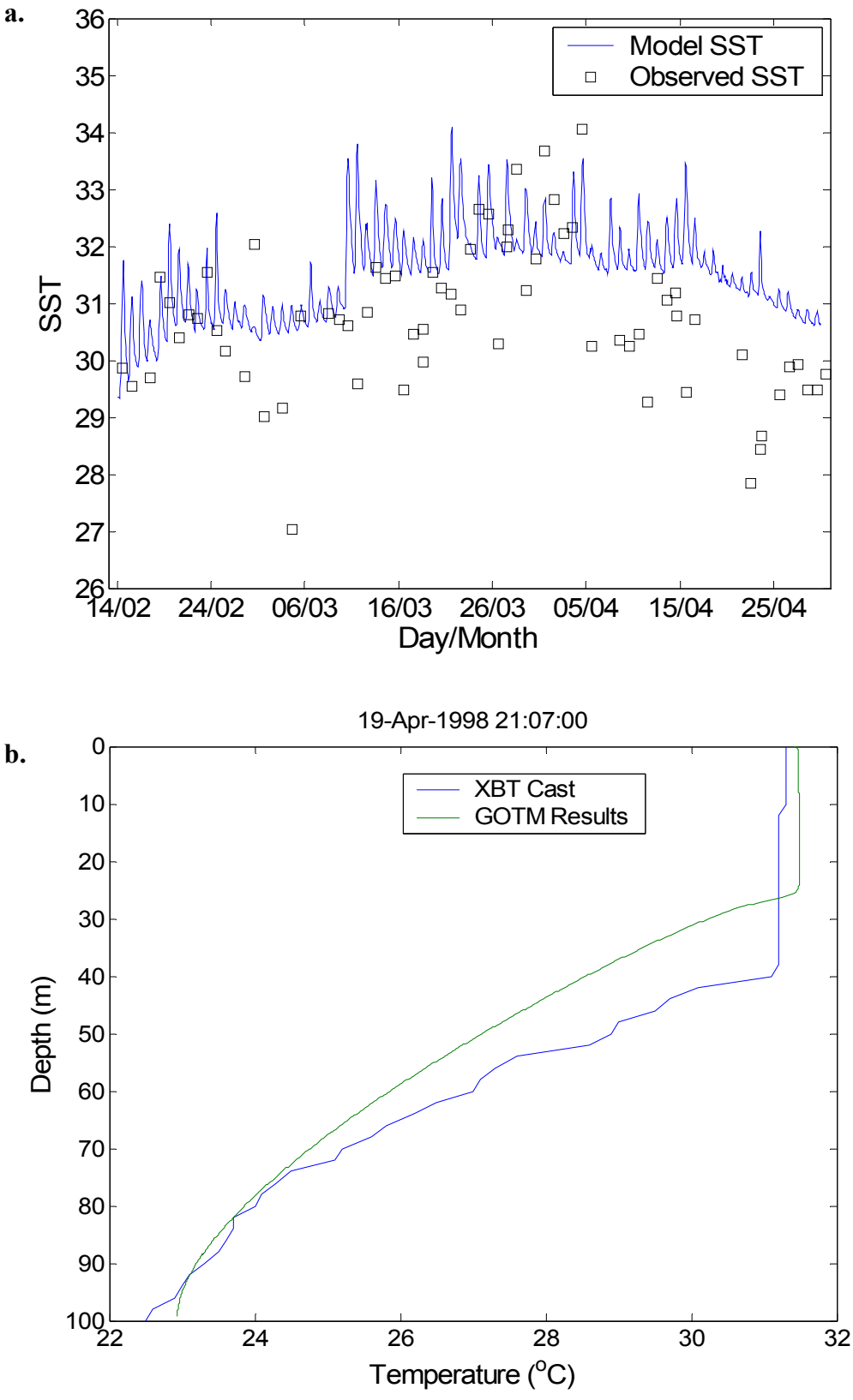

Figure 4.18 The modelled temperatures for the 1998 bleaching period are compared with sea surface temperature observations (top) and a temperature profile record (bottom).

The 1998 XBT cast is much closer to the 1998 GOTM results (Figure 4.18b) than the 2003 XBT cast was to the 2003 GOTM results (Figure 4.7). The fact that the deep-water (100 m) temperatures in the 1998 XBT cast, 1998 simulation, and 2003 simulation were roughly the same (22–23°C) suggests that the abnormally high temperature observed at 100 m in the 2003 XBT cast (24–25°C) was more likely due to a local effect (such as internal tides) than to enhanced deep-water mixing. Both the 1998 XBT cast and the 1998 model results show a distinct thermocline in the top 50 metres. The XBT cast indicates that the thermocline is at a depth of 40 metres, whereas GOTM hindcasts the thermocline to be at a depth of 25 metres. Thermoclines can rise and fall quickly from internal oceanographic processes not accounted for in the model. Because only one profile was observed, it is impossible to determine a representative height of the thermocline from the observation. At the same time, the model neglects some oceanographic processes (e.g. advection and salinity) which may lead to a shallower mixed depth layer. Overall, the oceanographic records available in 1998 support the model results.

Vertical Temperature Anomalies and Coral Bleaching

The hindcast shows that water temperatures in 1998 exceeded the expected temperatures during that time period by several degrees (Figure 4.16). However, the high water temperatures do not show the degree to which the corals may be stressed.

As described in Chapter 1, the NOAA-NESDIS product, HotSpots, locates areas of potential coral stress by mapping the difference between the observed anomalous SST temperature and the maximum monthly mean at that location (Liu et al., 2003). Motivated by the HotSpot technique, a similar methodology can be applied vertically through the water column. In this case, the maximum climatological average at each depth is chosen as a reference (as opposed to the maximum monthly mean). These temperatures are derived from the CARS data set. It is important to note that these reference temperatures are not necessarily taken from the same time period. In the case of Scott Reef, the maximum temperatures in the top 20 metres typically occur in late December. However, temperatures around 40 metres reach their maximum in May.

The corals at a particular depth are adapted to the average maximum temperatures at that depth; therefore the time that the maximum is reached should not be a factor.

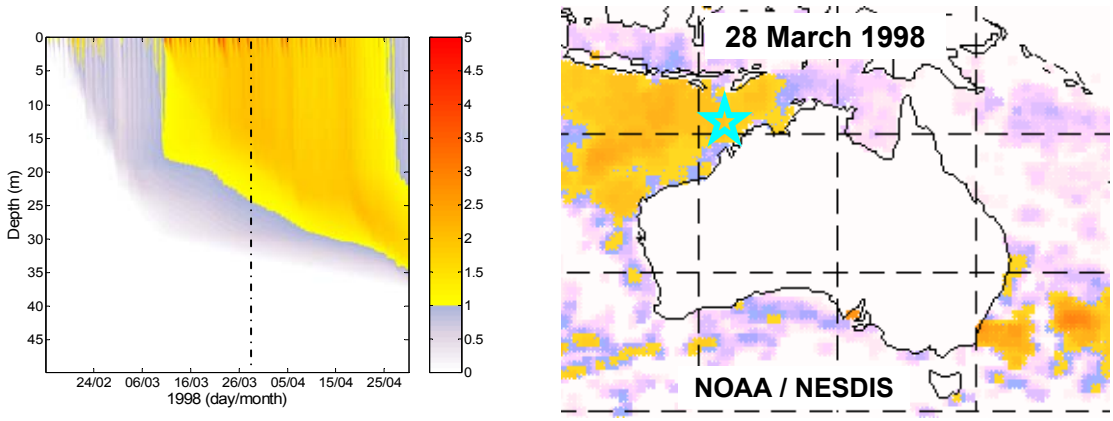

Figure 4.19 HotSpot products: **a. (left)** Prototype vertical water column through time and **b. (right)** the established spatial NOAA-NESDIS satellite product. The vertical line in Figure 4.19a denotes the vertical temperature profile that corresponds to Figure 4.19b.

The Water-column HotSpot map shows that the predicted water temperature in the top five metres exceeded the maximum average by over 3°C (Figure 4.19a). Additionally, the model shows water as deep as 35 metres became warm enough to stress corals. The model simulation ends before the deeper water drops below the 1°C anomaly mark; however, it seems likely that the warm water would continue to mix downward as the water column mixed. The plot suggests that while the hottest SST temperatures were measured at the end of March, the corals were under thermal stress until the end of April.

As mentioned earlier, coral bleaching and mortality depend not just on the intensity of stress, but also on its duration. NOAA-NESDIS investigates the duration of temperature stress through their Degree-Heating-Weeks product. Degree-Heating-Weeks are a time integration of satellite-observed temperature stress. Since temperature stress starts to occur roughly 1°C above the maximum monthly mean temperature, only temperatures at or above this threshold are included the Degree-Heating-Weeks product. Using the same criteria, a time-integration of the water column temperature stresses can be calculated (Figure 4.20a). The scale on the Degree-Heating-Weeks product and the vertical coral stress indicator is in°C-Weeks. A value of 10°C-Weeks would result from 5 weeks of 2°C above maximum expect temperatures or 2 weeks of temperatures 5°C above the maximum expected, etc. Surveys have shown that bleaching begins to occur when the Degree-Heating-Weeks reaches a value of around 4°C-Weeks. Major

bleaching and mortality have been correlated with Degree-Heating-Weeks values of 10 and above (Liu et al., 2003).

An elevation plot of the degree-heating-weeks (Figure 4.20) indicates that the coral bleaching threshold (4°C-Weeks) was reached at depths of 30 metres at Scott Reef. This finding is in line with observations recorded at the Reef directly following the 1998 bleaching episode. The results indicate that while bleaching may have reached 30 metres, the severe bleaching and mortality were limited to the top 20 metres of the water column.

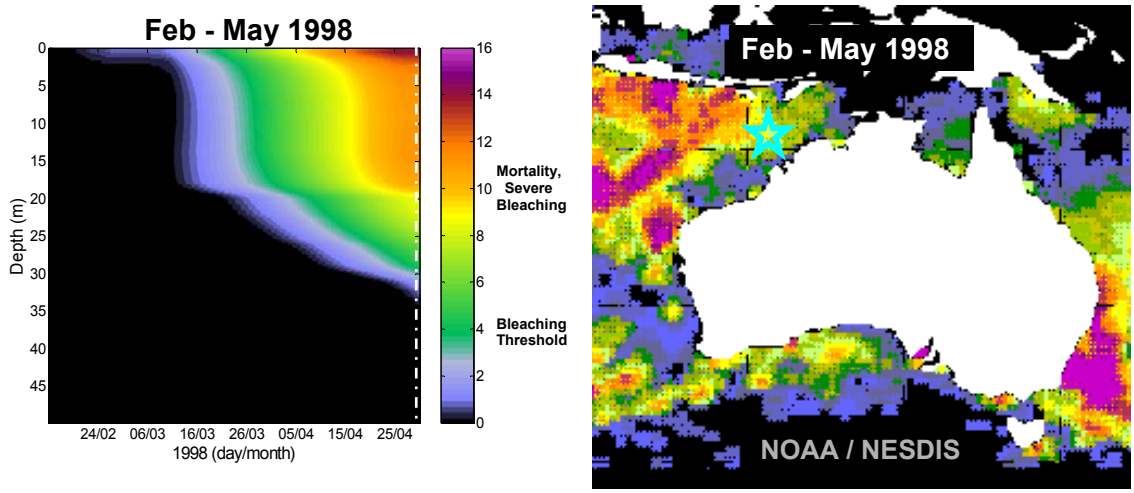

Figure 4.20 Degree-Heating-Week products: **a. (left)** Prototype vertical water column through time and **b. (right)** the established spatial NOAA-NESDIS satellite product.

The NOAA HotSpots image taken on the 28th of March, 1998 shows a similar surface temperature to the water column results for that day (Figure 4.18b). However, the NOAA Degree-Heating-Weeks product and the water column equivalent show discrepancies in the time-integrated temperature stress at Scott Reef. Figure 4.20b shows the cumulated stress over a 90 day period ending the 30 of April, 1998 (courtesy of NOAA / NESDIS). At Scott Reef, this 90 day cumulation resulted in a temperature stress of 8°C-Weeks. The water column time-temperature integration was run over roughly the same period; the vertical model starts on the 14th of February instead of the 31st of January. The only effect possible for a shortened time-temperature integration period is a lower Degree-Heating-Weeks value, as only temperatures above the 1°C threshold are included. However, the water column model indicates that by the last day of April, the surface reached 14°C-Weeks. Such discrepancies are significant and should be investigated further. It is worth noting that the water column model neglects horizontal advection and may over-simplify some of the mixing processes. At the same

time, the NOAA model is derived from satellite temperature observations; this period in 1998 was abnormally cloudy and an underestimation in the time-temperature integration may have resulted. As mentioned earlier, major bleaching and mortality have been correlated with Degree-Heating-Weeks values of at least 10°C-Weeks (Liu et al., 2003). Therefore, it would be surprising if the unprecedented coral mortality observed at Scott Reef corresponded with a lower Degree-Heating-Weeks value.

Summary and Concluding Remarks

In this chapter, the numerical water column model, GOTM, was used to simulate the water temperature profiles in the Scott Reef region. The model was set up to investigate the role of wind stress, tidal currents, and internal mixing. The simulations were compared to temperature observations taken during 2003, and it was found that model results were realistic when the Jerlov water type was approximated as Type I. One of the key findings is that the temperature simulations were able to match the major thermal features observed at Scott Reef during that period, despite the distance of the weather stations.

The temperature simulations of the 1998 bleaching episode were also successful. The model results provide insight into how the atmospheric conditions affected the temperatures in the water column. The similarity between the observed and simulated temperatures is evidence that the elevated water temperatures at Scott Reef were generated from local atmospheric conditions rather than by an alternative oceanographic process, such as advection.

The simulations also provide a new technique to predict coral bleaching at various depths. The simulated temperature profiles were converted into a format analogous to the NOAA's HotSpot and Degree-Heating-Weeks products. These results illustrated that anomalously warm water temperatures penetrated to depths of 30 metres and persisted over a period of time that is consistent with the severity of coral bleaching observed at those depths.

Chapter 5 – Scott Reef Mixing and Thermodynamics

The temperature profiles hindcast for the Scott Reef region in Chapter 4 can account for the 30 m deep bleaching of corals in March and April of 1998. However, the single profile cannot explain why corals in particular locations were more susceptible to bleaching than corals in other locations around Scott Reef. One explanation is that the temperature profile developed in Chapter 4 neglected tidal mixing in the topographically complex reef environment. Although tidal mixing is negligible in the deep, slow moving water surrounding Scott Reef, tidally-driven currents closer to the reef can dramatically enhance mixing, especially in the shallower regions. It is quite possible that mechanisms other than temperature were responsible for the spatial variability of the bleaching. However when investigating any other factors, one must first control for temperature, as thermal stress is the primary cause for mass coral bleaching (Hoegh-Guldberg, 1999). Therefore, regardless of the cause of the spatial discrepancies in bleaching, the first step is to estimate the importance of temperature in controlling the patchiness of coral bleaching.

The best method to determine the three-dimensional temperature distribution around and on Scott Reef would be to use a full three-dimensional, baroclinic hydrodynamic model. Such models are difficult to set up and are computationally expensive. The goal of this chapter is to determine if an economical combination of GOTM and a two-dimensional barotropic model can adequately approximate any sub-reef-scale temperature variations along Scott Reef in lieu of a full three-dimensional, baroclinic model.

Spatial Variability in Coral Mortality at Scott Reef

Coral Cover Surveys

Smith et al. (2003) surveyed coral cover by video techniques at six locations around Scott Reef (Figure 5.1). Each location is comprised of 3 sites separated by 100 to 200 metres. Within each site, corals are surveyed along five 8–9 metre deep, 50 metre long transects, each separated by 10 metres. Therefore a total of 90 coral cover surveys are taken each year. For each survey, the video is analysed to determine the proportion of

each coral family as well as the percentage coverage of coralline algae, turf, and any other category deemed relevant.

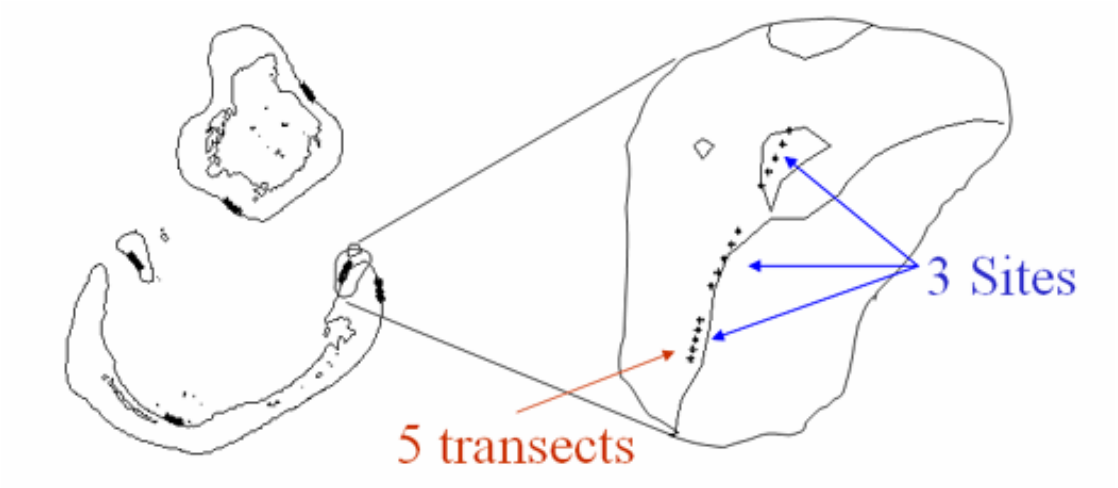

Figure 5.1 Coral cover measurements are collected along 90 transects at Scott Reef. Five transects are taken at each of the 18 sites situated at 6 distinct locations. The transects are at a depth between 8 and 9 metres and are plotted above with the eight-metre contour of Scott Reef.

As part of this project, the pre- and post-bleaching coral coverage records gathered and analysed by Smith et al. (2003) are converted into a coral survival rate (Figure 5.2). The percent survival at each transect is calculated as the difference in coral cover between November 1997 and December 1998 (pre- and post-bleaching) divided by the November 1997 coverage. The results are averaged over the 15 transects at each location. Figure 5.2 shows that on average, more corals survived at Sites 3 and 4 than at the other locations. Corals at Sites 2 and 5 fared the worst.

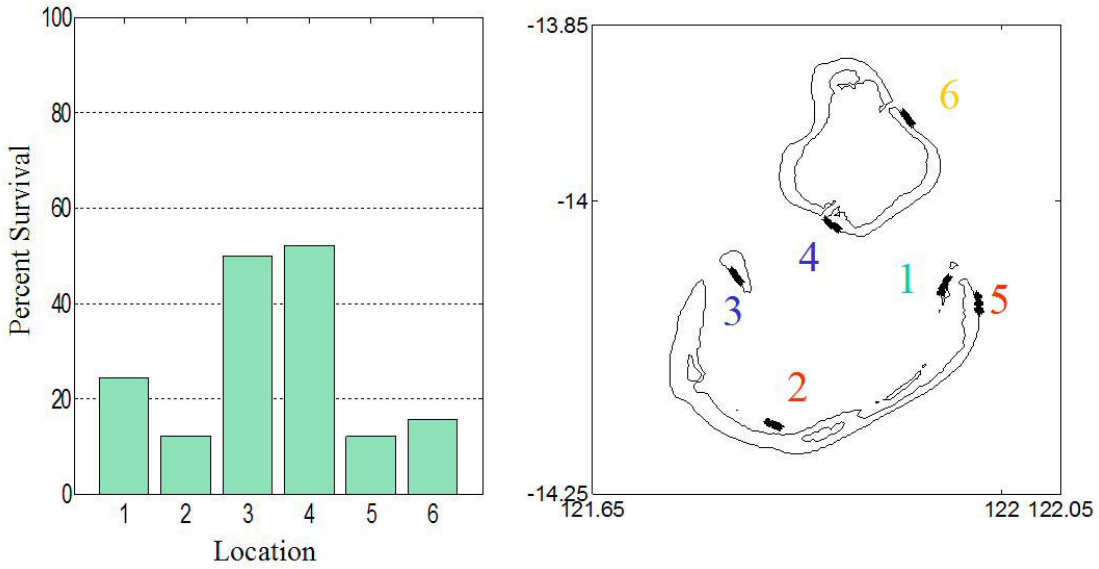

Figure 5.2 Plot showing the percentage of coral survival at each of the monitoring locations after the 1998 coral bleaching event.

Accounting for Coral Taxonomy

As discussed in Chapter 1, different types of coral exhibit varying reactions to thermal stress. Marshall and Baird (2000) found that *Acropora* and other faster-growing corals were more prone to bleaching and temperature-induced mortality than the massive corals, such as *Porites*. Therefore it is necessary to confirm that the coral survival results shown in Figure 5.2 are not due to differences in coral taxonomy – such as a disproportionately large population of *Porites* at Locations 3 and 4.

Smith et al. (2003) determined the percentage of coral coverage of each family along each of the 90 transects. The majority of corals at Scott Reef belong to the *Acroporidae* family although the *Poritidae*, *Alcyoniidae*, *Faviidae*, and *Pocilloporidae* families are also found in large numbers (Figure 5.3).

When the coral survival at each location is controlled for family (Figure 5.3), it is still clear that corals at Sites 3 and 4 survived more than those at the other locations. All five families had the largest survival rates at Sites 3 and 4, although the survival rates of the *Portidae* family at Sites 5 and 6 were surprisingly high. There is no statistically significant difference between the survival rates at Sites 1, 2, 5, and 6, but when only the most vulnerable corals (Pocilloporids and Acroporids) are considered, Sites 2 and 5 have significantly lower survival rates than Sites 1 and 6.

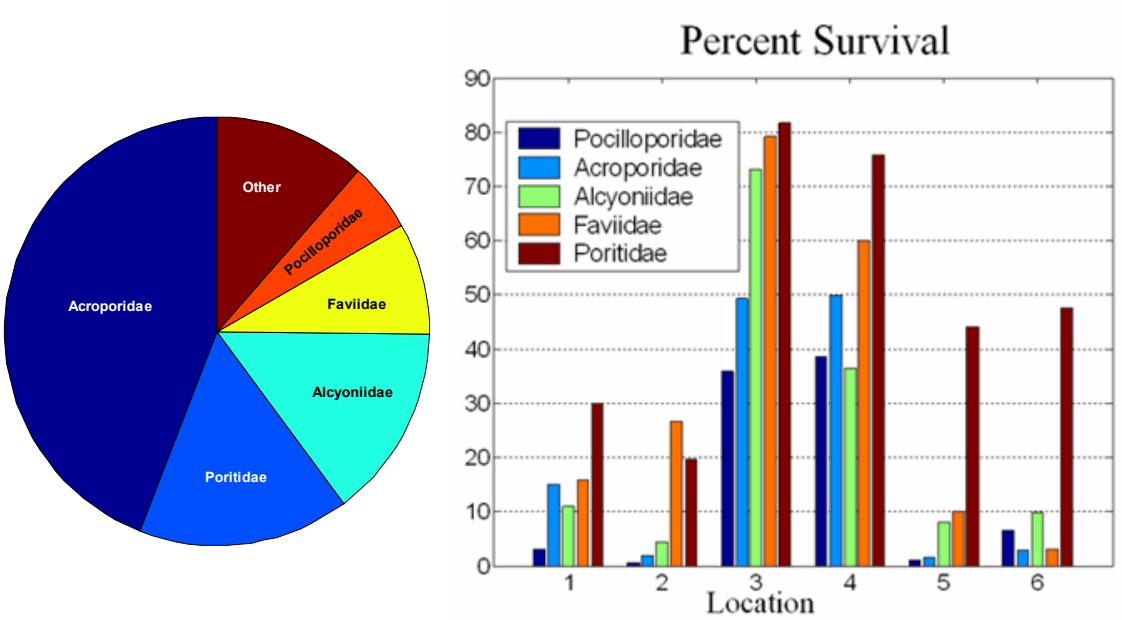

Figure 5.3 The percentage survival after the 1998 coral bleaching event is shown for each of the five most common families at each of the six locations. The relative areal representation of the families averaged over all of the location is shown in the pie graph.

Tidal Mixing

Tidal currents interact with the bottom through friction to create bottom-up mixing. Simultaneously, solar heating acts to stabilise the water column. Simpson and Hunter (1974) discovered that the vertical mixing in the water column can be described by a balance between turbulent mixing from the kinetic energy of the tidal current, and a demand for potential energy to maintain a stratified condition due to the buoyancy input to the sea surface by solar heating.

This vertical mixing scales as u^3/h, where u is the magnitude of the current and h is the water depth. Solar stratification dominates for small values of u^3/h, whereas for large values, tidal mixing dominates. The transition value between the two regimes is roughly $10^{-2.7}$ W kg^{-1} (Simpson et al., 1982). As is often done elsewhere, we adopt the terminology of Pingree and Griffiths (1978) and define the Stratification parameter, $S = \log_{10}(h/u^3)$, as a measure of the mixing. Thus the transition value generally occurs when $S = 2.7$. Below this critical value, the water can be considered stratified and any surface heating would not be dispersed throughout the water column.

Figure 5.4 depicts how different tidal current speeds affect the temperature profile at Scott Reef during the height of the 1998 coral bleaching episode. GOTM is run using

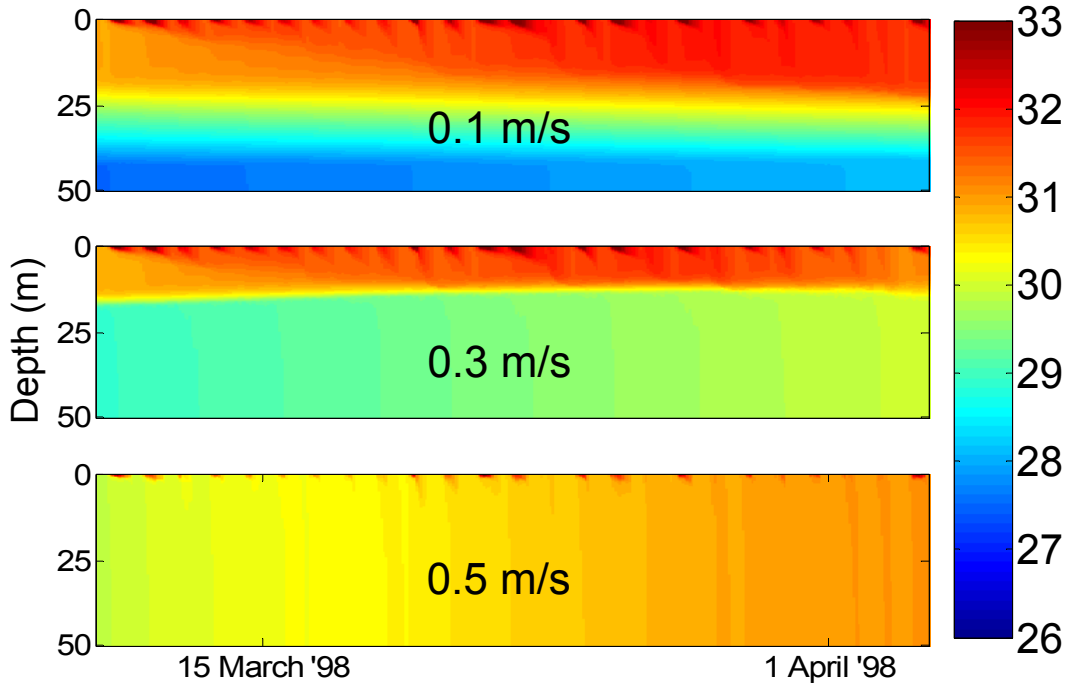

Figure 5.4 The effects of current on modelled water temperature profiles (50 metres deep) at Scott Reef during the height of the bleaching episode (March 1998). Diurnal currents of 0.1 m s^{-1} (top), 0.3 m s^{-1} (middle), and 0.5 m s^{-1} (bottom) lead to stratification numbers of $S = 4.7$, 3.3, and 2.6 respectively and can dramatically change the distribution of water temperature.

the same conditions as in Chapter 4, except that the water column is now specified to be 50 metres deep with a current velocity of 0.1 m s^{-1}, 0.3 m s^{-1}, or 0.5 m s^{-1}. The stratification parameter is therefore 4.7, 3.3, and 2.6 respectively. With a 0.1 m s^{-1} current, the mixed layer depth is around 25 metres. When the current velocity is increased to 0.3 m s^{-1}, the mixed layer depth is raised to 15 metres. Finally when the current is 0.5 m s^{-1}, the water column is well-mixed. As predicted, the water column becomes well-mixed when the stratification parameter is below 2.7.

It is important to note that surface water became cooler as soon as the water column became well-mixed. The goal of this chapter is to estimate the depths and currents around the reef so that areas of well-mixed water can be identified. The degree of cooling in these well-mixed regions is calculated and compared to coral bleaching records and temperature observations.

Hydrodynamic model development

A two-dimensional depth-averaged barotropic numerical hydrodynamic model (Bode and Mason, 1994) was employed to describe the depth-averaged tidal hydrodynamics of Scott Reef. This model includes wetting and drying of the reef flats, a feature that improves predictions in shallow regions. The model was run with a spatial resolution of 250 metres and a time step of 5 minutes. The goal of the model is to produce currents which are representative of those during any bleaching period at Scott Reef. Wind stresses are neglected as they tend to be negligible during bleaching-like conditions. Additionally, the field observations demonstrated that tidal currents dominated lower frequency currents; thus only tidal currents are considered.

Calculating tidal forcing on the boundary

Tidal boundary conditions were provided by nesting the model within a tidal model of the Southeast Asian area that utilised a reef/island parameterization scheme (Bode et al., 1997). A three step process was used to determine the phase and amplitude of the tidal constituents modelled. First, the barotropic model was run for the extended Timor Sea, by using a global ocean tide model (Eanes and Bettadpur, 1995) to provide boundary conditions. The phase and amplitude of the tidal constituents were calculated at each point on this large-scale bathymetry. In the second step, the model was run with a smaller bathymetry set surrounding Scott Reef. For this run, the tidal amplitude and phase around the boundary were calculated from the results of the larger, Timor Sea, model. The results of this model drove a yet smaller and finer-scale model surrounding Scott Reef. Again, the phase and amplitude of the tidal constituents were calculated at each point on this finest-scale bathymetry. The last step in determining the tidal forcing along the boundary was to calibrate the model results against observations from tide gauges. At Site L, just south of North Scott (Figure 2.2), a year-long tidal record for 2002 was obtained. Through harmonic tidal analysis, the amplitudes and phases of the significant tidal constituents at Site L were calculated and compared to the model result. The differences in phase and the ratios of amplitudes for each constituent were calculated. These ratios and differences were then applied to the corresponding constituents on the boundary, thus calibrating the tidal forcing on the boundary of the model.

Bathymetry

An accurate description of the regional bathymetry is of fundamental importance to the development of an accurate numerical model. Therefore considerable effort was expended in synthesizing a number of bathymetric data sets in and around Scott Reef. The range in the bathymetry of Scott Reef is extreme, in that it contains shallow (<10 m), intermediate (10–100 m), and deep (>100 m) water. There is limited traditional bathymetric information available for the extremely shallow areas on the reef crests of both North and South Scott Reef, on the reef flat surrounding the Sandy Islet, and also close to the reef front drop-off on both North and South Scott Reef. Sixty-metre-resolution bathymetry for these shallow environments was extracted from Landsat imagery utilising an algorithm detailed by Andrefouet et al. (2003). The shallow-water bathymetry was then merged with data holdings provided by Woodside and AGSO. The enhanced bathymetric data set is shown in Figure 5.5.

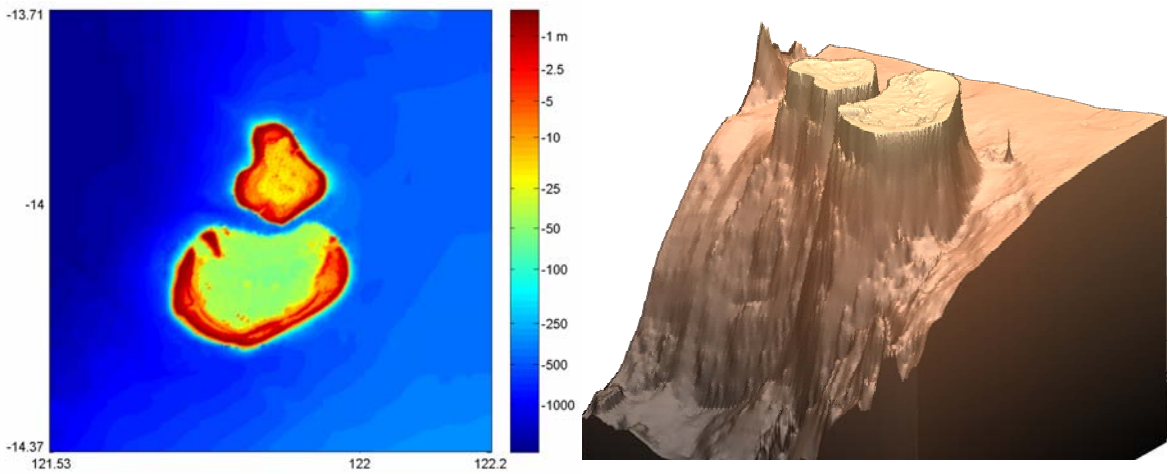

Figure 5.5 A colour contour map and a three-dimensional rendering of the merged bathymetric data sets (the aspect ratio in the rendering is modified to reveal the depth).

Coral Bleaching Hazard Map

The output of the two-dimensional hydrodynamic model was combined with the bathymetry to estimate the vertical mixing following the approach of Simpson and Hunter (1974). This method had first been used to help explain the frontal features observed by the NOAA satellite imagery in the shallow seas around the United Kingdom (Simpson and Hunter, 1974). Regionally, this approach has been applied with success south of Scott Reef at Shark Bay, WA (Ranasinghe and Pattiaratchi, 1999) and farther north off the Kimberley coast (Cresswell and Badcock, 2000). A map of the vertical mixing at Scott Reef is generated by calculating the mixing parameter, $S = \log_{10}(h^3/u)$, at each of the grid points of the model.

Tidal cooling map

The method above is taken a step further to estimate the potential for cooling by applying the temperature profile obtained from the one-dimensional water column model described in Chapter 4. This simple but effective approach was pioneered on the Great Barrier Reef to help explain the complex SST patterns found in the region during low winds and bleaching periods (Skirving and Steinberg, 2003). For each horizontal grid point, the stratification parameter is calculated as outlined above. If the water in a location is considered well-mixed ($S \leq 2.7$), then the surface water temperature is estimated as the mean temperature of the initial temperature profile. If the water is deemed stratified ($S \geq 2.7$), then the surface water remains at the same temperature as the surface water in the initial temperature profile. Figure 5.4 illustrates why this scheme is appropriate to estimate surface water temperatures. In those GOTM calculations, the surface waters remained at the same temperature until the stratification parameter dropped below 2.7. At this point the water column became well-mixed, and surface temperatures cooled to approximately the average of the stratified profiles.

If a region is considered to be tidally well-mixed, it does not imply that the water in that region is any cooler. Water on the reef flat may be shallow enough that there is a negligible difference between temperatures when the water column is stratified and well-mixed. The process to determine the amount of cooling in well-mixed regions is illustrated in Figure 5.6. The top left panel shows a temperature profile found from the

water column model (black curved line). By moving around the numerical model grid, different depths are found. The top right panel shows a 10 m depth which is in the unstratified portion of the surface heat layer. If the currents are strong enough to mix it, it remains quite warm (orange line). However at greater depths, cool, deep water is available for surface cooling. The bottom left panel shows the profile to 30 m which is well below the thermocline. If the water column at this depth becomes well mixed, the resulting temperature profile (blue line) is significantly cooler than the initial temperature at the surface. Given a general, deep water temperature profile and a depth, the amount of surface cooling in well-mixed regions can be estimated by this process.

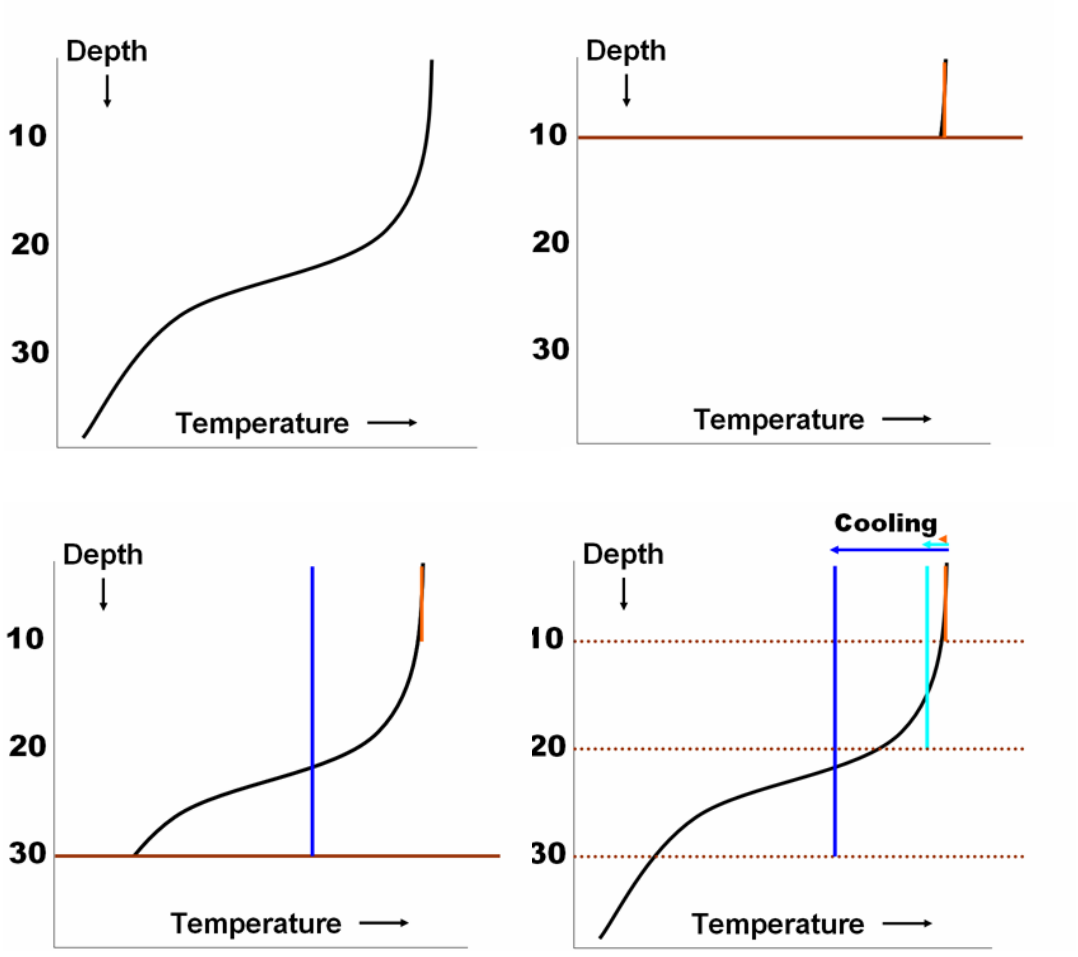

Figure 5.6 a. (top, left) A hypothetical temperature profile similar to the output of GOTM. **b. (top, right)** In shallow water, mixing the water column (orange line) does not significantly change the surface temperature. **c. (bottom, left)** In deeper water (below the thermocline), mixing the water column has a large effect on the surface temperature. **d. (bottom, right)** Given a general, deep water temperature profile and a depth, the amount of surface cooling in well-mixed regions can be estimated.

Hydrodynamic model validation

The numerical model was validated against in situ observations of sea-surface elevation at East Hook, North Scott and in the main Channel. A comparison of observed and computed elevations is shown in Figure 5.7. The model was able to simulate the observed tidal heights accurately, including the irregular tidal height observation in the North Scott lagoon.

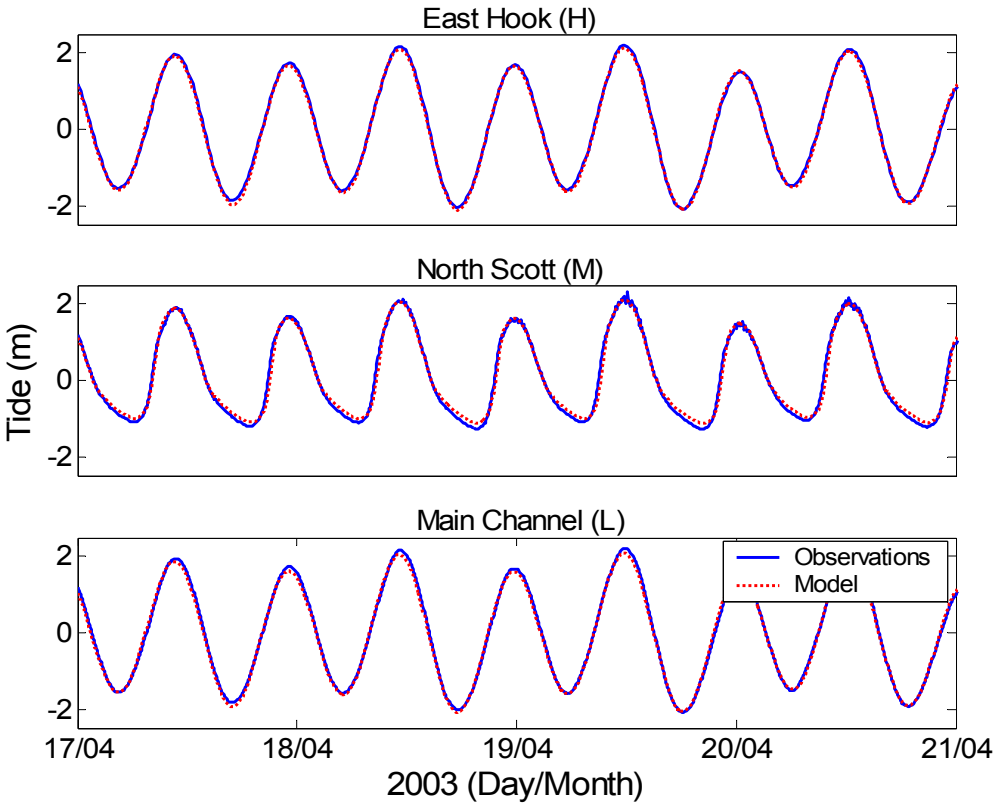

Figure 5.7 Observed and modelled sea-surface elevation at East Hook, North Scott, and in the Main Channel.

The model was also validated against observed velocities at a number of mooring locations. Currents are much more difficult to predict and measure than sea elevation for several reasons, one of which is the extra degree of freedom (Godin, 1983). Additionally, rapidly changing topography can break down the simple harmonic theory behind the analysis and produce high spatial gradients in the current regime, which cannot be resolved by a numerical model.

Figure 5.8 illustrates observed, tidally predicted, and modelled currents in the north-south and east-west directions at Site D, located in the channel between West Hook and Sandy Cay. The current observations were recorded using an Acoustic Doppler Current

Profiler and the particular currents illustrated in Figure 5.8 were measured at 20 metres below the datum (lowest astronomical tide). The model underestimates the north-south component of the current by about 30%, while the amplitude of the modelled east-west component agrees fairly closely with those observed and tidally predicted.

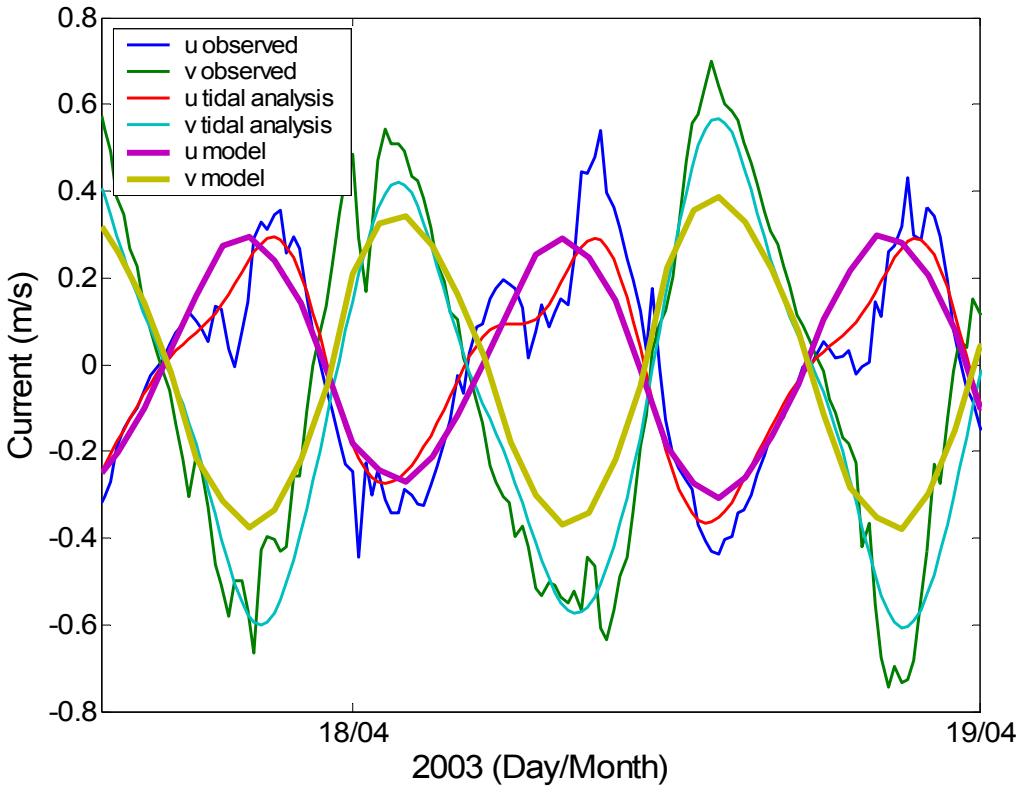

Figure 5.8 Observed, tidally predicted, and modelled currents in the north-south and east-west directions at Site D, located in the channel between West Hook and Sandy Cay.

It is interesting to note that the hydrodynamic model did not simulate the inflection points observed in the eastward currents. The inflection points are characteristic of the presence of horizontal eddies; the fact that the model did not simulate them may suggest that these eddies exist only near the surface. This particular site is 100 metres deep and since currents in the model are depth-averaged, if this feature was restricted to the upper layers of the water column, then they might not be produced in the model. It would be interesting to note whether these inflection points could be simulated using a three-dimensional barotropic model.

Another way to determine how well the model simulates observed currents is to plot both the modelled and observed currents on a hodograph (Figure 5.9). In this approach the direction and magnitude of the currents can be compared quickly. Figure 5.9a

shows a hodograph plot of the simulated currents at Site D overlaying the corresponding observations. The overall magnitude and direction of the model is roughly correct, although the magnitude of the modelled currents are less than those observed and upon closer inspection, the plots reveal that the principal directions between the observed and modelled currents differ by a few of degrees.

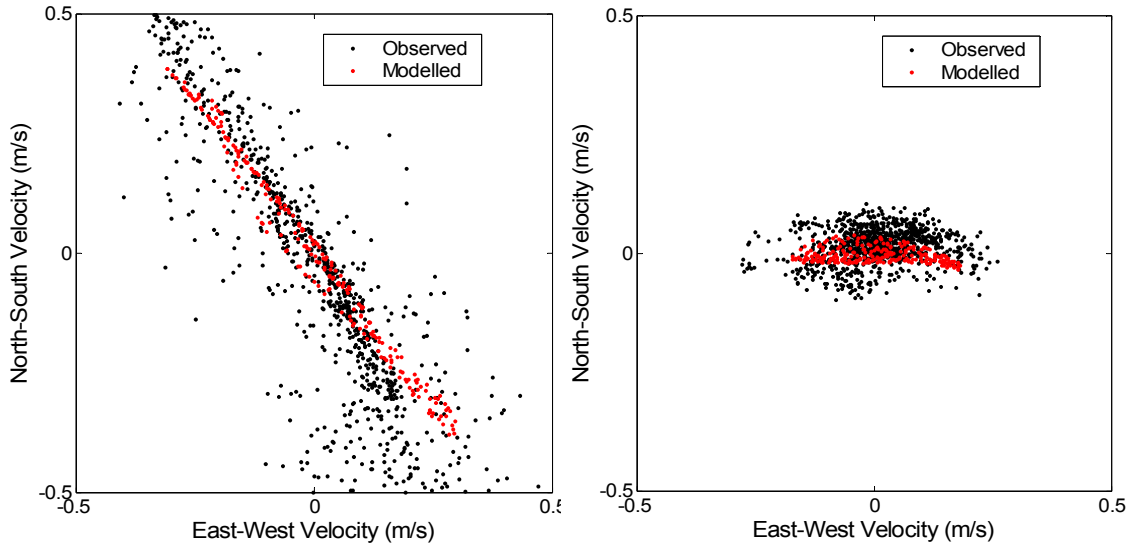

Figure 5.9 Hodograph plots of the simulated and observed currents at **a. (left)** Site D and **b. (right)** Site F.

Inside the main lagoon at Site F, a hodograph plot of the modelled and observed currents shows better results (Figure 5.9b) with the direction and magnitude of the modelled and observed currents being nearly identical. However, there appears to be a slight offset in the north-south direction, suggesting that during this period the observed currents had a net northward flow of a few centimetres per second. However, a better fit between the observed and modelled currents could be achieved by removing the non-tidal signal from the observed data set.

At one of the sites, Site H, the direction between the observed and modelled currents was significantly different, even though the magnitude of the current was accurately modelled (Figure 5.10). The satellite image in Figure 5.10 shows the location of the measurements as well as an indication of the local bathymetry. Site H is located on a sharp bathymetric gradient with the predominant isobaths in the north-south direction. In this case the local bathymetry may be the cause of the discrepancy in the observed and modelled currents. The resolution of the model is too coarse to discern small scale features such as bommies; in fact, the model currents are so sensitive at this site that

moving over just one pixel can halve or double the angle between the observed and model current ellipses. Nonetheless, the two-dimensional hydrodynamic model produces realistic results and is suitable for the level of accuracy required for this project.

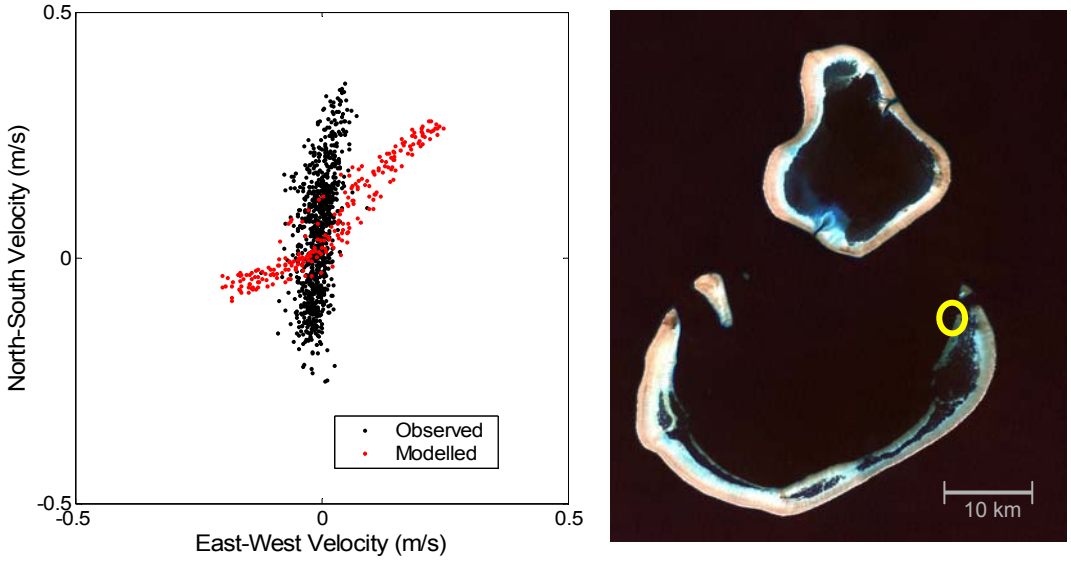

Figure 5.10 Hodograph plot (left) of the simulated and observed currents at Site H (yellow ellipse).

Coral Bleaching Hazard Map Results

Velocity measurements for the more than 90,000 points (250 metre resolution) are calculated by the two-dimensional hydrodynamic model at each time-step (every 5 minutes). From these velocities, a map of the spring-tide velocity at each of these points is created. Areas of pronounced vertical mixing are visualized by calculating the mixing parameter, computed from the velocity and depth at each grid point. Finally, a temperature profile is included in order to create a map which estimates tidally-driven surface cooling.

Velocity Map

In order to characterize the extent of mixing, it is necessary to calculate the upper range of tidal current velocity at each point in the model grid. The maximum tidal velocity occurs at slightly different times for different parts of the reef, though overall it will occur during the peak spring tide. Using the maximum velocity at each point is

potentially misleading as the model may calculate an anomalously strong current at one time which is not representative of the stronger currents at that point. Points that wet and dry, such as reef tops, are especially prone to anomalously strong currents. To control for these outliers as well as to account for the difference in times when peak currents are experienced, a near-maximum velocity was calculated. Here, we define a near-maximum velocity to be the sum of the time-averaged velocity and standard deviation of that velocity over a three day period surrounding the peak of the spring tide. The near-maximum velocities of Scott Reef are shown in Figure 5.11.

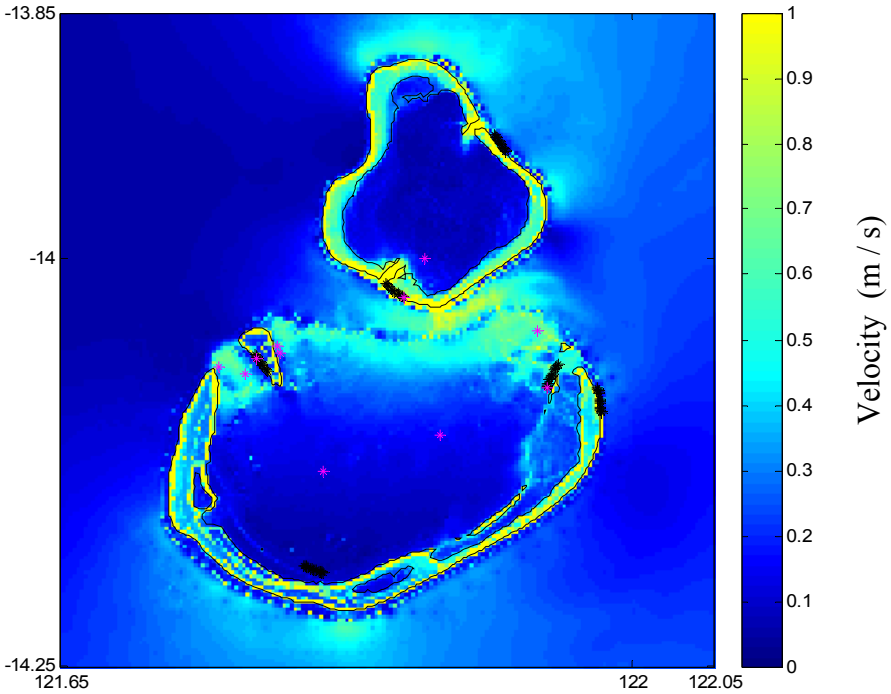

Figure 5.11 Near-maximum spring tide velocities (m s^{-1}) around Scott Reef. The black dots show the location of coral surveys and the magenta dots identify where oceanographic measurements were collected in 2003.

The strongest currents are located around the perimeter of the reef flat. Strong currents are found in all the main channels, with the strongest of these leading into North Scott. Currents inside the lagoons are much smaller, though the currents in the parts of the lagoon that are nearest the main channels are much stronger. Somewhat surprising are the currents around the top of North Scott and the bottom of South Scott. The higher speeds at these locations are due to the NW-SE direction of the tides; water blocked by the reef is quickly swept past these points.

Tidal Mixing Map

A mixing map is created by combining the depths and the tidal currents at each point (Figure 5.12). As mentioned earlier, the strength of mixing is characterised by $\log_{10}(h/u^3)$ where h is the depth and u is the near-maximum velocity. The map shows that the reef flats are very well-mixed, as would be expected. The water in the channel between the west lagoon and Sandy Cay is well-mixed as is the water in the eastern part of the southern lagoon. The water in the centre of both lagoons is shown to experience negligible tidal-mixing. Additionally, there is a band of well-mixed water that stretches across the northern part of the southern lagoon. This band corresponds to strong currents in the 400-metre-deep channel being pushed onto the shallower, 50-metre-deep ledge (see Figure 5.5). Even in the deep channel between the north and south reefs there are isolated spots of well-mixed water. These spots occur where there are strong currents (1 m s^{-1}), a speed which can vertically mix water as deep as 400 metres.

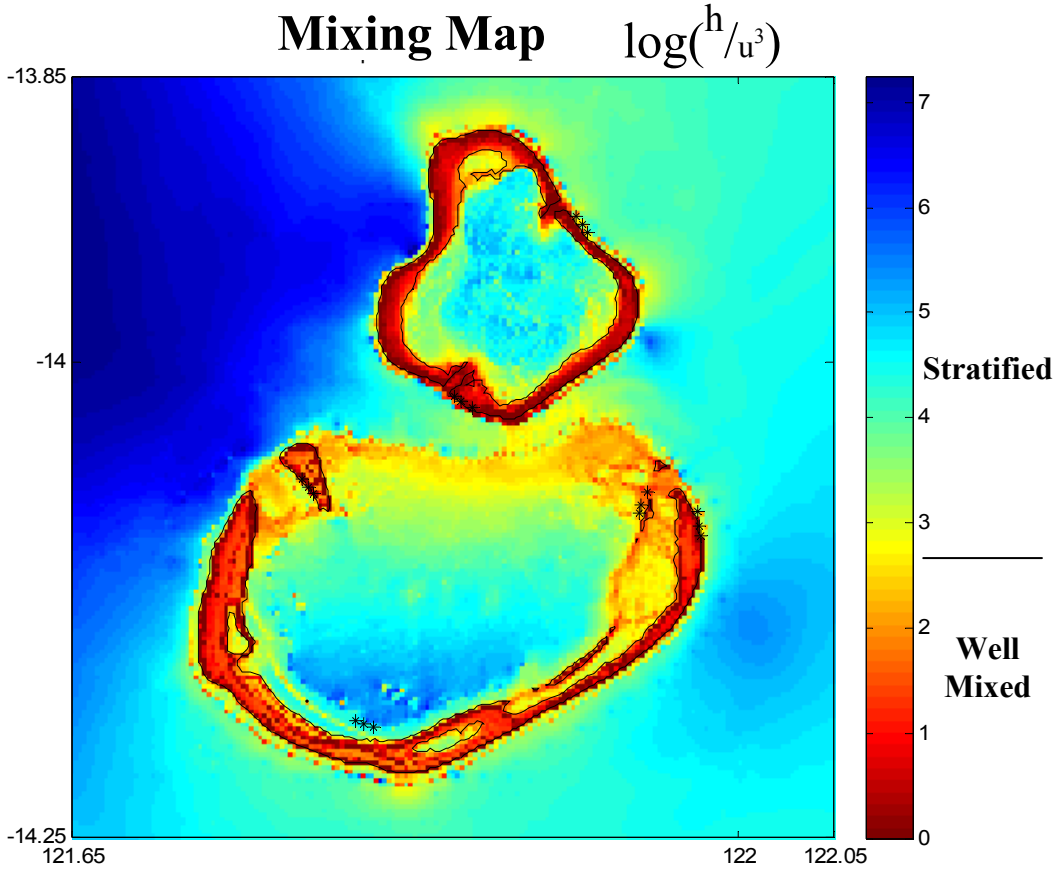

Figure 5.12 A tidal mixing map of Scott Reef which identifies stratified and well-mixed regions from the computer values of the parameter *S*. The black dots show the location of coral surveys.

Tidal cooling map

The tidal cooling map (Figure 5.13) was produced in the manner described earlier in this chapter. It provides a different insight to the mixing map as it highlights those regions that are well mixed and deep enough to generate significant surface cooling. The map was created by using a measured temperature profile for Scott Reef during the beginning of April, 1998 (Figure 5.14). Therefore this map gives insight into regions of Scott Reef which may have received respite from the record-breaking, warm temperatures during that period. As was expected, the shallow reef flats were extremely well-mixed (Figure 5.12) but not cooled from the mixing (Figure 5.13). Additionally, the well-mixed water in the eastern part of the southern lagoon is not cooled. However significant cooling is identified in the channel between the west lagoon and Sandy Cay, as well as in the band of well-mixed water stretching across the northern part of the southern lagoon. The greatest surface cooling occurred in the deep channel between north and south reefs where there are isolated spots of well-mixed water.

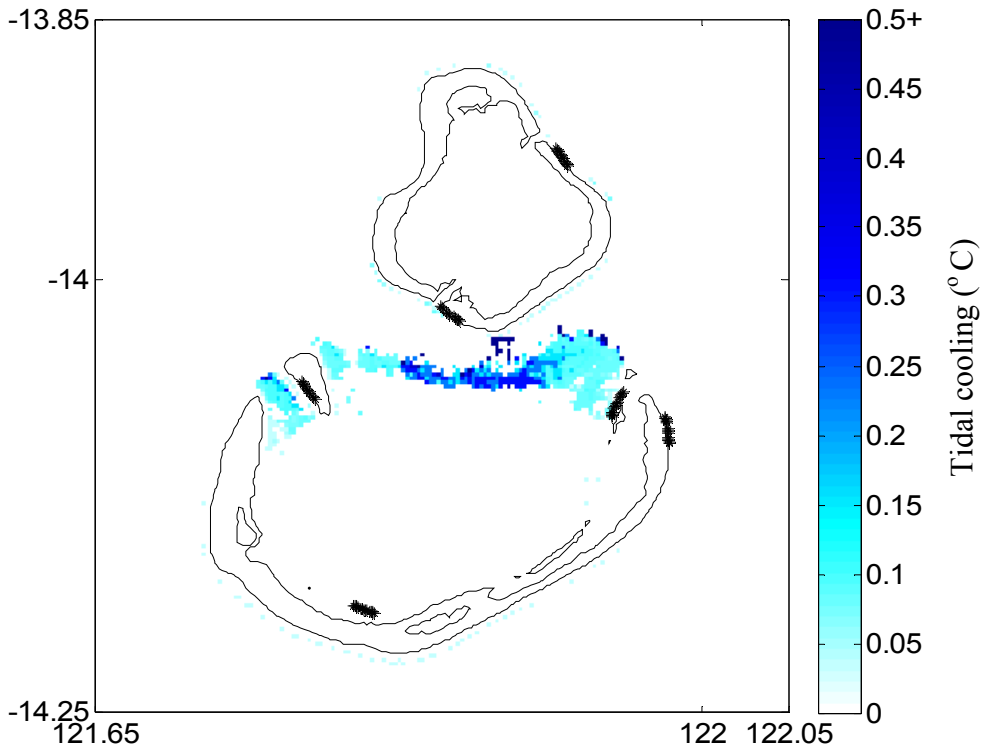

Figure 5.13 A map of tidal cooling (°C) at Scott Reef estimated from a temperature profile during the height of the 1998 coral bleaching period.

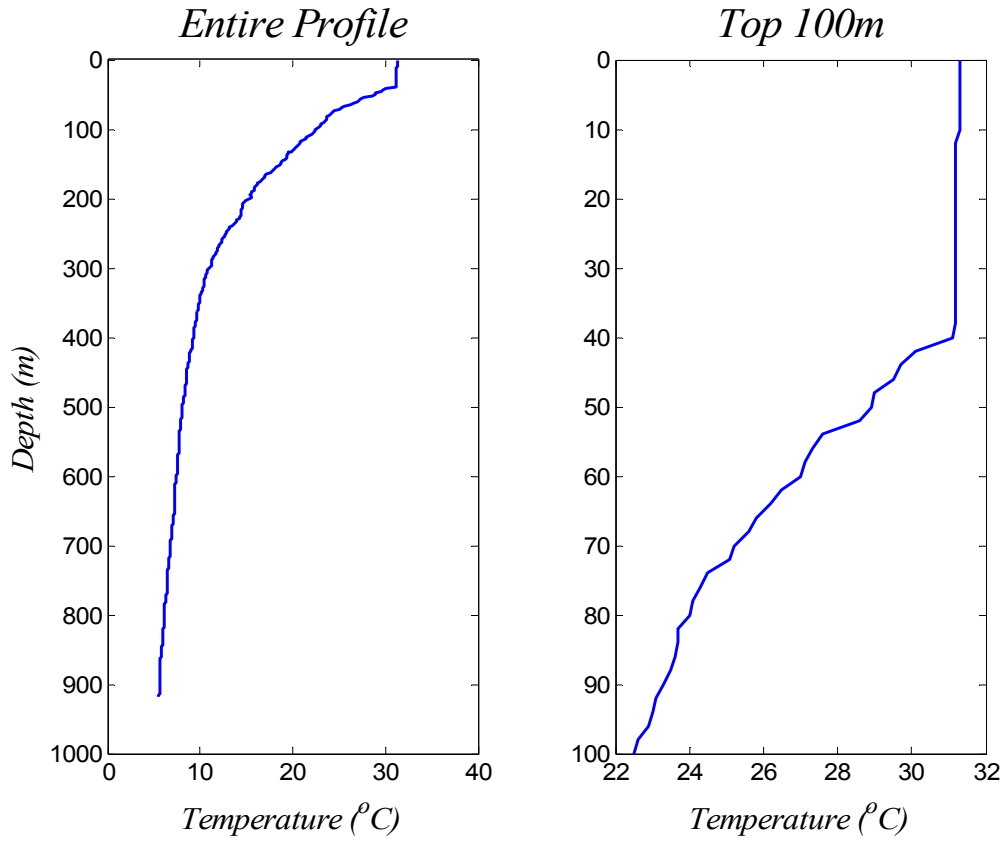

Figure 5.14 The XBT temperature profile used to generate the cooling map. This profile was taken at 13.92 S, 121.23 W on 19-Apr-1998 at 21:07:00. (*Profile data courtesy of CSRIO*)

Cooling Exposure Map

The maps shown in the prior sections are static in time. The temporal development of these maps can be computed so that the mixing and cooling can be observed over different tidal and weather regimes. This section attempts to determine where the well-mixed cooler waters shown in Figure 5.13 move during a few tidal cycles. Tidal advection allows the water to potentially move past other coral regions and thus expands the regions that experience cooler waters. Figure 5.15 shows that the major cooling generating area on the northeast side of Scott Reef produces water that moves through the channel separating North and South Scott Reefs. The channel between Sandy Cay and West Hook also shows the limited incursion of cooler water into South Scott lagoon.

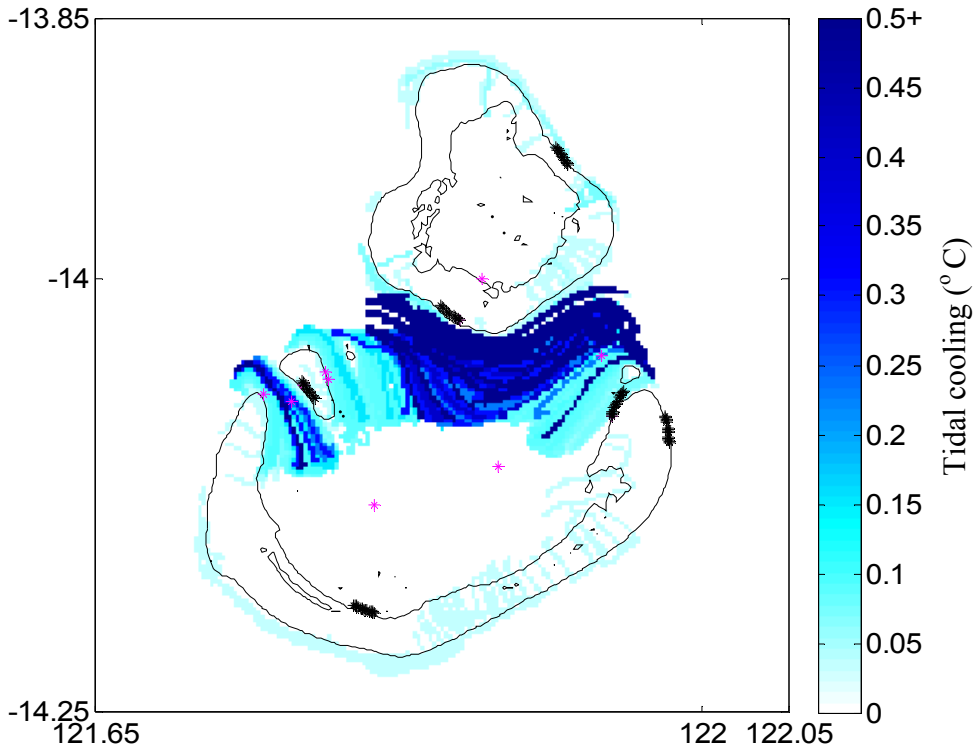

Figure 5.15 Cooling exposure map at Scott Reef over one tidal cycle. The black dots show the location of coral surveys and the magenta dots identify where oceanographic measurements were collected in 2003.

Cooling exposure maps generated from alternative profiles show similar results, though at different magnitudes. The cooling exposure map generated from a GOTM profile (Figure 5.16) shows cooling in the same regions as in Figure 5.15. However due to a combination of a shallower mixed layer depth and more stratified profile, the magnitude of cooling is significantly larger when the GOTM profile is used.

It is interesting to compare the cooling exposure maps during a bleaching event (Figures 5.15 and 5.16) with a cooling exposure map generated from a climatological profile. Doing so gives an indication of any cooling that might be expected on an average day. An average temperature profile was generated from the CSIRO Atlas of Regional Seas (CARS) for mid-April, and was then used to create a cooling exposure map (Figure 5.17). As expected, the climatological temperature profile was less stratified than the other two profiles and had a deeper mixed layer depth. The cooling that results is still in the same region, though the magnitude of cooling is significantly less. In the rest of this chapter the measured profile will be used so that the results do not depend on any of the assumptions and simplifications of the vertical model.

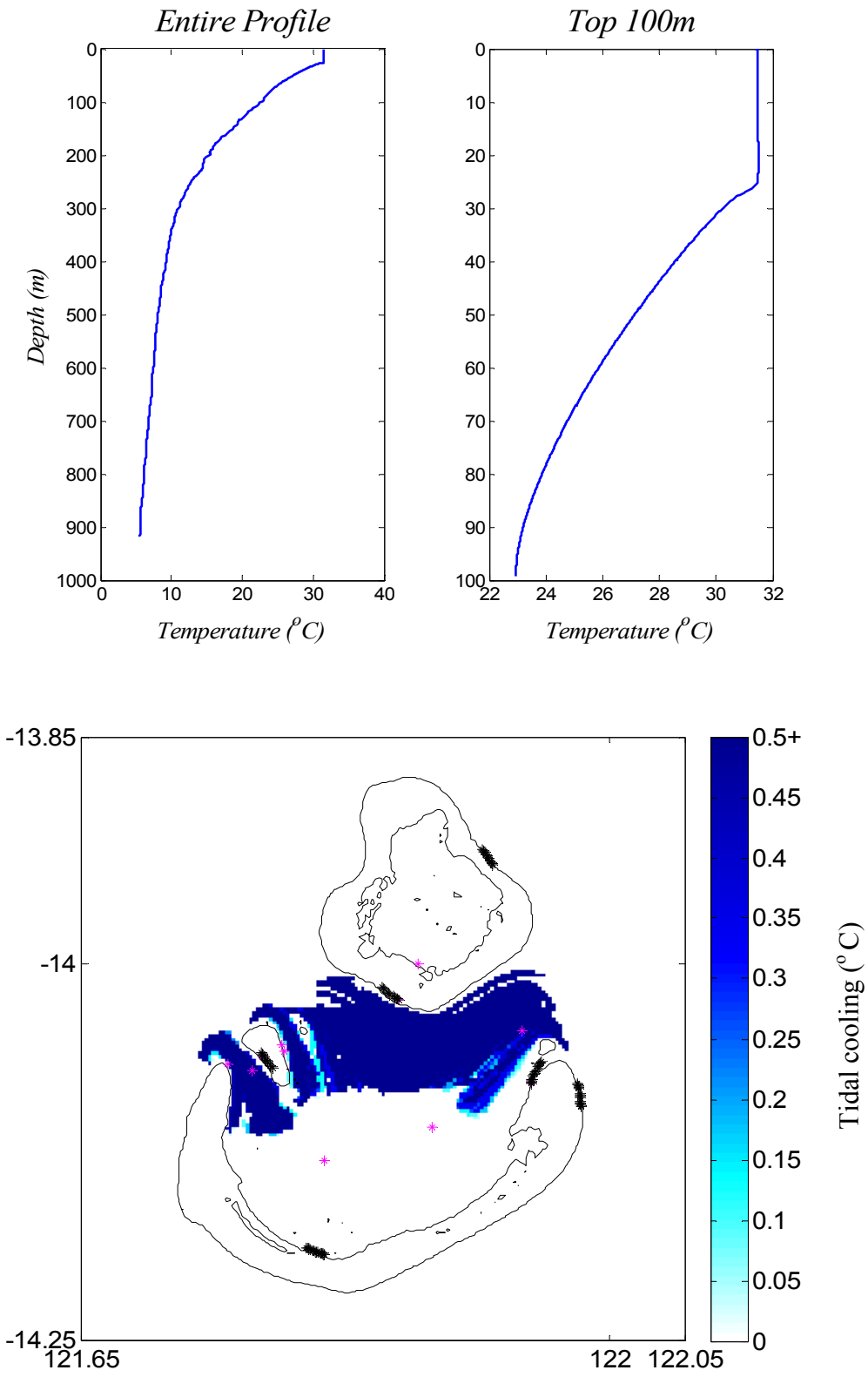

Figure 5.16 Cooling exposure map (*bottom*) at Scott Reef over one tidal cycle using a temperature profile from GOTM (*top*). The profile selected was for 19-Apr-1998 at 21:07:00 (see Figure 4.18).

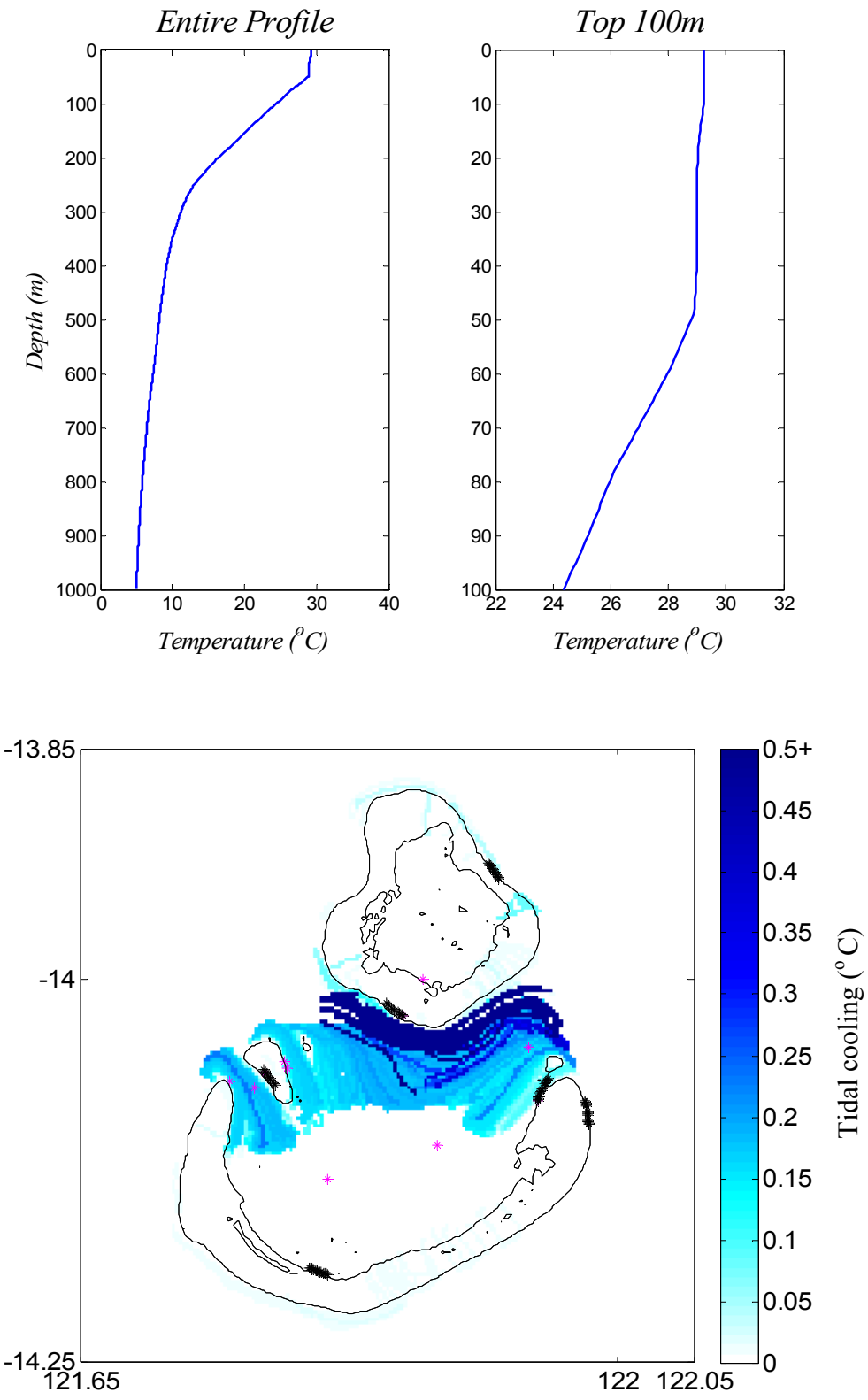

Figure 5.17 Cooling exposure map (*bottom*) at Scott Reef over one tidal cycle using a climatological temperature profile for 19-Apr-1998 at 21:07:00 (see Figure 4.14).

Correlation between Hazard Maps and Coral Survival

The goal of the hazard maps is to identify areas that are susceptible to coral bleaching at the sub-reef scale. Of all the maps, the cooling exposure map is the most appropriate as it estimates temperature variations due to tidal mixing. Validation of the cooling exposure map can be made by comparing it with actual bleaching mortality caused by the 1998 bleaching event (Figure 4.15). The best survival occurred at Sites 3 and 4, regions adjacent to where the coolest water was predicted. Site 1 at East Hook showed a relatively moderate level of bleaching, consistent with the level of cooling estimated. The other sites, 2, 5 and 6, also agree with the poor survivability and the lack of cooling predicted.

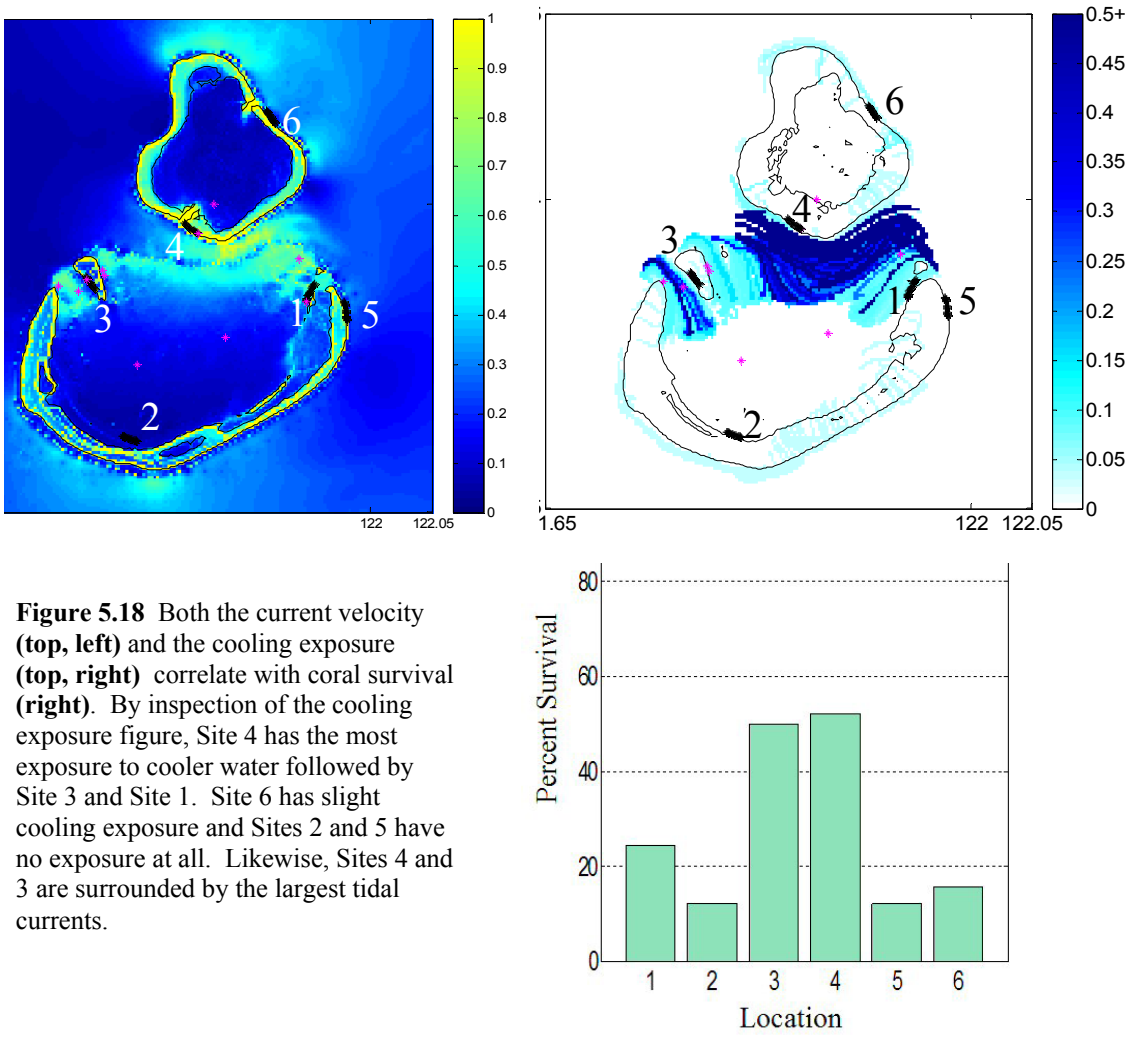

Figure 5.18 Both the current velocity **(top, left)** and the cooling exposure **(top, right)** correlate with coral survival **(right)**. By inspection of the cooling exposure figure, Site 4 has the most exposure to cooler water followed by Site 3 and Site 1. Site 6 has slight cooling exposure and Sites 2 and 5 have no exposure at all. Likewise, Sites 4 and 3 are surrounded by the largest tidal currents.

It has also been well established that the flow rate of water across corals is correlated with bleaching and recovery (Nakamura and van Woesik 2001; Nakamura et al. 2003) as described in Chapter 1. Figure 5.18 additionally illustrates that more corals survived in areas with larger tidal currents. Both the tidal cooling and the current velocity significantly correlated with survival rates of the major families. Because it is inaccurate to assume that cooling exposure or tidal flow has a linear effect on coral survival, a nonparametric correlation (Spearman's *rho*) was used to carry out these calculations. Additionally, a nonparametric correlation was appropriate since the survival rates were strongly skewed.

Correlations - Spearman's rho

		Tidal Cooling	Current Velocity	Acroporidae	Alcyoniidae	Faviidae	Pocilloporidae	Poritidae
Tidal Cooling	Correlation Coefficient	1.000	-.758**	-.815**	-.589**	-.561**	-.362**	-.355**
	Sig. (2-tailed)	.	.000	.000	.000	.000	.001	.001
	N	90	90	89	86	89	85	86
Current Velocity	Correlation Coefficient	-.758**	1.000	.573**	.349**	.247*	.317**	.292**
	Sig. (2-tailed)	.000	.	.000	.001	.019	.003	.006
	N	90	90	89	86	89	85	86

**. Correlation is significant at the 0.01 level (2-tailed).

*. Correlation is significant at the 0.05 level (2-tailed).

Table 5.1 There is significant correlation between coral survival and tidal cooling and between coral survival and current velocity for each of the coral families along each of the transects. It is difficult to separate the two effects as they are strongly correlated (ρ = -0.758).

The correlation results sufficiently validate the effectiveness of the cooling exposure map. However, it is not immediately clear whether this success should be attributed to tidal cooling or to tidal currents. The correlation between tidal cooling and bleaching mortality is consistently better than the correlation between current velocity and bleaching mortality. However, tidal cooling and current velocity are strong correlated ($\rho = -0.758$) and therefore difficult to separate. The next section discusses evidence of actual cooling.

Cooling in Field Data

During the 2003 field campaign (described in Chapter 2), temperature loggers were deployed around Scott Reef. If tidal cooling occurs, it would be expected that temperature records from these instruments would show a temperature decrease during strong tides. Successful temperature measurements were taken at Sites D, E, F, and G (Figure 5.19). The cooling map predicts that Sites D and G would experience cooling during strong tides. However, the map predicts that Locations E and F are too far within the lagoon to experience this cooling, and thus the temperature at these points would not correlate with tide.

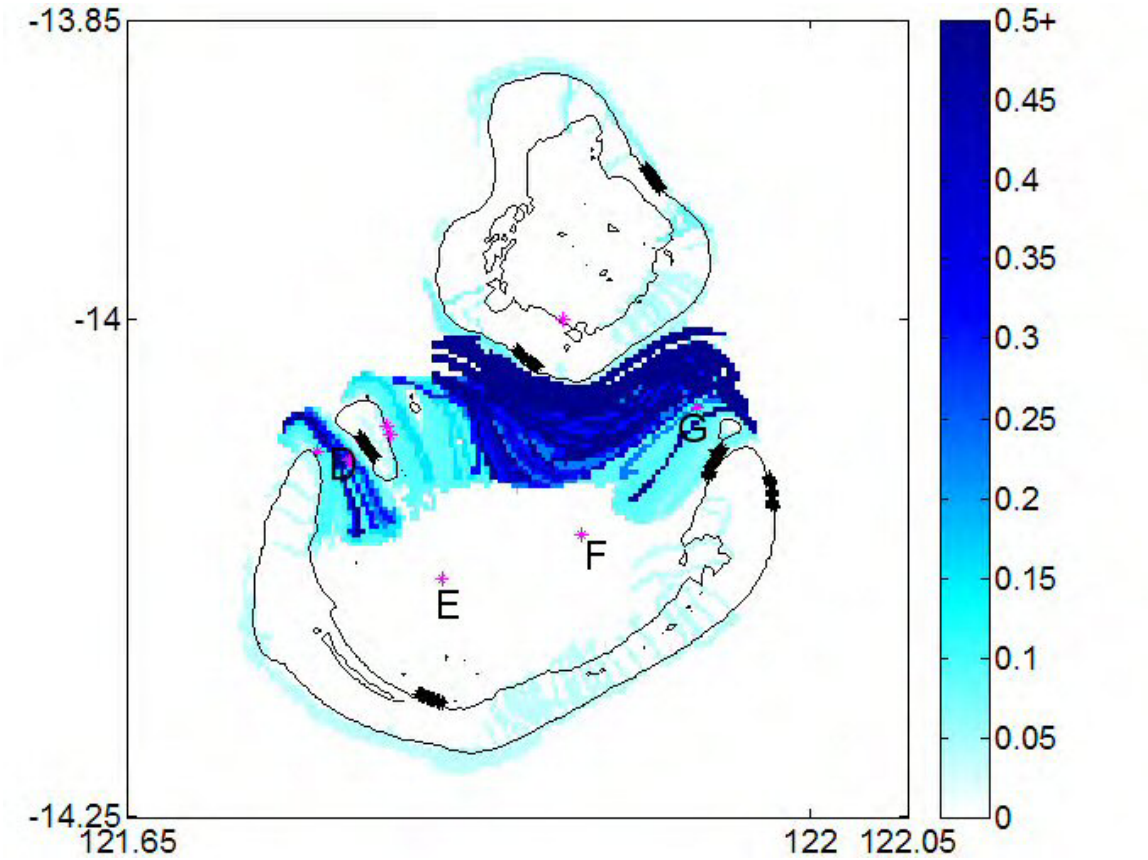

Figure 5.19 Cooling exposure map of Scott Reef. Sites D, E, F, and G correspond to mooring observations from 2003.

Actual temperature observations from moorings at Sites D, E, F and G (Figure 5.20) support the tidal cooling hypothesis. Site D is located in the channel between Sandy Islet and West Hook and exhibits significant tidal cooling. Site G is located in the eastern entrance of the channel between North and South Scott where significant cool

water is also generated. By contrast, the South lagoon moorings, E and F, show little tidal cooling.

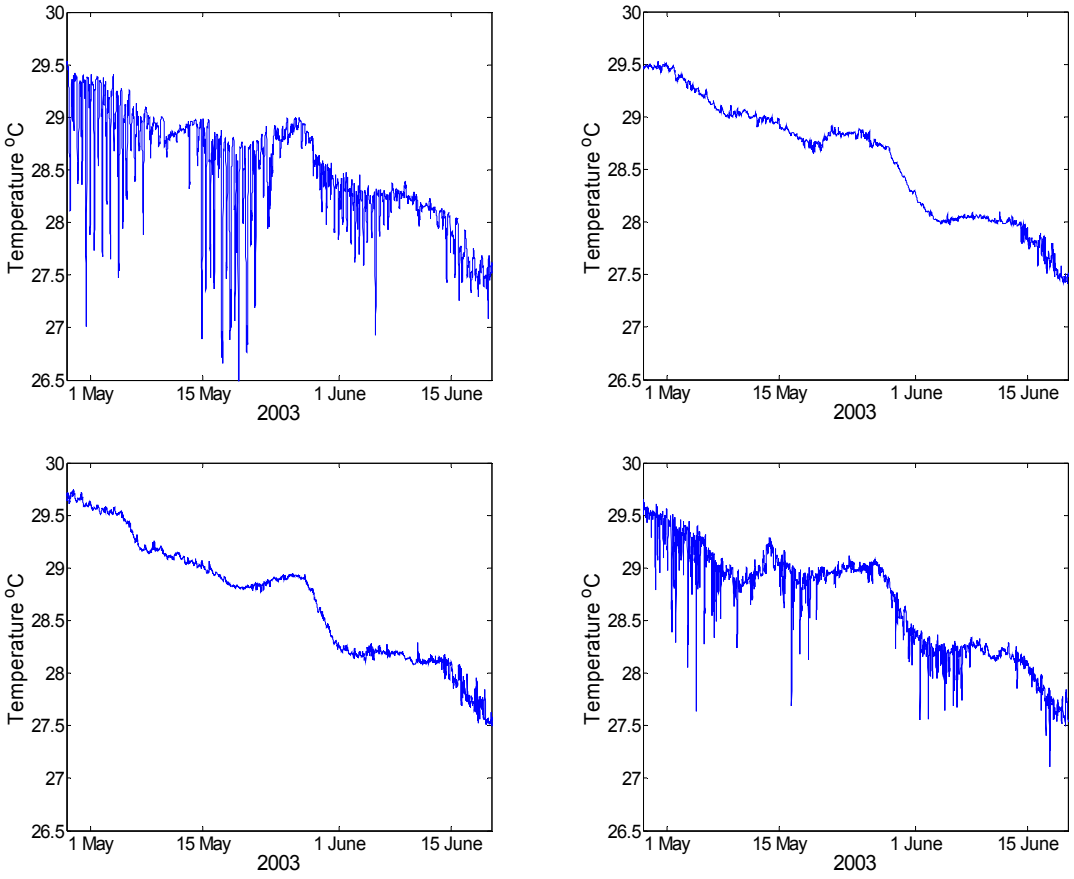

Figure 5.20 Observed temperatures from Locations D **(top left)**, E **(top right)**, F **(bottom left)**, and G **(bottom right)**. Locations D and G show tidal cooling during spring tides, as opposed to Locations E and F which show no tidal cooling.

The predicted cooling is actually a lower limit for what would be expected. The methods laid out in this thesis all assume a horizontal, two-dimensional flow along a flat ocean floor. Any three-dimensional flow generated from topography would increase mixing and thus the potential for cooling. A three-dimensional baroclinic model would be needed to accurately model these more complex flows.

Summary and Concluding Remarks

Coral records at Scott Reef demonstrate that the coral mortality in 1998 differed between sites. In this chapter it has been shown that tidal upwelling may have cooled the water in particular regions, leading to higher survival rates in those areas. As demonstrated in Chapter 4, the water temperatures can increase rapidly during low-wind conditions. During these calm periods, the water column can become strongly stratified. However vertical mixing from tidal currents can mix the water column and thus cool off the upper layers (Figure 5.4).

The strength of vertical mixing is related to both the tidal current speed and the depth of the water column. Tidal current speeds were estimated by using a two-dimensional, hydrodynamic model. The simulated currents were then combined with local bathymetry to estimate the mixing strength. The amount of cooling near the surface (or near the corals), is finally approximated by using the scheme described in Figure 5.6. This technique appears to work well in locating where tidal cooling is generated; however, in coral bleaching prediction, it is just as important to locate the regions cooled by the tidal mixing.

A cooling exposure map is created by tracking the cool water patches over one tidal cycle (Figure 5.15). Two other cooling maps are generated using alternative profiles (Figures 5.16 and 5.17). The similarities in these maps highlight the fact that the particular regions that tidal cooling affect are not overly sensitive to the temperature profile. Therefore we expect tidal cooling to be present in these lower-risk areas during normal times, which we observed in Figures 5.19 and 5.20. A key point is that during bleaching conditions the water column becomes more stratified (and the mixed layer depth becomes shallower) which leads to an increase in the magnitude of cooling experienced.

It was found that regions where corals had higher rates of survival during the 1998 bleaching episode correlated with the predicted areas of cooling. Temperature records in 2003 provided additional evidence that tidal cooling can significantly lower the temperature in parts of the reef during Spring tides. It is believed that these techniques can be applied to other tidally-driven reef systems in order to predict which regions of the reef are prone to coral bleaching.

Chapter 6 – Conclusions

Coral bleaching is a serious threat to the health of reefs around the world. The link between global warming and mass-coral bleaching is now considered "incontrovertible" (Hughes et al., 2003), and results from global warming models have suggested that over half of the coral reefs in the world may be gone by 2030 (Wilkinson, 2002). While ocean heating is a global issue that is difficult for individual countries to combat, predicting where and when bleaching events are likely to occur is a first step mitigating the problem. Results from this thesis demonstrate that relatively simple numerical models can offer insight into the depth of anomalous temperatures as well as into the spatial location of tidally-induced cooling.

This thesis is a case study focusing on Scott Reef. Of all the reefs bleached in 1998, Scott Reef is an excellent test site for this study for several reasons. First, the coral coverage was well documented before and after the bleaching event. Second, there are strong tidal currents in many areas of Scott Reef. Strong currents are necessary for tidal cooling to occur. Finally Scott Reef is surrounded by deep water. The water depth provided a greater range in temperature between surface and bottom water and therefore may have amplified the difference in coral survival rates between corals living near the lagoon and those living near the channels.

This thesis had two key objectives. First, we were interested in investigating water temperature at various depths. This is important because the magnitude of coral bleaching depends on the depth of the surrounding water. We were able to use a one-dimensional model to hindcast the mixed layer depth at Scott Reef during the 1998 bleaching episode. Second, we were interested in investigating whether certain spatial locations were more susceptible to coral bleaching. Although coral bleaching is not uniform across reefs or even colonies, most previous models have assumed that temperature is uniform at these scales and have neglected tidal mixing.

In order to interpret how the vertical temperature profiles may have affected corals, the temperature profiles were converted into bleaching-prediction products such as the HotSpots and Degree-Heating-Weeks products distributed by NOAA-NESDIS (Liu et al., 2003). The bleaching 'prediction' from the 1998-simulated temperatures hindcasted that severe bleaching would occur down to depths of 30 metres, a result that was

validated with field observation. The success and robustness of this approach is even more significant, considering the distance of the weather stations used.

In summary, the results from this thesis demonstrate that an intelligent combination of one- and two-dimensional numerical models can be used to provide accurate and useful predictions of where and when coral bleaching may occur. The models calculate that particular regions have access to tidally upwelled, cooler water. The relative amounts of tidal cooling hindcasted for the 1998 bleaching episode significantly correlate with the coral survival rate (Table 5.1). Additionally, tidal cooling was observed in the 2003 field measurements at the same locations predicted with the modelling techniques.

Future research should extend these findings in a number of ways. First it may be possible to incorporate the one- and two-dimensional models used in this thesis into a more global three-dimensional model. The most accurate method to determine the three-dimensional temperature distribution around and on Scott Reef would be to use a fully three-dimensional, baroclinic hydrodynamic model. Within the next few years, it is expected that researchers at the Australian Institute of Marine Science will develop this type of model for Scott Reef. Such a model would hopefully verify the results presented in this thesis as well as provide more information on whether cool water protected some of the corals. Although a three-dimensional model may be the most accurate option, such a model is computationally expensive and difficult to set up. The results from this thesis demonstrate that an intelligent combination of one- and two-dimensional models can also provide accurate, economical, and useful results.

Future research should also apply the approaches laid out in this thesis to other locations, especially those with records during coral bleaching periods. It is important to note that in order to extend this research to other locations, the reef may need to be located in an area with strong tidal currents. Work is already under way on some sites in the Great Barrier Reef (Steinberg and Choukroun, in preparation) and Palau (Craig Steinberg, personal communication). It is the author's hope that one day the vertical bleaching-prediction products outlined in Chapter 4 will one day be incorporated into the real-time monitoring network of NOAA-NESDIS.

Finally the work in this project could be incorporated into existing work on coral bleaching such as the recent application of Bayesian Belief Networks (Wooldridge and Done, 2004). Bayesian Networks offer a holistic approach to coral bleaching

predictions. The networks rely on several "evidence" nodes that describe a certain aspect of the system. It is the author's opinion that the cooling exposure maps (Chapter 5) would make an ideal node in a larger BBN model.

Given that coral bleaching has already been well correlated with high SST, the prediction of spatially complex SST through modelling, validated against satellite observations, is a significant result in its own right. Interestingly, surface cooling was not detectable at Scott Reef from satellite images. A careful analysis of high-resolution (1 km^2) SST records from both 1998 and 2003 did not reveal any tidal cooling; yet *in situ* field instruments recorded substantial cooling at the depths where corals were observed. This is evidence that coral bleaching prediction should not rely simply upon satellite imagery, and therefore it is worthwhile, perhaps essential, to use hydrodynamic modelling to better describe the bleaching response.

Appendix A – Nomenclature

a	Weight factor in shortwave radiation calculation
C_p	Specific Heat
h	Height (depth) of water column
I_o	Intensity of shortwave radiation entering the water
$I(z)$	Intensity of shortwave radiation
N^2	Brunt-Vaisaila frequency
$R(T)$	Shortwave radiation absorption
Ri	Richardson number
Q_E	Latent heat flux
Q_H	Sensible heat flux
Q_{LW}	Longwave radiation flux
S	Stratification parameter
α	Molecular diffusivity
α_t	Eddy diffusivity
u, U	Current velocity (often in the East-West direction)
v, V	Current velocity in the North-South direction
z	Depth coordinate starting at water surface.
η_1	Attenuation length for the longer shortwave radiation
η_2	Attenuation length for the shorter shortwave radiation
ρ_o	Relative density
ν_t	Eddy viscosity

Appendix B – Mooring and Transect Summary

Below is a summary of all the moorings and transects at Scott Reef. The tables provide the instrument make, measurement capabilities, and location and position within the water column relative to the surface. Each location is denoted by a letter (A – M) that corresponds to the map shown in Figure 2.2. Each letter is followed by a location code that corresponds to nomenclature used by AIMS during deployment and recovery. All depths are relative to Lowest Astronomical Tide (LAT). Acronyms are listed at the end of the section.

Italicized logger entries indicate data recovery failure.

Mooring Summary

A (S1) 14° 14'.205 S 122 ° 06'.422 E 400m Total Depth

First Good : 22 Mar 2003, 06:00:00 WST
Last Good : 24 Jun 2003, 01:30:00 WST

Depth	Instrument	Measurement
100m	RDI	Current Profile
395m	ACR 865	Acoustic Release

B (S5) 14° 00'.851 S 121 ° 55'.203 E 400m Total Depth

First Good : 23 Mar 2003, 11:30:00 WST
Last Good : 22 Jun 2003, 14:10:00 WST

Depth	Instrument	Measurement
10m	SBE 39	Temperature
100m	*AQD*	*Current Profile*
395m	ACR	Acoustic Release

C (S3) 14° 00'.751 S 121 ° 46'.436 E 800m Total Depth

First Good : 22 Mar 2003, 09:27:30 WST
Last Good : 19 Jun 2003, 07:30:00 WST

Depth	Instrument	Measurement
80m	RDI	Current Profile
800m	ACR	Acoustic Release

D (S2) 14° 04'.257 S 121 ° 45'.812 E 39m Total Depth

First Good : 23 Mar 2003, 09:49:59 WST
Last Good : 20 Jun 2003, 09:30:00 WST

Depth	Instrument	Measurement
5m	*Odyssey*	*Temperature*
7.5m	*Odyssey*	*Temperature*
10m	*Odyssey*	*Temperature*
20m	SBE 39	Temperature
35m	RDI	Current Profile
36m	SBE 39	Temperature
39m	ACR 866	Acoustic Release

E (S10) 14° 07'.843 S 121 ° 48'.668 E 46m Total Depth

First Good : 23 Mar 2003, 16:00:00 WST
Last Good : 20 Jun 2003, 13:45:00 WST

Depth	Instrument	Measurement
5.0m	Odyssey	Temperature
7.5m	Odyssey	Temperature
10m	*Odyssey*	*Temperature*
15m	SBE 39	Temperature
20m	S4	Current / Temperature *(died at end of May)*
25m	SBE 39	Temperature
40m	SBE 16	Salinity / Temperature
40m	ACR 866	Acoustic Release

F (S9) 14° 06'.494 S 121° 52'.924 E 58m Total Depth

First Good : 23 Mar 2003, 15:00:00 WST
Last Good : 20 Jun 2003, 14:55:00 WST

Depth	Instrument	Measurement
12.0m	*Odyssey*	*Temperature*
14.5m	*Odyssey*	*Temperature*
17.0m	*Odyssey*	*Temperature*
30m	S4	Current
32m	SBE 16	Salinity / Temperature
52m	SBE 39	Temperature
52m	ACR 866	Acoustic Release

G (S6) 14° 02'.670 S 121° 56'.534 E 37m Total Depth

First Good : 23 Mar 2003, 14:12:30 WST
Last Good : 24 Jun 2003, 15:18:00 WST

Depth	Instrument	Measurement
7.3m	*Odyssey*	*Temperature*
9.8m	*Odyssey*	*Temperature*
12.3m	*Odyssey*	*Temperature*
22.3m	SBE 39	Temperature
33.3m	RDI	Current Profile
35.3m	ACR	Acoustic Release

Transect Summary

H (East Hook Transect)
14° 04'.749 S 121° 56'.864 E 19.7m Total Depth

First Good : 25 Mar 2003, 13:05:00 WST
Last Good : 15 Jun 2003, 21:05:30 WST

Depth	Instrument	Measurement
1.9m	*Odyssey*	*Temperature*
1.2m	*Odyssey*	*Temperature*
2.2m	*Odyssey*	*Temperature*
6.3m	*Tidbit*	*Temperature*
10.0m	*Odyssey*	*Temperature*
19.7m	AQD	Current Profile

I (West Hook Transect)

14° 04'.013 S 121 ° 44'.797 E **16.4m Total Depth**

First Good : 01 Apr 2003, 10:50:00 WST
Last Good : 19 Jun 2003, 10:50:00 WST

Depth	Instrument	Measurement
0.5m	*Odyssey*	*Temperature*
1.5m	*Odyssey*	*Temperature*
4.5m	*Odyssey*	*Temperature*
9.5m	SBE 39	Temperature
16.4m	TG WLR5	Tide Gauge

J (Scott Cay West Transect)

14° 03'.710 S 121 ° 46'.211 E **19.8m Total Depth**

First Good : 24 Mar 2003, 16:45:00 WST
Last Good : 19 Jun 2003, 14:30:00 WST

Depth	Instrument	Measurement
-2.0m	*Odyssey*	*Temperature*
-1.0m	*Odyssey*	*Temperature*
1.8m	*Odyssey*	*Temperature*
4.8m	*Tidbit*	*Temperature*
19.8m	S4	Current
19.8m	SBE 16	Salinity / Temperature

K (Scott Cay East Transect)

14° 03'.484 S 121 ° 47'.059 E **17.1m Total Depth**

First Good : 24 Mar 2003, 14:10:00 WST
Last Good : 21 Jun 2003, 15:00:00 WST

Depth	Instrument	Measurement
-2.2m	*Odyssey*	*Temperature*
-0.9m	*Odyssey*	*Temperature*
0.6m	*Odyssey*	*Temperature*
3.4m	*Odyssey*	*Temperature*
5.4m	SBE 39	Temperature
17.1m	AQD	Current

L (North Scott South Transect)

14° 01'.438 S 121 ° 51'.626 E 14m Total Depth

First Good : 30 Mar 2003, 10:50 WST
Last Good : 23 Jun 2003, 13:30 WST

Depth	Instrument	Measurement
0.3m	*Odyssey*	*Temperature*
0.2m	*Odyssey*	*Temperature*
2.0m	*Odyssey*	*Temperature*
6.3m	*Tidbit*	*Temperature*
14m	TG WLR7	Tide Gauge

M (North Scott North Transect)

14° 00'.036 S 121 ° 52'.392 E 13.8m Total Depth

First Good : 30 Mar 2003, 16:00:15 WST
Last Good : 23 Jun 2003, 15:15:00 WST

Depth	Instrument	Measurement
2.0m	*Odyssey*	*Temperature*
5.0m	*Odyssey*	*Temperature*
9.8m	SBE 39 PT	Temperature
13.8m	SBE 39	Temperature

Acronyms:

AQD Nortek Aquadopp - manufacturer
LAT Lowest Astronomical Tide
RDI RD Instruments - manufacturer
S4 Interocean S4 current meter
SBE Sea Bird Electronics - manufacturer

Appendix C – Data Processing

Isolating Good Data from Field Measurements

Calculating instrument position.

Once all the data have been downloaded from the instruments, there are several crucial steps to give the numbers meaning. The first step is to determine the exact position of each data logger. As simple as it sounds, this process was quite time-consuming, as there were numerous occasions where field notes and mooring diagrams were contradictory. For example, a CTD cast taken in the lagoon during the recovery was planned to be as close as possible to the Site F mooring. However after the cast was taken, the mooring was popped but could not be found; shortly thereafter it was spotted at the horizon. While the field notes clearly stated that the position for the Site F mooring was 14° 06.494 S, 121° 5**3**.924 E, a separate document that was used to originally plan the survey suggested the position was 14° 06.494 S, 121° 5**2**.924 E. Thus it became clear that someone had miswritten one digit in the field notes. This mistake meant that the CTD cast taken in June deployment was not taken at the same location as the one in March. Temperature profiles from the CTD casts are used to verify the temperature loggers; therefore it is crucial to know if there is any reason to believe that the temperatures from the loggers and the profile should not match up. When mapping the oceanography of a single reef, one minute of a degree can be significant.

A more common problem was determining the depth of instruments on a mooring and transect. A mooring is designed to be at a particular depth and the instruments are attached to the mooring accordingly. Because of variation in bottom topography, the actual deployed depth may be slightly different from the intended depth, and it is therefore crucial to measure the water depth at the time of deployment. To account for the large tidal range (4 m) at Scott Reef, all depths are recalculated to a common datum. In this thesis, the depths of all field data are referenced to the lowest astronomical tide (LAT). The fact that so many different measurements of depth are recorded and managed increases the chances of human error.

There were several instances where field notes and mooring diagrams disagreed on the depth of an instrument on a mooring. There was even a case where a single instrument was reported to be located at two different heights on separate moorings. In order to

verify and correct any mistakes, the data had to be compared with other instruments on the mooring or transect and temperature profiles.

In-water points

Instruments are switched on and off while on land (or on a boat); thus there will be several data points which need to be trimmed. It is important not to trim off the first and last in-position points, as these may need to be compared with temperature profiles from CTD casts taken when the instruments were deployed and recovered. For temperature loggers, the transition between being in air and water is fairly apparent in the temperature record. However, there may be several points recorded while the instrument is being put into position under the water (this is especially true for transects). The most reliable method to determine when an instrument is in position is to look at the recorded depth, provided that a depth sensor is used on the particular mooring. For moorings without depth sensors or for instrument on transects (which are deployed individually), in-position points need to be determined from field notes and temperature fluctuations.

Determining if all the data are valid

The final step in isolating good data is to determine which points are good. There were cases in the data where a logger would record completely unrealistic measurements. It is important to note that unrealistic measurements do not necessarily indicate that the instrument is malfunctioning, but rather that the instrument is not measuring what was intended. An example is a current meter that has been covered with barnacles; in this case the currents measured by the current meter may not be representative of currents surrounding the sensor.

Unfortunately, removing data can be subjective, as the distinction between unrealistic and unexpected can at times be fuzzy. Perhaps even more unnerving are points that need to be modified. In the Scott Reef data set, a depth sensor at a mooring in the middle of the lagoon suddenly reported depths 20 metres shallower for a couple of readings and then returned to the expected depths. Meanwhile, none of the temperatures on the mooring changed, indicating that the mooring depth most likely did not decrease. Since a tidal analysis on the depth data required an equally spaced data

set, these anomalous points needed to be modified rather than just removed. Great care was taken in all cases where data points were removed or modified to keep the original data and to flag any changes.

Processing and Storing Instrument Data

Having a systematic data storage procedure is crucial to handling such a large and diverse data set. Extensive software was written in MATLAB to help isolate good data as well as perform the analysis. The key to this software is its versatility. One script is used to convert the unique instrument data format into a generic format. Included in this generic format is auxiliary information such as the position, type, and serial number of the instrument. Additionally, units of each of the measurements are written in the file. The main advantage of standardizing the data is that any sequential processing or analysis can be written generically and used for any of the instrument types. The data format developed can be used for virtually any oceanographic instrument and has already been used in other field projects with other kinds of instruments.

Consolidation

Instruments on a transect or mooring record a combination of temperature, salinity, and sea-level data. These data are consolidated into a temperature profile with corresponding salinity and sea level for each transect and mooring. While moorings and transects may have roughly the same start and end time, the individual instruments may not be in synch or may have different sampling intervals. Special care has been taken to preserve the original data in a format that allows the data from each instrument to be viewed simultaneously. In addition to this format, instrument data are interpolated onto the same timescale and sorted by depth to allow for simplified future processing and analysis.

Calibration

While all the instruments were at one point calibrated, sensor measurements may drift over time from the absolute. Certain models of sensors tend to maintain accuracy for years while others tend be precise but contain an offset. A large portion of the field data

analysis was devoted to determining which instruments were logging the correct data and if offsets could be used to correct data shown to be unrealistic. To achieve this task, the questionable data were compared with either initial temperature profiles from CTD casts or with other temperature measurements acquired from that site.

CTD Comparison

Temperature profiles at many of the sites were measured by a CTD cast immediately following the deployment of a mooring or transect. The temperature profile from the CTD cast is known to be accurate and can therefore be compared to the first temperatures that were recorded on the mooring or transect. At the East Hook transect (Site H), only data from one temperature logger were successfully recovered. Compared with other loggers at other sites, the temperatures measured at East Hook were significantly higher (almost one degree Celsius). If these measurements are correct, then one would be pressed to find an oceanographic explanation for the presence of higher temperature water. In this case, the first reading in the time-series was 30.24°C. A temperature profile taken nearby and shortly before, indicates that the temperature at 19.8 metres (the depth of the time-series logger) was 29.51°C on the way down and 29.49°C on the way back up. Therefore it becomes apparent that the time-series temperature logger has roughly a +0.74° C offset which is rounded to +0.7°C. When corrected, the temperatures from the East Hook transect are much more similar to other temperatures measured around the reef and there is no longer reason to believe that this particular site somehow has access to warmer water.

Intercalibration

The best method to calibrate temperature data is to compare temperature measurements on the same mooring line. For example, three temperature loggers were located on the Site D mooring at depths of 20, 27, and 35 metres. Figure C.1 shows the temperature from these three instruments over 5 days. The temperatures were always decreasing with depth and there appeared to be a persistent temperature drop between the 27 and 35 metre loggers. The data seemed realistic, though the shapes of the temperature time-series for the 27 and 35 metre loggers seemed surprisingly similar compared with the shape of the 20 metre time-series. However, when it became evident from mooring

diagrams that the 27 metre logger was more likely located at 36 metres, the story changed completely. It now became apparent that the water was not stratified, but rather that the temperature logger located at 35 metres had an offset of –0.29°C. Measurements from older instruments, such as the one at 35 metres, can drift over the years if not recalibrated. The corrected data are plotted over the same period in Figure C.2.

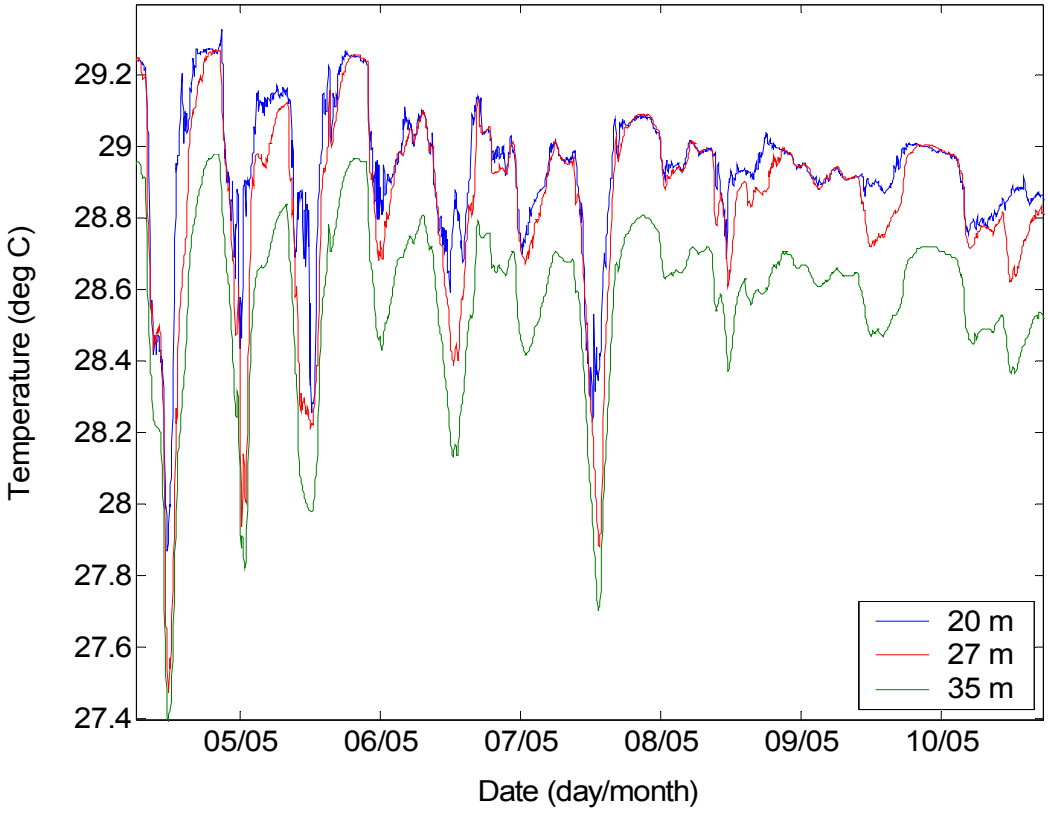

Figure C.1 Temperature records for loggers believed to be at 20, 27, and 35 metres below surface at Site D.

From the plot, it is apparent that there are times when the water temperature is the same at both 27 metres and 36 metres. For density reasons, it would be expected that the water measured at 35 metres would be at a temperature between that measured at 27 and 36 metres. This condition is met when the measured temperatures at 35 metres are offset by 0.29°C. There are two reasons to include this example. First, it illustrates how one sensor can be accurately calibrated using other sensors on a mooring. The second reason to include this example is that it demonstrates the importance of careful and thorough data processing. Initially, there was little reason to dispute the uncorrected temperature results. Had these results gone unchallenged, the reports from

the field data would have described persistent temperature stratification in the channel, which was not evident at any of the other sites. The implications of misleading field data can easily go beyond the field report and confuse modellers and theorists. Thus while thorough data processing for the Scott Reef field data set was quite time-consuming, accurate results are vital to other aspects of this project.

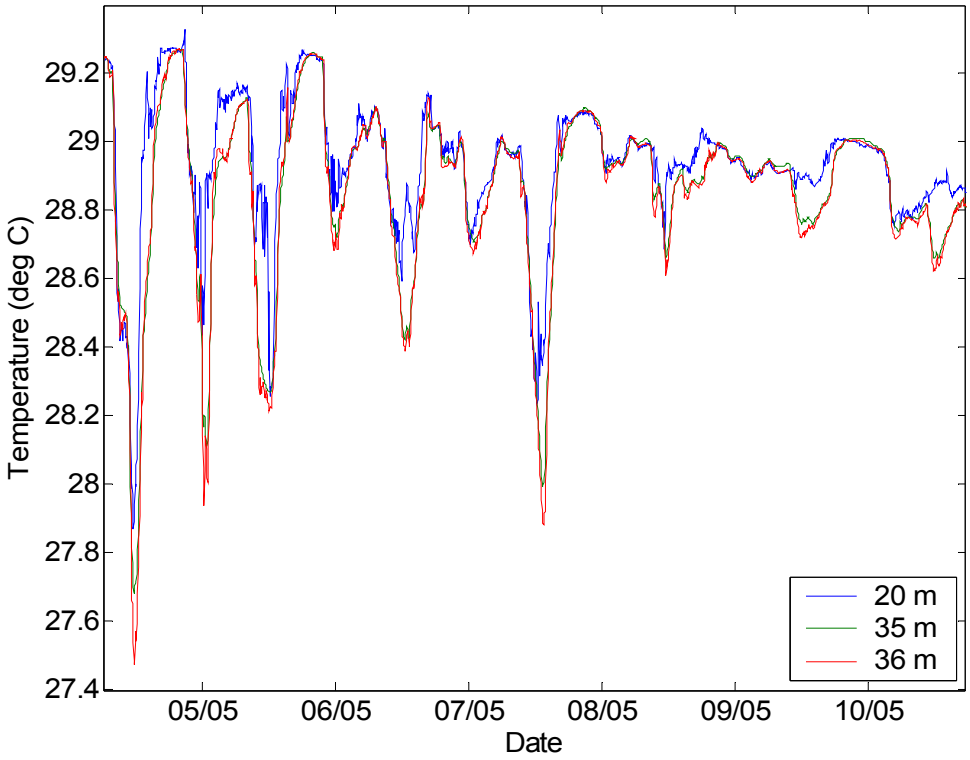

Figure C.2 Modified temperatures for loggers at Site D, now believed to be at 20, 35, and 36 metres below surface.

Appendix D – Tidal Analysis

Tidal harmonic analyses were performed for both the sea-level elevations and the current meters using a combination of MATLAB code written by Pawlowicz et al. (2002) and Fortran code written by Lou Mason of James Cook University. The length of measurements needed for a tidal analysis depends on which constituents are needed. Longer periods of measurements are required to discern between similar-frequency constituents. After 90 days the major constituents can usually be extracted; however time series of over a year are necessary to extract many of the minor components. Even longer time series may be necessary to accurately describe lower frequency terms.

Tidal Heights

Water surface elevation at Site L was measured hourly for 395 days starting on the 28th of February, 2002. From the tidal analysis the amplitude and phase of most of the major and minor constituents was calculated and are shown below. The predicted tide from this analysis could explain 99.8% of the variance in the original data. It was found that most of the energy at Scott Reef is contained in the M2, S2, K1, and N2 constituents (in that order). In the table below all error measurements are reported with a 95% confidence interval.

Tide	Frequency (cycles/day)	Amplitude (m)	Amplitude Error	Phase (deg)	Phase Error	SNR
*SA	0.0001141	0.0420	0.008	123.36	14.76	25
*SSA	0.0002282	0.0227	0.009	195.54	28.98	6
*MSM	0.0013098	0.0080	0.009	268.76	78.25	0.75
*MM	0.0015122	0.0065	0.009	14.07	89.28	0.51
*MSF	0.0028219	0.0012	0.007	270.56	203.25	0.029
*MF	0.0030501	0.0120	0.010	32.54	49.65	1.5
*ALP1	0.0343966	0.0010	0.001	243.89	72.38	0.94
*2Q1	0.0357064	0.0033	0.001	241.00	21.82	8.6
*SIG1	0.0359087	0.0056	0.001	245.79	12.16	16
*Q1	0.0372185	0.0361	0.001	256.60	2.05	9.2e+002
*RHO1	0.0374209	0.0065	0.001	262.03	12.33	26
*O1	0.0387307	0.1541	0.001	275.12	0.44	1.4e+004
*TAU1	0.0389588	0.0032	0.001	289.14	26.68	5.8
*BET1	0.0400404	0.0008	0.001	234.37	97.23	0.43
*NO1	0.0402686	0.0091	0.001	300.31	4.87	79
*CHI1	0.0404710	0.0029	0.001	294.14	23.74	7.8
*PI1	0.0414385	0.0055	0.001	299.01	14.76	14
*P1	0.0415526	0.0725	0.001	287.63	1.14	2.5e+003
*S1	0.0416667	0.0120	0.002	320.78	9.91	37

*K1	0.0417807	0.2416	0.001	292.17	0.31	2.9e+004
*PSI1	0.0418948	0.0028	0.001	252.69	23.65	4.2
*PHI1	0.0420089	0.0032	0.001	295.48	21.61	5.5
*THE1	0.0430905	0.0024	0.001	304.06	32.34	4.2
*J1	0.0432929	0.0130	0.001	320.28	5.72	85
*SO1	0.0446027	0.0024	0.001	351.28	32.26	3.5
*OO1	0.0448308	0.0096	0.001	346.53	6.16	1.1e+002
*UPS1	0.0463430	0.0014	0.001	24.60	39.14	1.9
*OQ2	0.0759749	0.0017	0.003	204.58	115.62	0.28
*EPS2	0.0761773	0.0031	0.003	217.37	76.75	0.88
*2N2	0.0774871	0.0160	0.004	228.64	12.99	15
*MU2	0.0776895	0.0162	0.004	250.05	15.28	16
*N2	0.0789992	0.1741	0.003	259.99	1.29	2.8e+003
*NU2	0.0792016	0.0344	0.004	267.44	6.51	71
*H1	0.0803973	0.0068	0.004	45.51	36.21	3.4
*M2	0.0805114	0.9894	0.004	291.77	0.21	5.8e+004
*H2	0.0806255	0.0083	0.004	147.74	26.81	4
*MKS2	0.0807396	0.0023	0.003	104.49	91.90	0.49
*LDA2	0.0818212	0.0120	0.004	287.69	19.67	9.1
*L2	0.0820236	0.0332	0.005	306.75	9.78	45
*T2	0.0832193	0.0349	0.004	353.88	5.76	72
*S2	0.0833333	0.5649	0.004	353.78	0.37	1.9e+004
*R2	0.0834474	0.0078	0.003	12.30	26.21	6.1
*K2	0.0835615	0.1580	0.004	351.68	1.35	2e+003
*MSN2	0.0848455	0.0021	0.003	195.67	106.63	0.41
*ETA2	0.0850736	0.0074	0.003	33.04	23.58	5.6
*MO3	0.1192421	0.0017	0.001	267.15	40.23	2
*M3	0.1207671	0.0029	0.001	11.90	24.65	4.2
*SO3	0.1220640	0.0004	0.001	266.44	139.84	0.16
*MK3	0.1222921	0.0010	0.001	250.55	71.73	0.83
*SK3	0.1251141	0.0026	0.001	269.28	25.98	5.8
*MN4	0.1595106	0.0034	0.003	279.78	58.83	1.6
*M4	0.1610228	0.0063	0.003	269.02	27.42	3.9
*SN4	0.1623326	0.0006	0.002	245.51	178.76	0.085
*MS4	0.1638447	0.0127	0.003	338.36	16.27	14
*MK4	0.1640729	0.0031	0.002	3.36	44.53	1.7
*S4	0.1666667	0.0030	0.003	73.52	62.86	1.2
*SK4	0.1668948	0.0002	0.002	301.17	226.59	0.013
*2MK5	0.2028035	0.0003	0.001	47.33	136.37	0.26
*2SK5	0.2084474	0.0005	0.001	342.36	93.29	0.51
*2MN6	0.2400221	0.0004	0.001	74.90	151.41	0.2
*M6	0.2415342	0.0026	0.001	60.07	25.55	4.1
*2MS6	0.2443561	0.0034	0.001	150.87	19.95	7.9
*2MK6	0.2445843	0.0013	0.001	203.68	48.74	1.5
*2SM6	0.2471781	0.0016	0.001	240.06	41.54	1.8
*MSK6	0.2474062	0.0007	0.001	243.90	86.12	0.78
*3MK7	0.2833149	0.0003	0.000	302.30	89.13	0.57
*M8	0.3220456	0.0003	0.000	32.29	69.23	0.54

Table D.1. Tidal elevation constituents at Site L derived from Harmonic Tidal Analysis.

Tidal Currents

Water currents were measured at several sites (see Appendix B) during the field campaign in 2003. At Site D, predictions from tidal analysis accounted for 82.1% of the variability in the 89 day current. By being in a channel, the currents at Site D are stronger and easier to detect than the currents in the surrounding areas. In the lagoon, only 54.3% of the variability could be explained by tidal predictions for the 89 day current at Site F. It has long been established that predicting currents is in general much more difficult than predicting sea-level (Godin, 1983) and this lower predictive capability is not surprising. The table below lists the tidal ellipse parameters for Site F.

Tide	Frequency (cycles/day)	Major (m/s)	Minor (m/s)	Inclination (deg)	Phase (deg)	SNR
*MM	0.0015	1.053	0.289	14.50	211.66	0.85
*MSF	0.0028	1.611	-0.013	159.80	330.12	1.9
*ALP1	0.0343	0.275	0.027	74.07	255.90	1.1
*2Q1	0.0357	0.310	0.031	161.44	284.16	1.5
*Q1	0.0372	0.184	-0.019	56.81	39.78	0.61
*O1	0.0387	1.020	-0.052	20.73	169.32	12
*NO1	0.0402	0.192	0.121	42.18	120.40	1.2
*K1	0.0417	1.270	0.215	21.63	161.00	16
*J1	0.0432	0.371	0.133	175.23	8.91	1.6
*OO1	0.0448	0.163	0.142	172.30	30.35	0.69
*UPS1	0.0463	0.117	0.072	52.88	51.91	0.45
*EPS2	0.0761	0.307	0.095	60.77	5.00	0.26
*MU2	0.0776	0.558	-0.197	6.08	147.13	0.52
*N2	0.0789	1.105	-0.413	175.35	351.09	1.3
*M2	0.0805	5.958	-0.797	1.54	197.64	36
*L2	0.0820	1.861	0.183	4.29	229.20	2.8
*S2	0.0833	4.020	-0.572	0.35	253.53	20
*ETA2	0.0850	0.256	-0.029	176.14	92.85	0.3
*MO3	0.1192	0.249	0.061	18.27	310.61	1.3
*M3	0.1207	0.234	-0.025	22.75	308.17	0.98
*MK3	0.1222	0.199	0.062	164.41	24.88	0.92
*SK3	0.1251	0.151	0.075	12.13	133.44	0.9
*MN4	0.1595	0.327	-0.176	111.72	21.73	1.5
*M4	0.1610	0.680	0.221	50.75	65.92	4.9
*SN4	0.1623	0.197	-0.038	110.74	95.10	0.6
*MS4	0.1638	1.223	0.020	26.26	133.73	13
*S4	0.1666	0.218	0.044	39.62	195.09	0.6
*2MK5	0.2028	0.127	-0.072	130.73	11.93	1.2
*2SK5	0.2084	0.063	-0.035	174.79	232.07	0.56
*2MN6	0.2400	0.175	-0.045	83.46	320.64	1.9
*M6	0.2415	0.203	0.010	106.84	12.08	2.8
*2MS6	0.2443	0.305	-0.045	135.46	127.46	4.9
*2SM6	0.2471	0.156	-0.011	138.36	177.91	1.5
*3MK7	0.2833	0.046	0.001	60.57	330.51	0.37
*M8	0.3220	0.040	-0.028	115.83	235.22	0.59

Table D.2. Tidal current constituents at Site F derived from Harmonic Tidal Analysis.

Appendix E – SST Iteration Procedure

In the ideal case, the sea surface temperature observed by satellite images could be used in flux calculations. Unfortunately, these measurements are easily tainted by clouds and can only be taken when satellites pass overhead. Furthermore even if SST were known perfectly, the rest of meteorological measurements contain uncertainty. SST depends on the rest of the meteorological measurements, but the meteorological measurements are independent of SST. This means that given a set of meteorological measurements and an initial profile, the SST corresponding to these measurements can be calculated. It is most logical to have the model calculate the SST diagnostically; given the fluxes at time, t, the model can calculate the temperature at the next timestep, t+1, which will be used to calculate the fluxes. When this option is chosen in GOTM, the user forsakes all control on how the fluxes are calculated. More importantly, results showed unrealistic responses to the fluxes. Without the time to debug and recode the basic structure of the numerical model, an alternative method was developed.

Flux measurements are entered into the numerical model prognostically, meaning that the flux entered at a given time is independent of the simulated SST the timestep before. Instead the flux is adjusted to the model SST through an iterative process. Starting with an initial estimate on the SST, fluxes are calculated from the bulk formulas. The resulting fluxes are inputted into GOTM to estimate vertical temperatures. The temperature time-series from the top layer gives an indication of the accuracy of the initial temperature estimate. If the initial estimate was accurate, then the skin layer temperatures from the model would be nearly identical to the initial value chosen. However when the initial estimate is not accurate, an important question is whether the resulting simulated skin layer temperature is closer to the true value. If the model results were closer to the true value than the initial estimate, a second model run using fluxes calculated from the skin layer temperature results from the first model run would produce an estimate for the skin layer temperature even closer to the true value. This iterative process could continue until the skin layer temperature used to calculate the fluxes and the next modelled skin layer temperature converged. Unfortunately when this technique is attempted over a two month period, the predicted skin layer temperatures (SSTs) diverge. Inspection of Figure E.1 reveals two noteworthy

observations of these skin layer temperature iterations. The first is that temperature errors accumulate over each time series as there is no dynamical method for the temperatures to correct themselves. The second observation is that each successive iteration flip-flops over the true value while diverging. An overestimation of SST used to compute the fluxes will generate fluxes that lead to an underestimate of the SST in the next iteration. When these underestimated SSTs are used to compute the next set of fluxes, the next set of fluxes will lead to an overestimate in the SST in the following iteration, and so on.

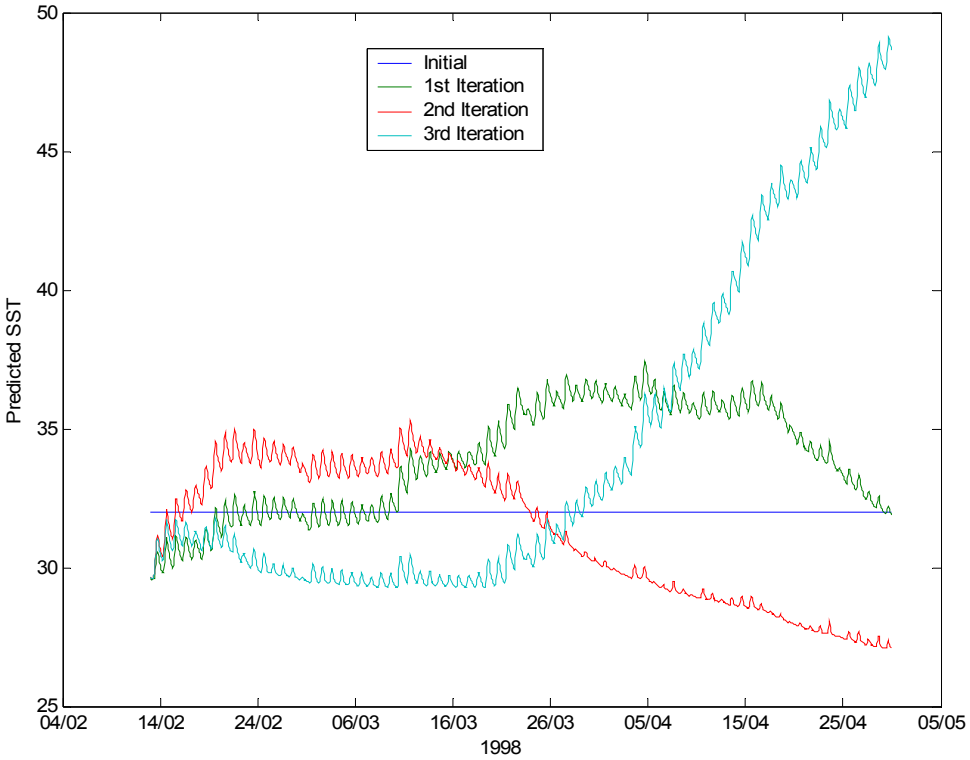

Figure E.1 Predicted SST for a 2-month GOTM simulation using a simple iteration technique. Each colour curve corresponds to an individual iteration.

By changing the iteration technique, it is possible to force the sequential SSTs to converge relatively quickly. The SST used to calculate fluxes in the new technique is an arithmetic average of SST from the previous two iterations. Figure E.2 illustrates this technique. The fluxes are first calculated using an initial estimate of the SSTs (blue line); the fluxes drive the numerical model which generates temperature time series at the sea surface (green line). As in the approach above, the temperature time-series at the sea surface (green line) is used to calculate fluxes which then drive the numerical model, producing a new temperature time-series at the sea surface (red line). Already

one can notice that the average temperature is diverging rapidly. However this time, instead of repeating the process with the red line, the first and second iterations (green and red lines) are averaged (cyan line). The averaged temperature time-series (cyan line) is used to calculate fluxes which then drive the numerical model, producing yet another temperature time-series at the sea surface (purple line). The fluxes are calculated next by the average of the last temperature time-series and the one before (in this case the purple and cyan lines). Repeating this method, the SST time-series eventually converges so that the 11^{th} and 12^{th} time-series are nearly identical. The number of iterations required for the SST time-series to converge depends strongly on how close the initial estimate is to the converged time-series.

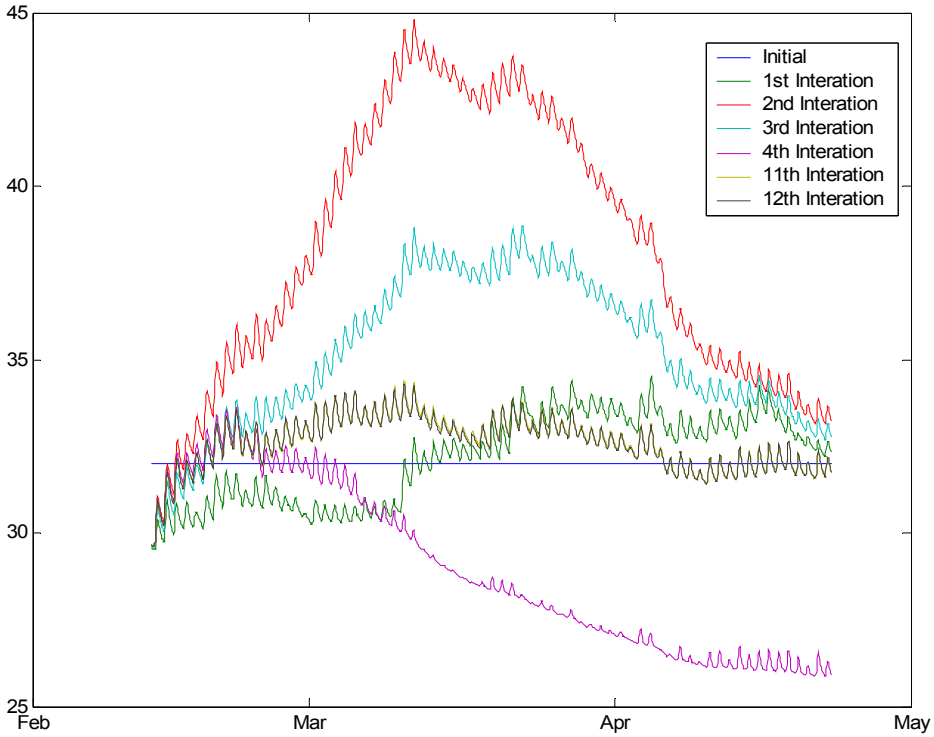

Figure E.2 Predicted SST for a 2-month GOTM simulation using a modified iteration technique. Each colour curve corresponds to an iteration.

The converged SST represents the SST that would result from those particular fluxes, given the assumptions of the one-dimensional numerical model. As these assumptions are changed, such as by changing the water turbidity in the model, the SST will change. It is important to note that the calculated SST was derived without any influence from the satellite observed SST. Therefore the observed SST can be used to judge the

performance of the numerical model as well as help determine what conditions (such as turbidity) lead to the best results.

References

Andrefouet, S. et al., 2003. Multi-site evaluation of IKONOS data for classification of tropical coral reef environments. Remote Sensing of Environment, 88: 128-143.

Berkelmans, R., 2002. Time-integrated thermal bleaching thresholds of reefs and their variation on the Great Barrier Reef. Marine Ecology-Progress Series, 229: 73-82.

Berkelmans, R., De'ath, G., Kininmonth, S. and Skirving, W.J., 2004. A comparison of the 1998 and 2002 coral bleaching events on the Great Barrier Reef: spatial correlation, patterns, and predictions. Coral Reefs, 23(1): 74-83.

Berkelmans, R. and Oliver, J.K., 1999. Large-scale bleaching of corals on the Great Barrier Reef. Coral Reefs, 18(1): 55-60.

Bode, L. and Mason, L.B., 1994. Application of an implicit hydrodynamic model over a range of spatial scales. In: D. Stewart, H. Gardner and D. Singleton (Editors), Computational Techniques and Applications: CTAC93. World Scientific Press, pp. 112-121.

Bode, L., Mason, L.B. and Middleton, J.H., 1997. Reef parameterisation schemes with applications to tidal modelling. Progress in Oceanography, 40(1-4): 285-324.

Brinkman, R., Wolanski, E., Deleersnijder, E., McAllister, F. and Skirving, W.J., 2001. Oceanic inflow from the Coral Sea into the Great Barrier Reef. Estuarine, Coastal and Shelf Science, 54: 655-668.

Burchard, H., 2002. Applied turbulence modelling in marine waters. Lecture Notes in Earth Sciences, 100. Springer, Berlin, Heidelberg, New York, 229 pp.

Burrage, D.M., Massel, S.R., Steinberg, C.R. and Skirving, W.J., 1996. Detecting Surface and Internal Wave Signatures on the North West Australian Shelf using the ERS1&2 Active Microwave Instrumentation (AMI), Proceedings of the First Australian ERS-1 Symposium during the 3rd AMOS National Conference, Hobart.

Coles, S.L. and Brown, B.E., 2003. Coral bleaching - Capacity for acclimatization and adaptation, Advances in Marine Biology, Vol 46. Advances in Marine Biology. Academic Press Ltd, London, pp. 183-223.

Coutis, P.F. and Middleton, J.H., 1999. Flow-topography interaction in the vicinity of an isolated, deep ocean island. Deep-Sea Research Part I-Oceanographic Research Papers, 46(9): 1633-1652.

Cresswell, G.R. and Badcock, K.A., 2000. Tidal mixing near the Kimberley coast of NW Australia. Mar. Freshwater Res., 51: 641-646.

Eanes, R.J. and Bettadpur, S., 1995. The CSR 3.0 global ocean tide model, Center for Space Research, University of Texas, Austin, Tx.

Fairall, C.W., Bradley, E.F., Rogers, D.P., Edson, J.B. and Young, G.S., 1996. Bulk parameterization of the air-sea fluxes for Tropical Ocean Global Atmosphere Coupled-Ocean Atmosphere Response Experiment. J. Geophys. Res., 101: 3747-3764.

Feng, M. and Wijffels, S., 2002. Intraseasonal variability in the south equatorial current of the east Indian Ocean. Journal of Physical Oceanography, 32(1): 265-277.

Fitt, W.K., Brown, B.E., Warner, M.E. and Dunne, R.P., 2001. Coral bleaching: interpretation of thermal tolerance limits and thermal thresholds in tropical corals. Coral Reefs, 20(1): 51-65.

Franklin, D.J., Hoegh-Guldberg, P., Jones, R.J. and Berges, J.A., 2004. Cell death and degeneration in the symbiotic dinoflagellates of the coral Stylophora pistillata during bleaching. Marine Ecology-Progress Series, 272: 117-130.
Fung, I.Y., Harrison, D.E. and Lacis, A.A., 1984. On the variability of the net longwave radiation at the ocean surface. Rev. Geophys., 22: 177-193.
Godfrey, J.S. and Mansbridge, J.V., 2000. Ekman transports, tidal mixing, and the control of temperature structure in Australia's northwest waters. Journal of Geophysical Research-Oceans, 105(C10): 24021-24044.
Godin, G., 1983. On the Predictability of Currents. International Hydrographic Review, 60(1): 119-126.
Goreau, T.J. and Hayes, R.L., 1994. Coral Bleaching and Ocean Hot-Spots. Ambio, 23(3): 176-180.
Heyward, A., Smith, L.D., Halford, A., R., Rees, M. and Meekan, M.G., 1999. Natural variability at Scott Reef: Short term response of coral and fish assemblages to a severe coral bleaching event, Australian Institute of Marine Science.
Hoegh-Guldberg, O., 1999. Climate change, coral bleaching and the future of the world's coral reefs. Marine and Freshwater Research, 50(8): 839-866.
Holloway, P.E., 1996. A numerical model of internal tides with application to the Australian North West Shelf. Journal of Physical Oceanography, 26(1): 21-37.
Holloway, P.E. and Nye, H.C., 1985. Leeuwin Current and Wind Distributions on the Southern Part of the Australian North-West Shelf between January 1982 and July 1983. Australian Journal of Marine and Freshwater Research, 36(2): 123-137.
Hughes, T.P. et al., 2003. Climate change, human impacts, and the resilience of coral reefs. Science, 301(5635): 929-933.
Jerlov, N.G., 1976. Marine Optics. Elsevier, Amsterdam, 194 pp.
Karl, T.R., Knight, R.W. and Baker, B., 2000. The record breaking global temperatures of 1997 and 1998: Evidence for an increase in the rate of global warming? Geophysical Research Letters, 27(5): 719-722.
Kondo, J., 1975. Air-sea bulk transfer coefficients in diabatic conditions. Boundary-Layer Meteorology, 9: 91-112.
Large, W.G., McWilliams, J.C. and Doney, S.C., 1994. Oceanic Vertical Mixing - a Review and a Model with a Nonlocal Boundary-Layer Parameterization. Reviews of Geophysics, 32(4): 363-403.
Lesser, M.P., 1996. Elevated temperatures and ultraviolet radiation cause oxidative stress and inhibit photosynthesis in symbiotic dinoflagellates. Limnology and Oceanography, 41(2): 271-283.
Liu, G., Strong, A. and Skirving, W.J., 2003. Remote Sensing of Sea Surface Temperatures During 2002 Barrier Reef Coral Bleaching. EOS, 84(15): 137.
Lough, J.M., 2000. 1997-98: Unprecedented thermal stress to coral reefs? Geophysical Research Letters, 27(23): 3901-3904.
Marshall, P.A. and Baird, A.H., 2000. Bleaching of corals on the Great Barrier Reef: differential susceptibilities among taxa. Coral Reefs, 19(2): 155-163.
Martin, P.J., 1985. Simulation of the mixed layer at OWS November and Papa with several models. Journal of Geophysical Research, 90: 903-916.
Maurer, J., 2002. Infrared and Microwave Remote Sensing of Sea Surface Temperature.
McClanahan, T.R., 2004. The relationship between bleaching and mortality of common corals. Marine Biology, 144(6): 1239-1245.
McPhaden, M.J., 1999. Climate oscillations - Genesis and evolution of the 1997-98 El Nino. Science, 283(5404): 950-954.

Mumby, P.J., Chisholm, J.R.M., Edwards, A.J., Andrefouet, S. and Jaubert, J., 2001. Cloudy weather may have saved Society Island reef corals during the 1998 ENSO event. Marine Ecology-Progress Series, 222: 209-216.
Nadaoka, K. et al., 2001. Regional variation of water temperature around Okinawa coasts and its relationship to offshore thermal environments and coral bleaching. Coral Reefs, 20(4): 373-384.
Nakamura, T. and van Woesik, R., 2001. Water-flow rates and passive diffusion partially explain differential survival of corals during the 1998 bleaching event. Marine Ecology-Progress Series, 212: 301-304.
Nakamura, T., Yamasaki, H. and van Woesik, R., 2003. Water flow facilitates recovery from bleaching in the coral Stylophora pistillata. Marine Ecology-Progress Series, 256: 287-291.
Pawlowicz, P., Beardsley, B., Lentz, S., Dever, E. and Anis, A., 2001. Software simplifies Air-Sea Data Estimates. EOS, 82(1): 2-4.
Pawlowicz, R., Beardsley, B. and Lentz, S., 2002. Classical tidal harmonic analysis including error estimates in MATLAB using T-TIDE. Computers & Geosciences, 28(8): 929-937.
Payne, R.E., 1972. Albedo of the Sea Surface. Journal of the Atmospheric Sciences, 29: 959-970.
Phongsuwan, N., 1998. Extensive coral mortality as a result of bleaching in the Andaman Sea in 1995. Coral Reefs, 17(1): 70-70.
Pingree, R.D. and Griffiths, D.K., 1978. Tidal Fronts on Shelf Seas around British-Isles. Journal of Geophysical Research-Oceans and Atmospheres, 83(NC9): 4615-4622.
Ranasinghe, R. and Pattiaratchi, C., 1999. Circulation and mixing characteristics of a seasonally-open tidal inlet: A field study. Marine Freshwater Reseach, 50: 281-290.
Reed, 1977. On Estimating Insolation over the Ocean. J. Phys. Oceanog., 7: 482-485.
Ridgway, K.R. and Dunn, J.R., 2002. Ocean Interpolation by Four-dimensional Weighted Least Squares - Application to the waters around Australasia. Journal of Atmospheric and Ocean Technology, 19: 1357-1375.
Riegl, B. and Piller, W.E., 2003. Possible refugia for reefs in times of environmental stress. International Journal of Earth Sciences, 92(4): 520-531.
Simpson, J.H. and Hunter, J.R., 1974. Fronts in Irish Sea. Nature, 250(5465): 404-406.
Simpson, J.H. et al., 1982. Mixing and Phytoplankton Growth around an Island in a Stratified Sea. Continental Shelf Research, 1(1): 15-31.
Skirving, W.J. and Steinberg, C.R., 2003. The hydrodynamics of a coral bleaching event, Coral Reefs, Climate, & Coral Bleaching, Oahu, Hawaii.
Smith, L., Gilmour, J., Heyward, A. and Rees, M., 2003. Biological and Physical Environment at Scott Reef: 1994-2003, II: Biological Environment, Australian Institute of Marine Science, Townsville.
Smith, N.P., 2001. Weather and hydrographic conditions associated with coral bleaching: Lee Stocking Island, Bahamas. Coral Reefs, 20(4): 415-422.
Wilkinson, C. (Editor), 2000. Status of coral reefs of the world: 2000. Australian Institute of Marine Science, Townsville, QLD, 376 pp.
Wilkinson, C. (Editor), 2002. Status of coral reefs of the world: 2002. Australian Institute of Marine Science, Townsville, QLD, 388 pp.
Wilkinson, C. et al., 1999. Ecological and socioeconomic impacts of 1998 coral mortality in the Indian Ocean: An ENSO impact and a warning of future change? Ambio, 28(2): 188-196.

Wolanski, E. and Deleersnijder, E., 1998. Island-generated internal waves at Scott reef, Western Australia. Continental Shelf Research, 18(13): 1649-1666.
Wooldridge, S. and Done, T., 2004. Learning to predict large-scale coral bleaching from past events: A Bayesian approach using remotely sensed data, in-situ data, and environmental proxies. Coral Reefs, 23(1): 96-108.